AD-A089 186 EFFECTS TECHNOLOGY INC SANTA BARBARA CA F/G 8/7
MISSILE SITE ROCK CHARACTERIZATION AND PENETRATION TEST RESULTS--ETC(U)
DEC 79 J D CARLYLE DNA001-79-C-0115
UNCLASSIFIED DNA-5144F NL

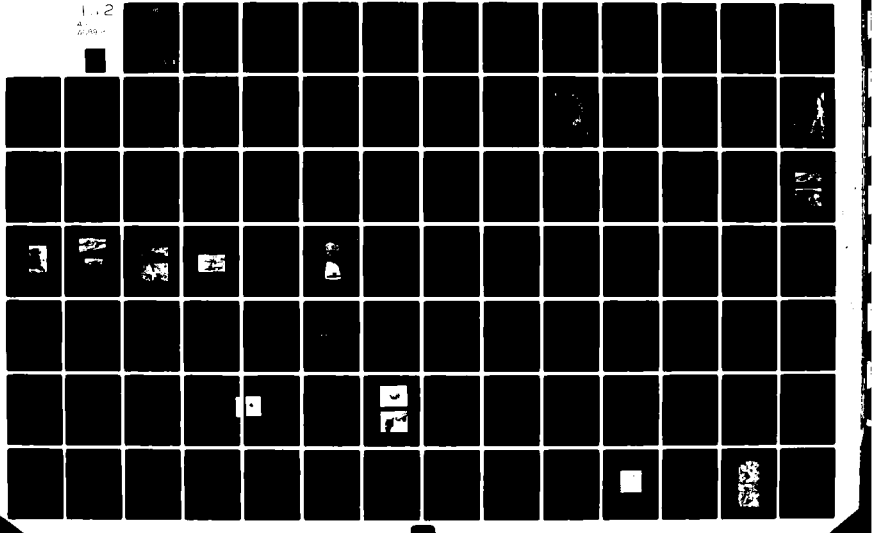

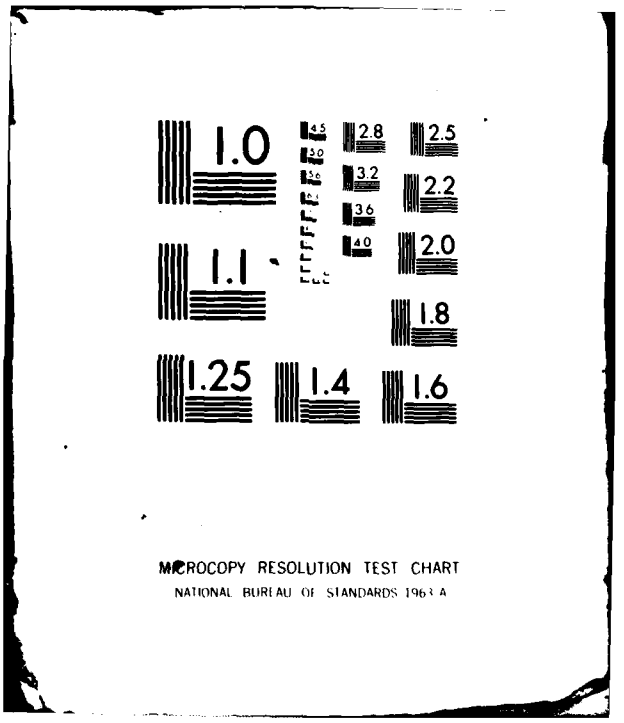
1.0
1.1
1.25
1.4
1.6
1.8
2.0
2.2
2.5
2.8
3.2
3.6
4.0
MICROCOPY RESOLUTION TEST CHART
NATIONAL BUREAU OF STANDARDS 1963 A

(12) LEVEL II

B.S.

DNA 5144F

MISSILE SITE ROCK CHARACTERIZATION AND PENETRATION TEST RESULTS

John D. Carlyle
Effects Technology, Inc.
5383 Hollister Avenue,
Santa Barbara, California 93111

14 December 1979

Final Report for Period 9 January 1979—1 November 1979

CONTRACT No. DNA 001-79-C-0115

APPROVED FOR PUBLIC RELEASE;
DISTRIBUTION UNLIMITED.

THIS WORK SPONSORED BY THE DEFENSE NUCLEAR AGENCY
UNDER RDT&E RMSS CODE B363076464 N99QAXAI12907 H2590D.

Prepared for
Director
DEFENSE NUCLEAR AGENCY
Washington, D. C. 20305

Destroy this report when it is no longer needed. Do not return to sender.

PLEASE NOTIFY THE DEFENSE NUCLEAR AGENCY, ATTN: STTI, WASHINGTON, D.C. 20305, IF YOUR ADDRESS IS INCORRECT, IF YOU WISH TO BE DELETED FROM THE DISTRIBUTION LIST, OR IF THE ADDRESSEE IS NO LONGER EMPLOYED BY YOUR ORGANIZATION.

12 130 18 DNA, SBIE

UNCLASSIFIED

SECURITY CLASSIFICATION OF THIS PAGE (When Data Entered)

REPORT DOCUMENTATION PAGE	READ INSTRUCTIONS BEFORE COMPLETING FORM
1. REPORT NUMBER: DNA 5144F	2. GOVT ACCESSION NO.: AD-A089186
3. RECIPIENT'S CATALOG NUMBER:	
4. TITLE (and Subtitle): MISSILE SITE ROCK CHARACTERIZATION AND PENETRATION TEST RESULTS	5. TYPE OF REPORT & PERIOD COVERED: Final Report for Period 9 Jan 79—1 Nov 79
6. PERFORMING ORG. REPORT NUMBER:	
7. AUTHOR(s): John D. Carlyle	8. CONTRACT OR GRANT NUMBER(s): DNA 001-79-C-0115
9. PERFORMING ORGANIZATION NAME AND ADDRESS: Effects Technology, Inc. 5383 Hollister Avenue Santa Barbara, California 93111	10. PROGRAM ELEMENT, PROJECT, TASK AREA & WORK UNIT NUMBERS: Subtask N99QAXAI129-07
11. CONTROLLING OFFICE NAME AND ADDRESS: Director Defense Nuclear Agency Washington, D.C. 20305	12. REPORT DATE: 14 December 1979
	13. NUMBER OF PAGES: 126
14. MONITORING AGENCY NAME & ADDRESS (if different from Controlling Office): 5144F AD-E300 905	15. SECURITY CLASS (of this report): UNCLASSIFIED
	15a. DECLASSIFICATION/DOWNGRADING SCHEDULE:

16. DISTRIBUTION STATEMENT (of this Report)

Approved for public release; distribution unlimited.

17. DISTRIBUTION STATEMENT (of the abstract entered in Block 20, if different from Report)

18. SUPPLEMENTARY NOTES

This work sponsored by the Defense Nuclear Agency under RDT&E RMSS Code B363076464 N99QAXAI12907 H2590D.

19. KEY WORDS (Continue on reverse side if necessary and identify by block number)

Nuclear Dust and Debris	Candidate Deployment Parcel
Penetration	In-Situ
Ballistic Limit	Rock Unit
Candidate Deployment Region	Missile Vulnerability

20. ABSTRACT (Continue on reverse side if necessary and identify by block number)

The in-situ particulates from representative candidate missile deployment parcels have been characterized as part of the effort described in this report. An assessment of the ballistic penetration for the range of rock types found at proposed basing sites has been made for a Ti(6Al4V) target material in order to evaluate the variation in the extent of damage to a missile shroud during ascent.

DD FORM 1 JAN 73 1473 EDITION OF 1 NOV 65 IS OBSOLETE

UNCLASSIFIED

SECURITY CLASSIFICATION OF THIS PAGE (When Data Entered)

405842

20. ABSTRACT (Continued)

The penetrability of the baseline tonalite granite was found to be comparable to several of the in-situ rock types for high impact velocities. Volcanic tuff and scoria which represent rock units that constitute 40 to 90% of the geology in any one candidate deployment sites surveyed were found to be two to three times less penetrating than the tonalite granite representative projectile types.

A correlation of data bases for various projectiles was obtained from the current test results and the literature. From this correlation and the approach used for this effort, a test methodology for the characterization of shroud materials/concepts and motor-case protection materials is recommended.

PREFACE

This report is submitted by Effects Technology, Incorporated (ETI), to the Defense Nuclear Agency (DNA). This report documents ETI's efforts to survey proposed basing areas and evaluate the effects of in-situ debris on ascent shroud concepts/materials for advanced strategic nuclear weapon systems.

Capt. A. T. Hopkins was the Contracting Officer's Representative for the program. Dr. T. J. Ahrens of California Institute of Technology provided geophysical consulting for the effort.

The author would like to take this opportunity to thank Dr. G. Ramanjaneya of Fugro National Incorporated for his assistance in providing particle size distribution data and information on candidate deployment region location and geology.

Table 1. Conversion factors for U.S. customary to metric (SI) units of measurement.

To Convert From	To	Multiply By
angstrom	meters (m)	1.000 000 X E -10
atmosphere (normal)	kilo pascal (kPa)	1.013 25 X E +2
bar	kilo pascal (kPa)	1.000 000 X E +2
barn	meter^2 (m^2)	1.000 000 X E -28
British thermal unit (thermochemical)	joule (J)	1.054 350 X E +3
cal (thermochemical)/cm^2§	mega joule/m^2 (MJ/m^2)	4.184 000 X E -2
calorie (thermochemical)§	joule (J)	4.184 000
calorie (thermochemical)/g§	joule per kilogram (J/kg)*	4.184 000 X E +3
curies	giga becquerel (GBq)+	3.700 000 X E +1
degree Celsius‡	degree kelvin (K)	$t_K = t°_C + 273.15$
degree (angle)	radian (rad)	1.745 329 X E -2
degree Fahrenheit	degree kelvin (K)	$t_K = (t°_F + 459.67)/1.8$
electron volt§	joule (J)	1.602 19 X E -19
erg§	joule (J)	1.000 000 X E -7
erg/second	watt (W)	1.000 000 X E -7
foot	meter (m)	3.048 000 X E -1
foot-pound-force	joule (J)	1.355 818
gallon (U.S. liquid)	meter^3 (m^3)	3.785 412 X E -3
inch	meter (m)	2.540 000 X E -2
jerk	joule (J)	1.000 000 X E +9
joule/kilogram (J/kg) (radiation dose absorbed)§	gray (Gy)*	1.000 000
kilotons§	terajoules	4.183
kip (1000 lbf)	newton (N)	4.448 222 X E +3
kip/inch^2 (ksi)	kilo pascal (kPa)	6.894 757 X E +3
ktap	newton-second/m^2 ($N-s/m^2$)	1.000 000 X E +2
micron	meter (m)	1.000 000 X E -6
mil	meter (m)	2.540 000 X E -5
mile (international)	meter (m)	1.609 344 X E +3
ounce	kilogram (kg)	2.834 952 X E -2
pound-force (lbf avoirdupois)	newton (N)	4.448 222
pound-force inch	newton-meter (N•m)	1.129 848 X E -1
pound-force/inch	newton/meter (N/m)	1.751 268 X E +2
pound-force/foot^2	kilo pascal (kPa)	4.788 026 X E -2
pound-force/inch^2 (psi)	kilo pascal (kPa)	6.894 757
pound-mass (lbm avoirdupois)	kilogram (kg)	4.535 924 X E -1
pound-mass-foot^2 (moment of inertia)	kilogram-meter^2 ($kg•m^2$)	4.214 011 X E -2
pound-mass/foot^3	kilogram-meter^3 (kg/m^3)	1.601 846 X E +1
rad (radiation dose absorbed)§	gray (Gy)*	1.000 000 X E -2
roentgen§	coulomb/kilogram (C/kg)	2.579 760 X E -4
shake	second (s)	1.000 000 X E -8
slug	kilogram (kg)	1.459 390 X E +1
torr (mm Hg, 0° C)	kilo pascal (kPa)	1.333 22 X E -1

*The gray (Gy) is the accepted SI unit equivalent to the energy imparted by ionizing radiation to a mass of energy corresponding to one joule/kilogram.
+The becquerel (Bq) is the SI unit of radioactivity; 1 Bq = 1 event/s.
‡Temperature may be reported in degree Celsius as well as degree kelvin.
§These units should not be converted in DNA technical reports; however, a parenthetical conversion is permitted at the author's discretion.

TABLE OF CONTENTS

LIST OF ILLUSTRATIONS

LIST OF ILLUSTRATIONS (continued)

LIST OF ILLUSTRATIONS (concluded)

LIST OF TABLES

LIST OF TABLES (concluded)

1.0 INTRODUCTION

In the event of a nuclear strike against U.S. ICBM forces, advanced missiles may be required to successfully launch and ascend through a variety of hostile environments as depicted in Figure 1.1.

Laboratory tests to evaluate missile design concepts and to screen candidate shroud and motor case protection materials have been developed to simulate anticipated particle encounters. Granite projectiles are used for testing to provide more realistic impact simulation. These granite projectiles, representative of current operational site geology, provided the existing data base for various shroud concepts and materials. However, the use of granite projectiles may be uncharacteristic of sites presently being considered for advanced ICBMs. Additionally, the relative penetration capability of in-situ debris versus granite spheres was unknown. Since the penetration capability of different types of projectiles will partially determine the performance requirements of a missile material and the material's weight contribution to the overall weight of the missile, it is imperative that representative projectile materials and impact conditions be used for shroud evaluation.

This program was initiated to evaluate the ballistic penetration of in-situ debris compared with the current baseline tonalite granite. The general approach is depicted in Figure 1.2. A two-phase program was pursued for site debris sampling (Phase I) and site debris characterization testing (Phase II). Phase I consisted of determining the location of proposed basing areas, conducting a geologic (map) survey of the sites, obtaining samples of the geology, and included sample preparation for Phase II of the program. Within Phase II uniaxial compression tests were conducted on in-situ samples to obtain a ranking of the rock types which may correspond to their capacity for ballistic penetration. Ballistic penetration tests using titanium (6Al4V) targets were carried out with spheres made from both in-situ debris samples and tonalite granite.*

*A quartz, plagioclase and horneblende igneous rock.

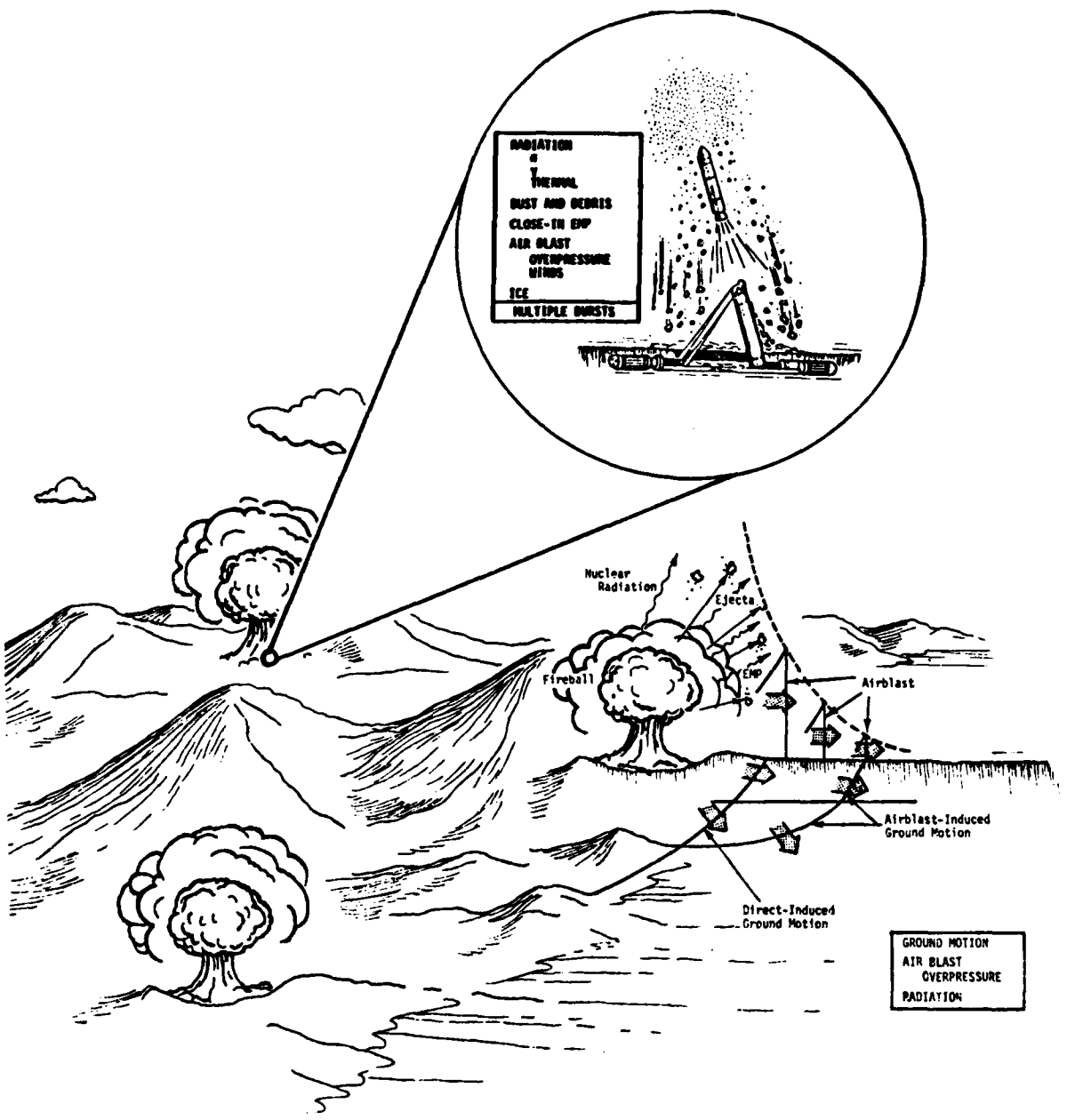

Figure 1.1. ICBM Launch and Ascent Environment.

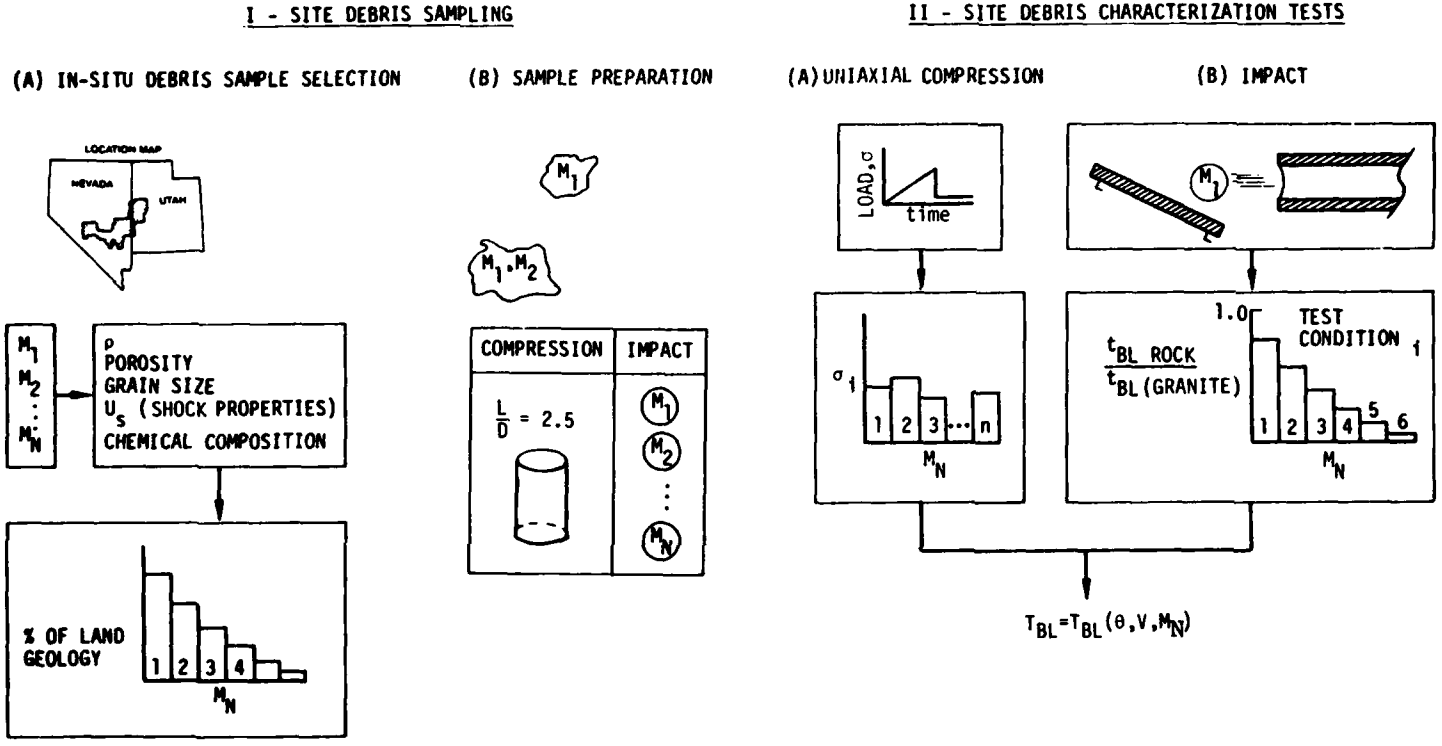

Figure 1.2. Site Debris Characterization Evaluation Overview.

The program provided a compilation of test data and rankings of the in-situ debris and granite spheres in terms of their relative penetration capability. The effort also documented in-situ particle size distributions for selected candidate basing sites. From the test results of the program and the literature, correlation of data bases for various projectiles (glass spheres, granite spheres, SAFR's*, and in-situ rock) was obtained. From this correlation and test results a test methodology for the characterization of shroud materials and shroud concepts is recommended.

*Standard Air Force Rock, cone/cylinder/cone geometry.

2.0 SUMMARY

The effort described in this report characterized and evaluated the in-situ lithology of several advanced missile Candidate Deployment Parcels (CDP)* located in Nevada. The objective of the program was to evaluate the use of in-situ materials for penetration testing and establish the difference in damage that would result using these materials versus the current baseline tonalite granite. To accomplish this, a test methodology was developed to rank in-situ debris materials against the baseline tonalite granite. This methodology included static and dynamic rock testing and ballistic impact tests on monolithic titanium.

The first task of the program consisted of a geological survey of candidate deployment parcels in order to determine the relative percentage of the geology represented by individual rock units which would contribute to the clasts and cobbles within the alluvium of each CDP valley. Results of the survey showed a predominance of siliceous tuff, rhyolite, and andesite rock masses in the geology. With the type and extent of geological units tentatively identified in the field, sampling of the regions was conducted for test specimens. In order to validate the field identification of various rock types we analyzed the test specimens in detail by using standard petrographic techniques.

An assessment of the ballistic penetration for the range of rock types found at Candidate Siting Region† (CSR) located in Nevada was made for a Ti6Aℓ4V target material in order to delineate the variation in the extent of the damage to the shroud during ascent. The introduction of in-situ rock types into the shroud evaluation procedure rather than a

*CDP - An area of 150 to 500 square nautical miles potentially suitable for MX siting.

†CSR - Potentially suitable area between 4000 and 6000 square nautical miles containing CDPs.

standard projectile material and shape will contribute to a more realistic specification of the cloud environment which may be encountered and provide an accurate definition of both thickness requirements and characteristics of the missile materials.

The capability to prepare spherical projectiles for all the site rock types was developed under this effort. This capability to manufacture spherical projectiles for the complete range of hardness represented by the in-situ rock types was previously unavailable. Techniques were developed to propel the spherical projectiles over the range of velocities anticipated to be encountered during the ascent phase. These techniques are also applicable to a wide variation in projectile geometry.

Ballistic impact tests using the various rock types were conducted at increasing impact angles at constant impact velocity until penetration (or tearing) of the titanium target occurred. A considerable spread of penetrability of the rock types was evident at the lower impact velocities (less than 1000 fps), while the penetration capability of many of the rock types converges at higher velocities (greater than >1000 fps). The penetrability of the baseline tonalite granite was found to be comparable to several of the in-situ rock types at the higher velocities. Volcanic tuff and scoria which represent rock units* that constitute from 40 to 90% of the geology at any one valley surveyed were found to be two to three times less penetrating than rock materials representative of other rock units identified in the survey.

Figure 2.1 gives a summation of the geological survey and of the ballistic impact response of the in-situ debris compared with tonalite granite. Figure 2.1a depicts the percentage of total geology of the CDP investigated represented by the individual rock units. Rock Unit I**

---

* Rock units - distinct rock masses with different characteristics (e.g., igneous, metamorphic, sedimentary).

** Refer to Table 3.4 for specific identification of rock units A through I.

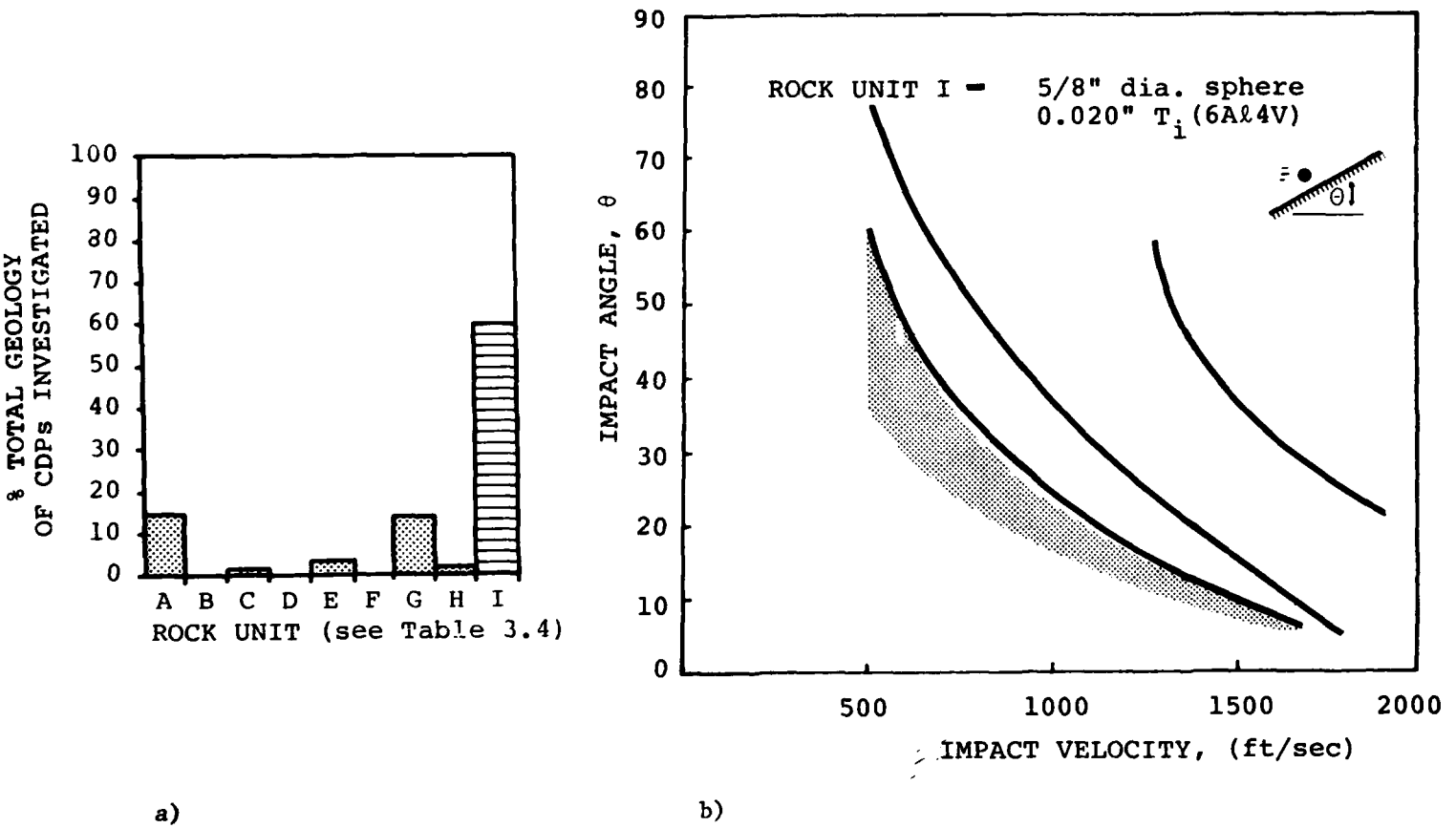

Figure 2.1. Summation of In-Situ Debris Characterization Program.

comprises greater than 60% of the total geology and represents anywhere from 40 to 90% of the geology in any one CDP. Figure 2.1b depicts the results of the ballistic impact tests. Impact angle versus impact velocity is plotted for different rock materials. The curves represent ballistic limits for three different rock materials from Rock Unit I. The shaded area represents the response of tonalite granite and of materials from rock units other than I.

When the program data was compared to previous literature data for thicker targets and applied to a representative shroud design (Kong, 1978), it was found that the volcanic tuff and scoria materials (Rock Unit I) would pose no single-pebble penetration threat. For the debris materials that had penetration responses comparable to tonalite granite, it was determined that a shroud thickness of at least 40 mils would be required to assure survival in the pebble environment.

Also, in-situ particle size distributions for selected candidate basing sites are tabulated and presented in Figure 3.5. This data summary indicates an in-situ particle size distribution several orders of magnitude finer than for a competent rock geology and at best an order of magnitude finer than for a previously considered site representative geology (Rosenblatt, 1979).

Due to the timing and scope of this program, the data presented in this report should not be considered totally representative of all the currently proposed candidate deployment parcels. CDPs are being considered for both Nevada and Utah and the area under consideration has more than doubled since the program inception.

3.0 SITE CHARACTERIZATION

Since the in-situ geological material at candidate siting regions (CSR) will influence the characteristics of airborne particles, characterization of the geological material at the CSRs is of prime consideration. In order to define the potential threat and guide materials test programs, it is necessary to describe the penetration potential of representative rock types and accurately define the distribution of each rock type at the CDPs. Procedures have been developed for classifying the geological material at the CDPs both with respect to areal extent and subsurface gradation distribution.

3.1 GEOLOGICAL SURVEY OF CANDIDATE MX SITING REGIONS

The locations of the proposed basing sites were identified and a geological survey* was made of candidate sites. This was accomplished through contacts with companies conducting siting investigations for the Government. Figure 3.1 shows the location of the CSRs evaluated under a geotechnical survey** recently conducted by Fugro National, Inc. (Fugro, 1979). The CSR of prime consideration is designated as F_1 on the figure and named the Great Basin CSR. Representative candidate deployment parcels are also shown in the Figure. For this effort the extent of the geological survey was confined to the valleys located between and including Ralston Valley and Dry Lake Valley. Figure 3.2 shows in more detail the valleys† surveyed and for which representative samples were obtained.

---

* Maps used to identify predominant rock units for which representative samples would be obtained.

** Table 3.1 defines several important terms relative to the geotechnical survey.

† Samples representative of Dry Lake Valley, White River Valley, Coal Valley, Garden Valley, Railroad Valley, Ralston Valley, and Big Smoky Valley were obtained for this evaluation.

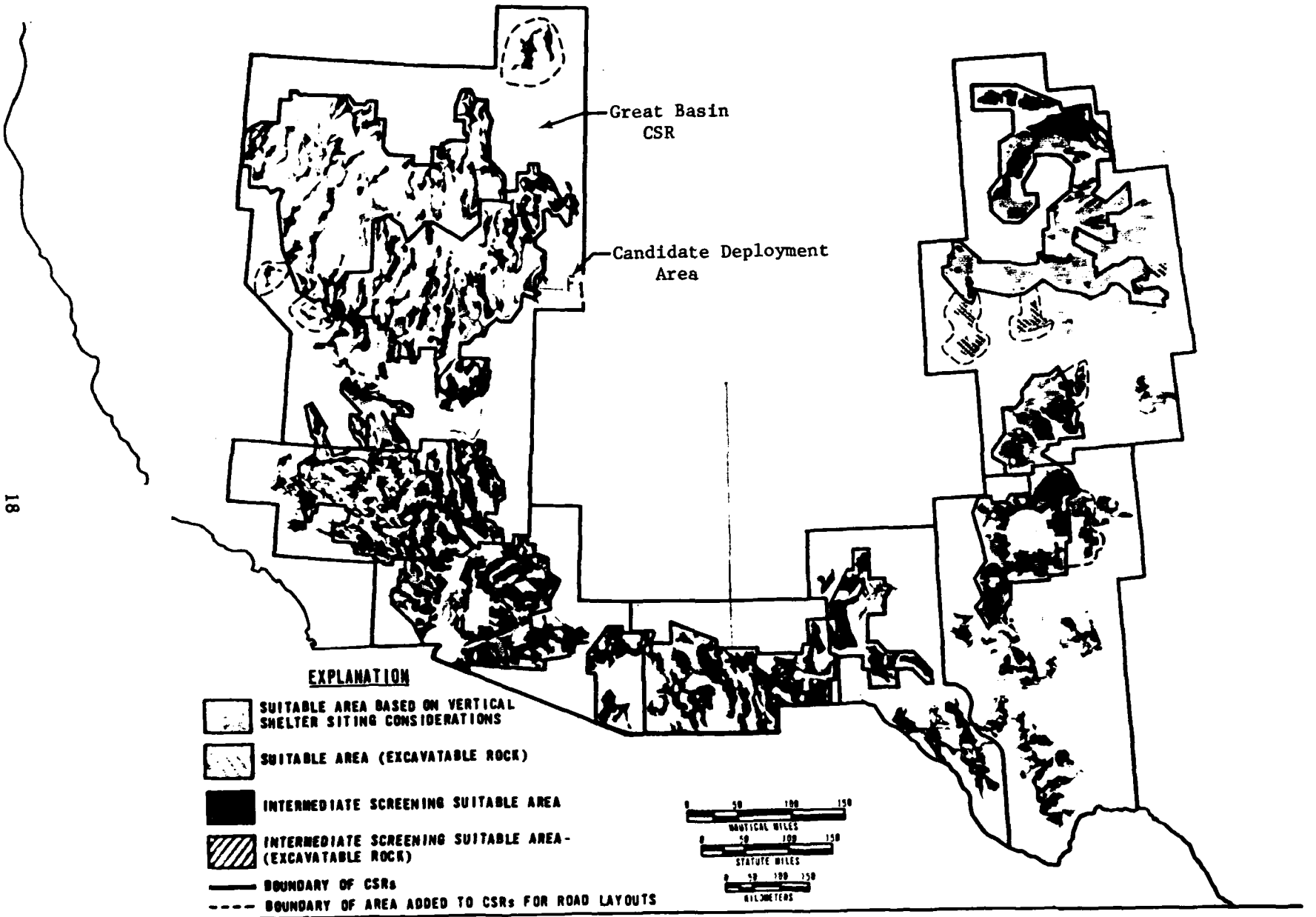

Figure 3.1. Designated Candidate Deployment Parcels (Fugro, 1979).

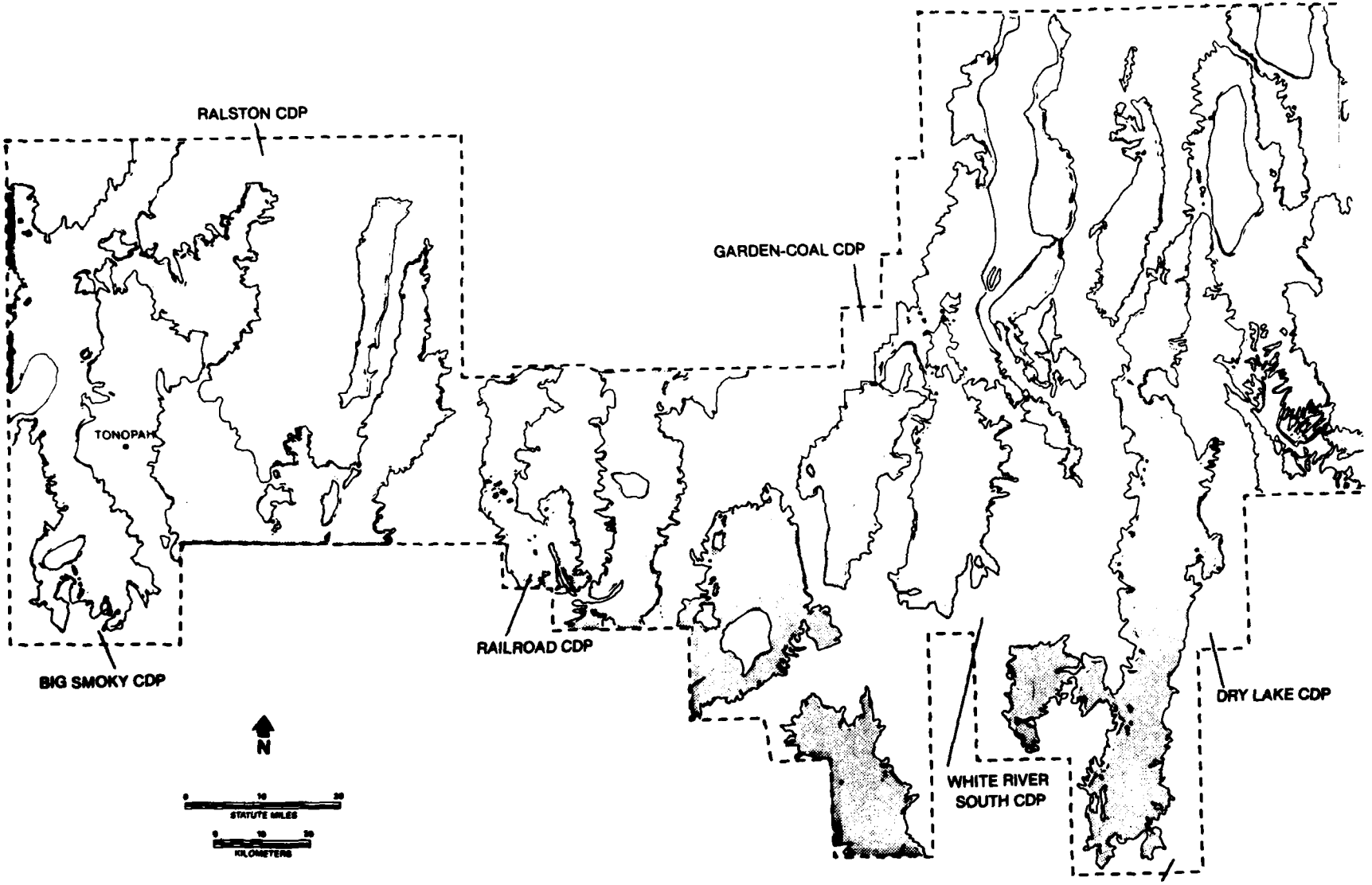

Figure 3.2. CDP's Surveyed (Designated as F_1 in Figure 3.1).

Table 3.1 . Glossary of Terms.

CANDIDATE - One of some group of regions, areas or sites being considered for MX deployment. Removal of candidate from a specifically named region, area or site term indicates selection by SAMSO/MNND.

CANDIDATE DEPLOYMENT AREA (CDA) - An area encompassing between 500 and 1000 square nautical miles of potentially suitable land with either naturally or artificially defined boundaries designated for convenience of study, discussion and data depiction. The candidate deployment area could be composed of two to four parcels and should have a specific plane name description.

CANDIDATE DEPLOYMENT PARCEL (CDP) - An area of 150 to 5000 square nautical miles potentially suitable for MX siting which, when aggregated with others, forms a Candidate Deployment Area. Each parcel should have a specific geographic description. (In the *Basin and Range Physiographic* province a parcel may correspond to a geographic valley and in Texas to some agri-economic unit.)

CANDIDATE DEPLOYMENT SITE (CDS) - A non-specific (i.e., not finally approved) site proposed for some element of the MX system within a chosen deployment area (i.e., trench or shelter site).

CANDIDATE SITING PROVINCE (CSP) - An area potentially suitable for deployment of the MX system generally encompassing more than 6,000 square nautical miles which, in a broad sense, is homogeneous with respect to most of the important characteristics governing siting of a total MX system.

CANDIDATE SITING REGION (CSR) - Potentially suitable area between 4000 and 6000 square nautical miles within one, or encompassing portions of more than one, candidate siting province which allows for full MX deployment.

All of the CDPs are valleys located between linearly extending mountains which are the source of the geologic material that fills the valleys. In order to determine the constituents of the alluvial fill, a survey was undertaken using available geological maps of the regions containing the CDPs. This survey concentrated on the mountains surrounding the valleys since they are the sources for the materials carried into the valleys.

In geological terms, bedrock is fragmented by the natural process of weathering over a long time period. This is true for all types of rocks that have exposed surfaces, but the resulting fragments (size and shape) are dependent on the rock type. Hard rock fragmentation is a very long process and the fragments tend to be large and very angular. Softer rocks tend to be weathered faster and are widely distributed (by water and wind). In order to minimize data scatter likely due to the fragmentation process and flaws introduced by weathering, virgin samples were obtained from outcroppings.

Additionally samples obtained directly from the valley floor could not be identified as to the rock unit source of the sample and it would be literally impossible to find samples of the specific rock units identified from the geological maps. Of primary importance in the sampling was to delineate the range of rock types that could comprise an explosion-induced debris cloud based on the major percentage of the geology. However the direct use of alluvium for further testing shroud vulnerability should not be ignored.

Figure 3.3 is a geologic map of the Dry Lake Valley, one of the CDPs from the large-scale map in Figure 3.2, which will be used to illustrate the procedure followed to establish the character of the geological material present at the sites considered to date. Table 3.2 is the legend for the geology shown in Figure 3.3 for the Dry Lake Valley. The geology is defined in terms of rock units.

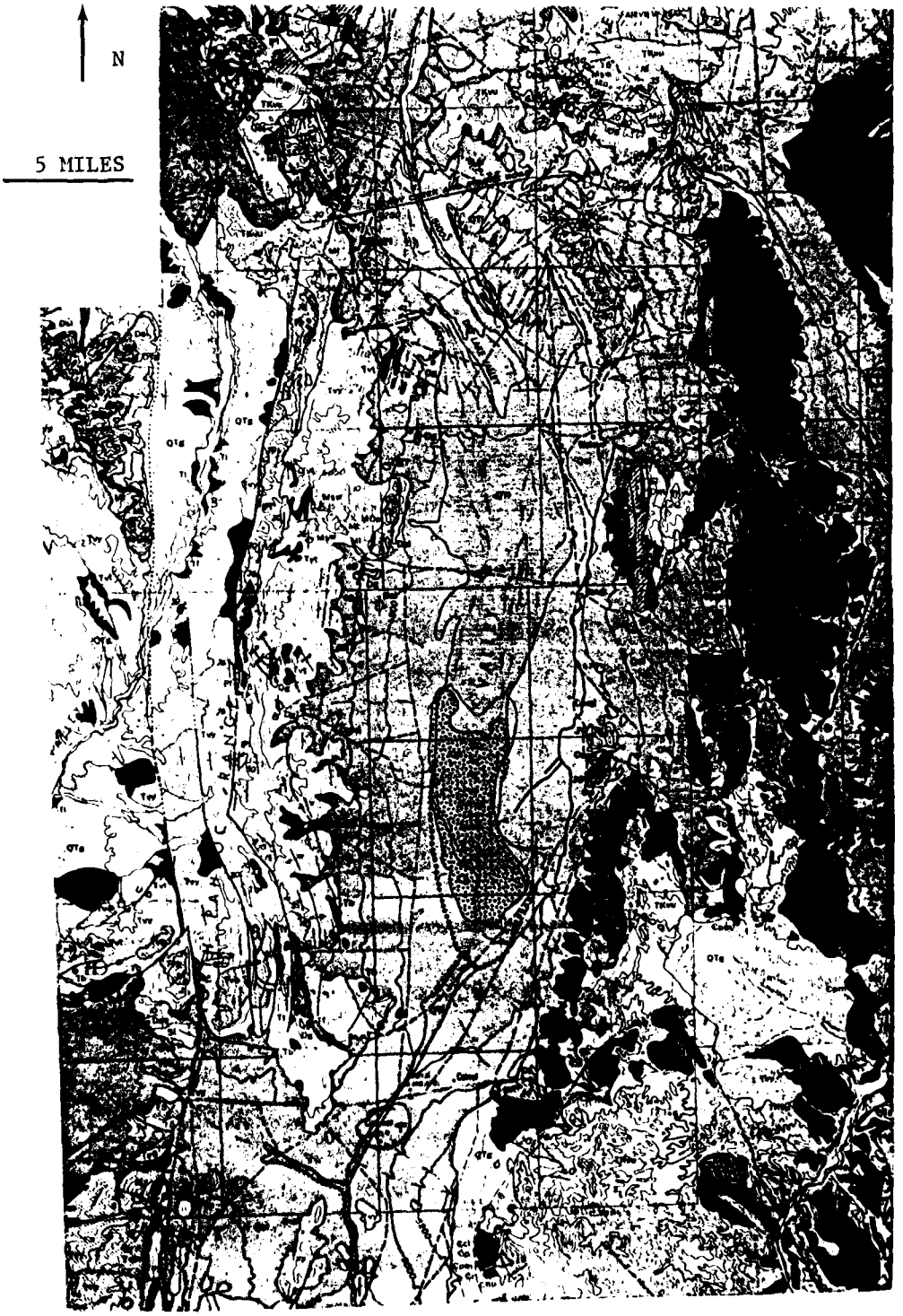

Figure 3.3. Geological Map of Dry Lake Valley, Nevada.

Table 3.2. Key to Figure 3.3.

LEGEND - DRY LAKE VALLEY - LINCOLN CITY, NEVADA

Q_p - recent playa deposits (unconsolidated)

Q_{tl} - intermediate lake beds (unconsolidated)

Q_{ol} - older alluvium (unconsolidated)

T_b - basalt (igneous) (unconsolidated)

T_{vy}, T_{va}, T_{vb}, T_{vd}, T_{vr}, T_{vt} - younger volcanic rock (igneous)

T^*_g, T_r, T^*_{gp}, T_{gd}, T^*_{qm}, T^*_d, T_{vn} - intrusive volcanic rock (igneous)

T_f - lucustrian (non-marine) limestone (sedimentary)

T_{kv} - older volcanic rocks (igneous)

T_{kvu} - volcanic rocks - undifferentiated (igneous)

O^*_e - pure quartzite (metamorphic)

NOTE: * indicates hard rock.

TERMINOLOGY

Playa - clay, silt, and salt remaining after evaporation of water in desert depressions.

Basalt - black to medium-grey aphantic rock (composed chiefly of tiny crystals). Most abundant lava.

Intrusive - masses of plutonic igneous formed by cooling of molten rock (magma) beneath the surface.

Quartzite - very hard, sugary-textured composed predominantly of interlocking quartz grains.

Rock units are distinct rock masses with different characteristics. They are typically classified as containing sedimentary, igneous or metamorphic rock. Sedimentary rock generally refers to the case where mechanical, chemical or organic sediments are transported, deposited, and either consolidated and/or cemented into a new rock type. Such deposits normally arise from wind, water, or glacial action. Igneous rock generally refers to rock formed by solidification of molten magma and may have been formed on or below the earth's surface. Metamorphic rock generally refers to rock formed by recrystallization of igneous or sedimentary rocks through the action of high pressure, heat, and hydrothermal alteration. Such general groupings, however, give little indication of the properties of the rock insofar as engineering applications are concerned (Hall, 1974).

A five mile wide border area consisting of the mountains surrounding the valley defined the basic land area used to obtain bounds on the percentage of the regional geology containing individual rock units. The total surface area contained in this border region (not including the valley area*) was surveyed to determine the relative percentage each rock unit represented in the total geology. Table 3.3 lists the areal percentage of the geology type as determined on this basis for Dry Lake Valley. Quartzite (Oe), which is probably the hardest material present, makes up less than one percent of the total area outlined by the five mile border. Based strictly upon the survey, the debris present in the Dry Lake Valley and within close proximity to the valley appears relatively innocuous compared with tonalite granite material. Thus it was necessary to obtain representative samples to test the in-situ ballistic response with that of tonalite granite. It must be remembered that this is an areal survey and does not account for the subsurface geology which would involve an expensive field survey.

The percentage geology containing each rock unit was determined in a similar manner for the seven valleys identified in Figure 3.2. The general rock units identified within close proximity of the seven valleys

*The valleys contain primarily alluvium for which the mountains are the source. Including the valley area would underestimate the relative percentages.

Table 3.3. Result of Areal Survey of Dry Lake Valley.

AREA OF DRY LAKE VALLEY 360 SQ. MI.

AREA OF 5 MI. BORDER AROUND VALLEY 1037 SQ. MI.

COMPOSITION OF VALLEY

Q_{tl}:	72 sq. mi.	(20%)
Q_{ol}:	288 sq. mi.	(80%)

COMPOSITION WITHIN 5 MI. BORDER OF VALLEY

Q_{ol}:	∿ 600 sq. mi.	(58%)
Q_{tl}:	∿ 77 sq. mi.	(7.5%)
T_{vy}:	∿ 105 sq. mi.	(10%)
T_{kvu}:	∿ 82 sq. mi.	(8%)
T_{vb}:	∿ 15 sq. mi.	(1.5%)
Q_{p}:	∿ 23 sq. mi.	(2%)
Q_{e}:	∿ 3 sq. mi.	(∿.3%)
Misc:	∿ 132 sq. mi.	(∿12.7%)
Total	1037 sq. mi.	(100%)

identified in Figure 3.2 are tabulated in Table 3.4. Nine distinct rock units were found. The primary rock types comprising each rock unit are also listed in Table 3.4. Rock units considered to contain the hardest of the rock materials found in the survey (e.g., quartzite and volcanic rocks) are denoted by an asterisk: rock units C, E, and G. Figure 3.4 is a graphical representation of the resulting estimates in terms of the rock units defined in Table 3.4.

It is important to note that the exact percentage of each rock type making up the individual rock units is not known and cannot be determined from the available geological maps. In order to obtain the more refined rock type distributions, an extensive and costly geological survey would be required. This would involve visiting all localities and doing large volume sampling. Such an evaluation would be a useful and informative undertaking once the exact basing sites have been identified, but it was beyond the scope of the current effort.

Based upon the survey of geological maps, it is apparent that in no one valley do rock units C, E, or G represent more than 30 to 40% of the geology. These rock units were determined to have the highest probability for containing a significant percentage of hard rocks. Rock unit I was the most widely distributed among the individual valleys as well as within the CDP as a group. It represents from 40 to 90% of the geology of the five valleys investigated. Rock unit A was the next most prevalent with the area of White River Valley consisting of almost 50% of this unit, but rock unit A represents only 0 to 15% of the geology of the other valleys.

With the relative percentages of each rock unit that constituted the geology of the mountains surrounding the valleys known, a field trip was organized to sample the rock units of interest for further characterization of the rock constituents and to provide specimens for mechanical property evaluations.

Table 3.4. Rock Units within CSR Sampled.

UNITS

A. UPPER PALEOZOIC SEDIMENTARY ROCKS
   - Conglomerates
   - Siltstone
   - Limestone
   - Shale
   - Sandstone

B. UPPER PALEOZOIC SILICEOUS & VOLCANIC ROCKS
   - Shale
   - Siltstone
   - Sandstone
   - Conglomerates
   - Mafic - nonquartzose volcanic

C. LOWER PALEOZOIC *
   - Siliceous and Volcanic Rocks
   - Chert
   - Shale
   - Siltstone
   - Sandstone
   - Quartzite
   - Limestone
   - Greenstone

D. MIDTERTIARY 16-17 x 10^6 YEARS OLD
   - Basalt
   - Andesite
   - Rhyolite
   - Siliceous Tuff

E. TERTIARY GRANITIC & DIORITIC ROCK *

F. MIDTERTIARY 6-7 x 10^6 YEARS OLD
   - Tuffaceous
   - Sedimentary

G. LOWER PALEOZOIC SEDIMENTARY ROCKS *
   - Limestone
   - Dolomite
   - Shale
   - Siltstone
   - Sandstone
   - Quartzite

H. RECENT VOLCANIC ROCKS 6 x 10^6 YEARS OLD
   - Mostly Basalt

I. LOWER TERTIARY VOLCANIC ROCK 17-43 x 10^6 YEARS OLD
   - Siliceous Tuff
   - Rhyolite
   - Andesite and Related Rocks

* Considered to contain mostly hard rocks.

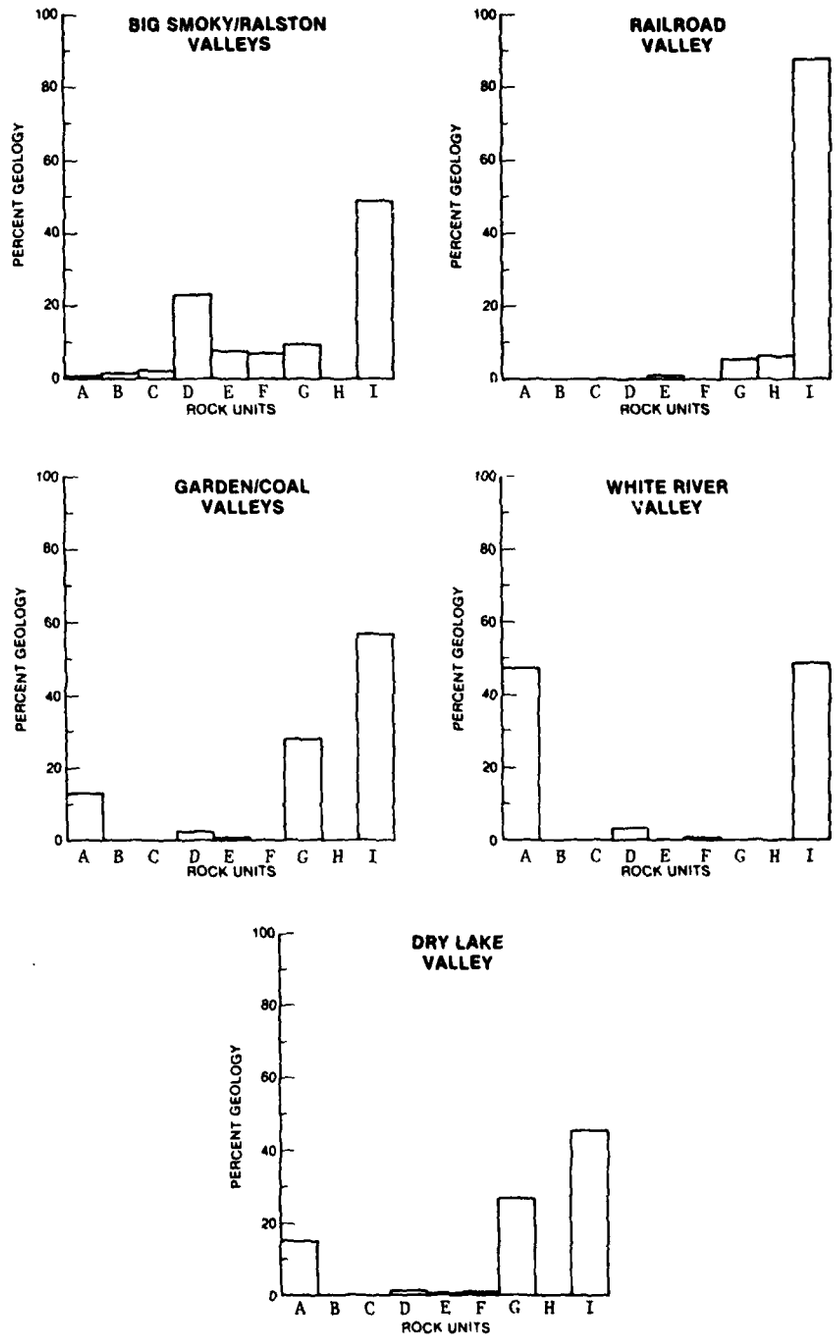

Figure 3.4. Percent Geology for Rock Units in CDPs Investigated.

As part of the geological survey of the CDPs, a compilation of particle size distribution (Fugro, 1979; and Ramanjaneya, 1979) was obtained from geotechnical work conducted under contract to the Air Force. This type of data provides input for the material/concept methodology discussed in Section 4.4. For particle impact testing of missile materials or concepts, it is required that representative particle sizes be used. For this reason and the fact that nuclear dust cloud models require representative particle size distribution, graphs similar to Figure 3.5 are important. Figure 3.5 plots particle size versus percent finer by weight and shows particle size distribution for an incohesive soil, an in-situ geology, advanced missile site representative geology, and a competent rock geology.

Included in particle size distribution data is data obtained from near surface (0 to 10 ft.) and from core samples (10 to 300 ft.). Although this data is highly pertinent to the description of the geology, it should be used with caution. To obtain the near surface data, the surface layers of cobbles and boulders are removed and then bulk samples are recovered for analyses. For the core samples, typically six inches diameter, subsurface geology can be mapped as shown in Figure 3.6. The problem with using core data is that if rocks are encountered with diameters larger than the core diameter, they cannot be recovered. Thus the exclusion of the larger particle (cobble) sizes systematically biases these data.

3.2 FIELD SURVEY AND SAMPLE ACQUISITION

After the rock units within the seven valleys were identified, sampling of several rock units within these valleys was accomplished. The rock samples collected during a single field trip are cataloged in Table 3.5. The list identifies the sample number, locality number, locality, rock type (initial identification), pertinent distribution or significance of the sample, measured bulk density, and rock unit represented.

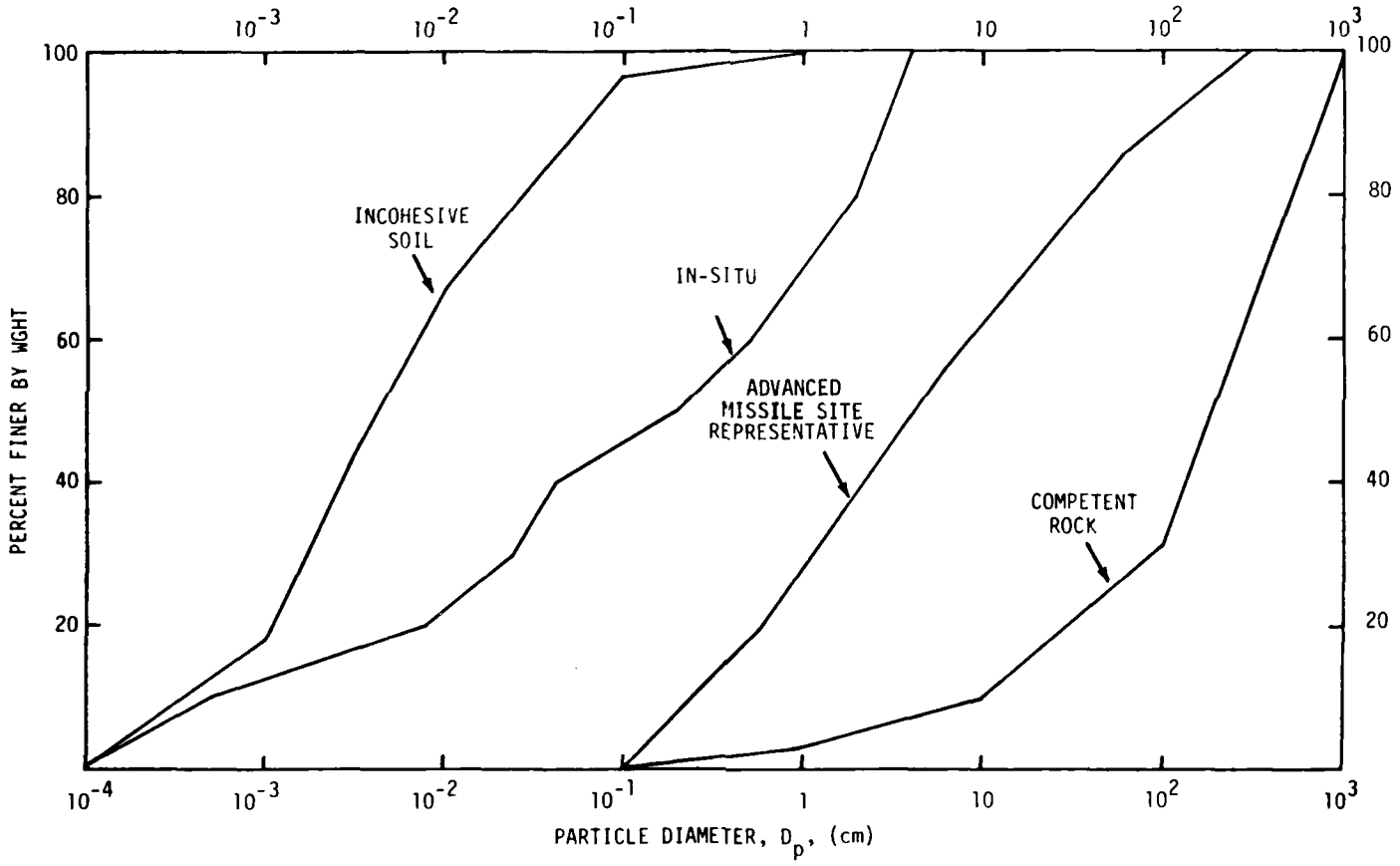

Figure 3.5. Particle Size Distribution for Several Geologies.

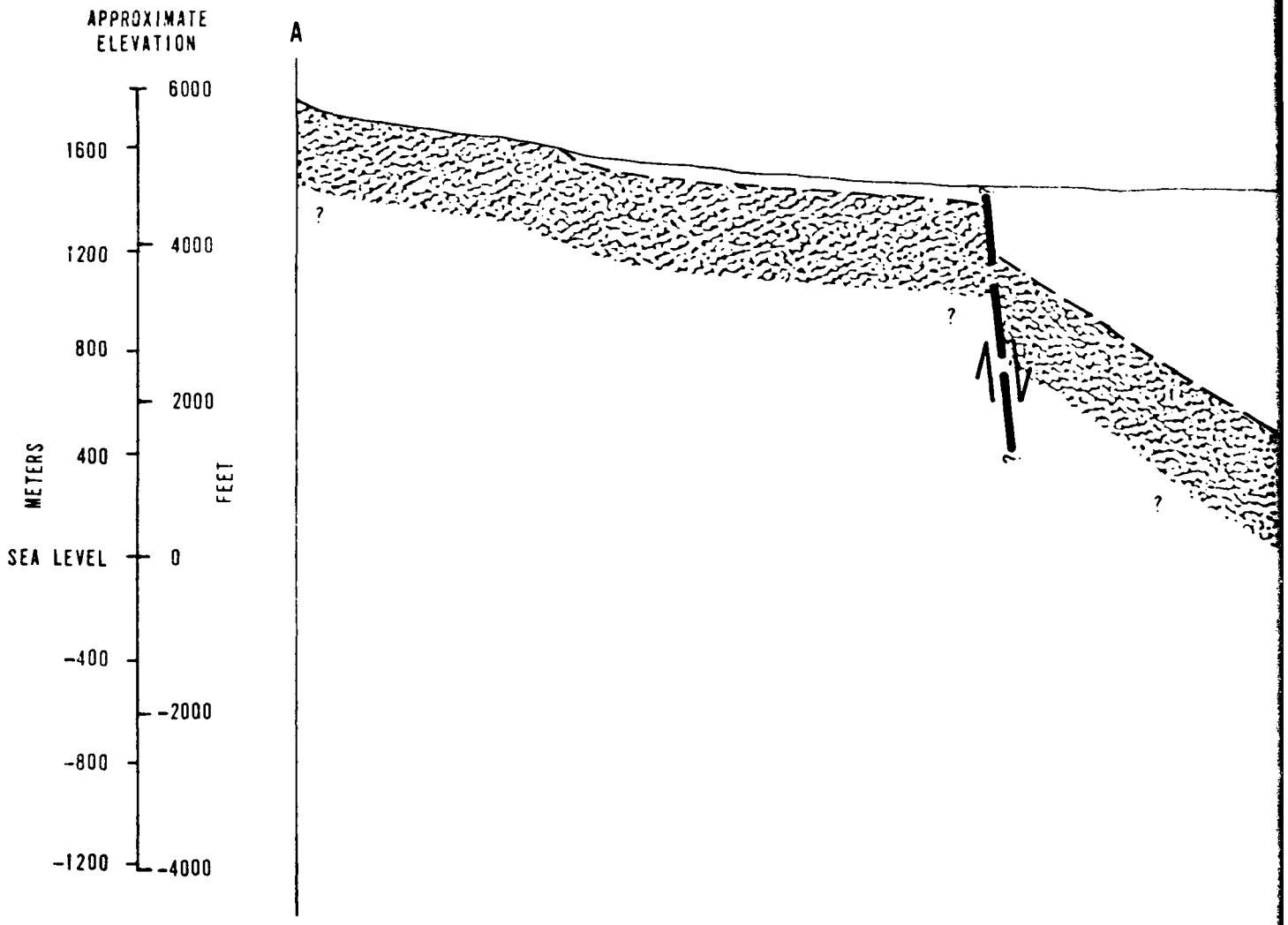

EXPLANATION

Playa (A4) and older lacustrine and or playa (A4o) deposits

Undifferentiated basin-fill deposits
Predominantly alluvial (A5) deposits, with fluvial (A1), stream terrace (A2s) and other non-rock deposits (Au)

Undifferentiated volcanic and sedimentary rock

NOTES: 1. T
the
data
high
2. F

BEND IN SECTION

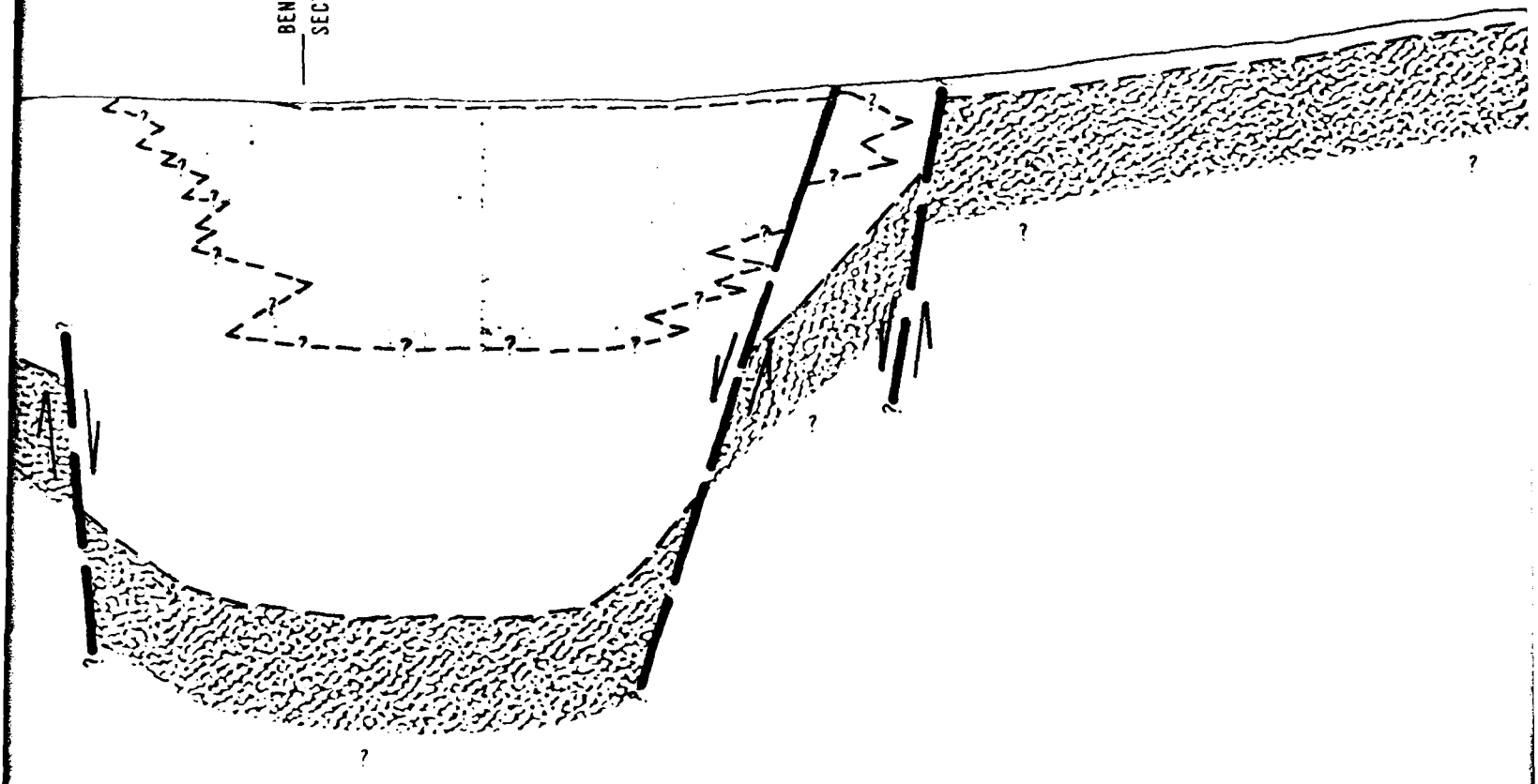

?— Approximate geologic contact queried where inferred

Fault, dashed where inferred from gravity interpretation

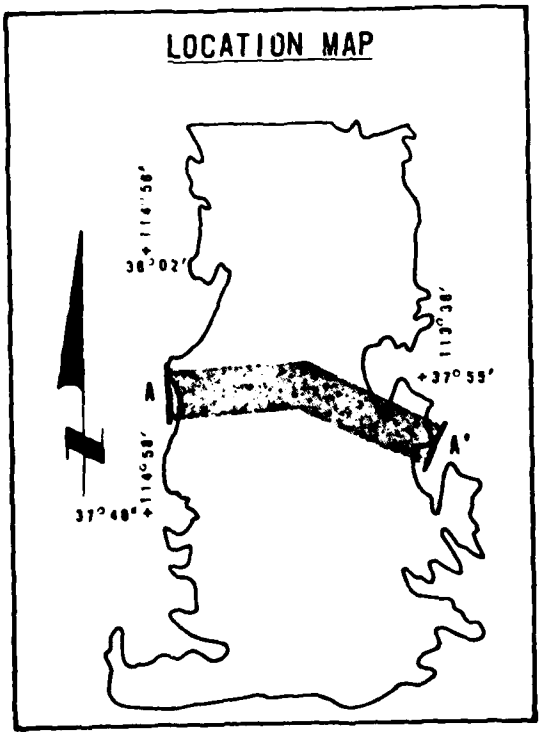

he cross section is generally representative of subsurface conditions within band shown on the location map. Due to the limited density of available and the sparseness of newly acquired data, the subsurface conditions are ly interpretive.

or a detailed description of geologic units see Table A-1

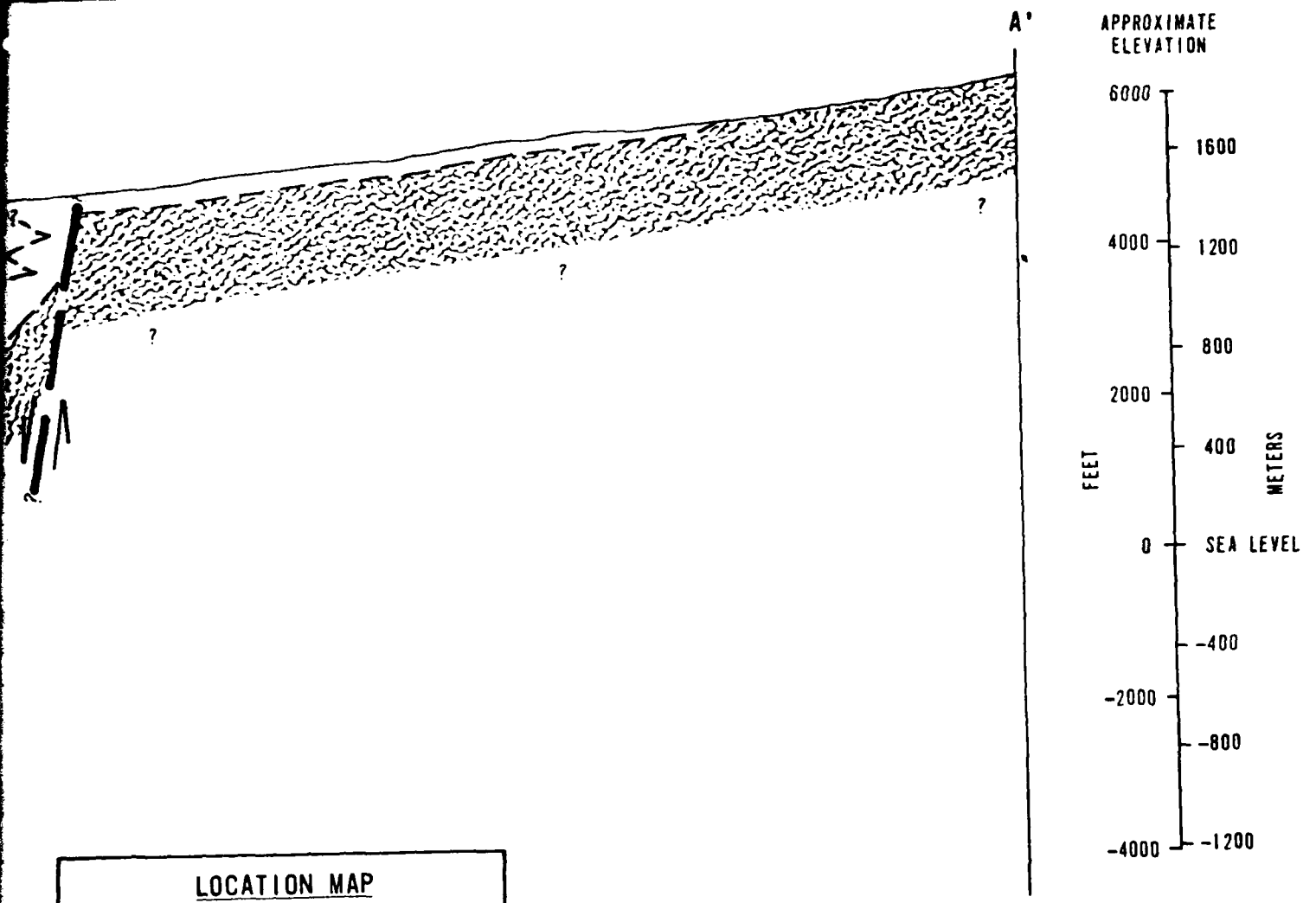

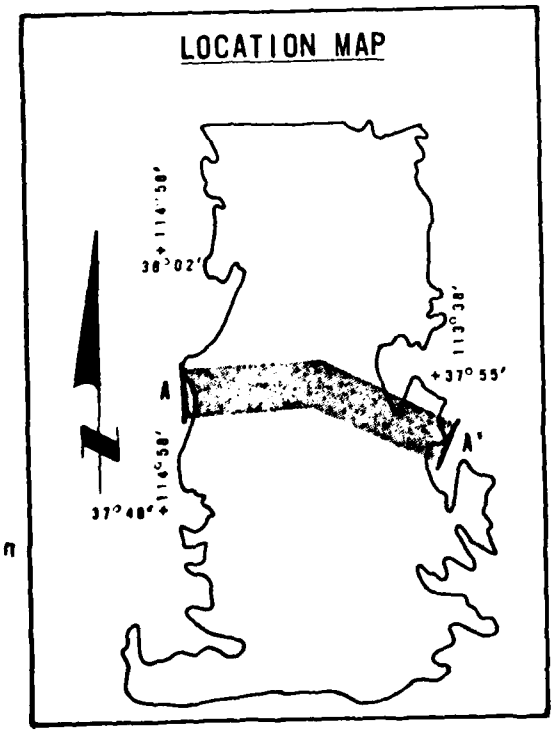

Horizontal Scale: 1"≈ 1 Mile (1.6 km)
Vertical Scale: 1"=2000' (610 m)
Vertical Exaggeration: 2.6X

HORIZONTAL SCALE

STATUTE MILES 0 1 2

KILOMETERS 0 1 2 3

Figure 3.6. Cross Section Geology (Fugro, 1979).

Table 3.5. Results of In-situ Sampling.

SAMPLE NUMBER	LOCALITY NUMBER	LOCALITY	ROCK TYPE	PERTINENT DISTRIBUTION OR SIGNIFICANCE	Measured Bulk Density gm/cm^3	Rock Unit*
1	1	12 km NE of Las Vegas along U.S. #15 (Clark County, 36°19'N, 114°57' W)	Upper Paleozoic Carbonate rock Well indurated, medium grey	N end of Dry Lake Valley, NE side of Garden Valley, NW side of White River Valley (inferred from geological mapping)	2.68	A
2	1				2.69	A
3	2	20 km N of Junction #15 and #93 along Rt. 93, N of Hidden Valley (Clark Co., 36°35'N, 114°56' W)	Upper Paleozoic carbonate rock Well indurated, medium grey	N end of Dry Lake Valley, NE side of Garden Valley; NW side of White River Valley (inferred from geological mapping)	2.68	A
3*						
4	3	1/2 km S of upper Pahranaga Lake along Hiway 93 (Lincoln Co., 37°17'N, 115°07'W)	Miocene or Pliocene quartz rhyolite (Large phenocryst quartz in glossary matrix)	NW side of Ralston Valley (inferred from geologic mapping)	2.24	D
5	4	4 km E of Hiway #93 and #93 intersection along Hiway #93 (Lincoln Co., 37°34'N, 115°12' W)	Mid tertiary coarsed-grained spheriodally weathered rhyiotitic ignimbrite	Western side of Dry Lake Valley	2.39	I
6	5	1.6 km W of Oak Spring Summit of U.S. 93 (Lincoln Co., 37°36'N, 114°42' W)	Undifferentiated acidic volcanic	Eastside of Dry Lake Valley	2.48	I
7	5'	1.4 km W of Oak Spring Summit, of U.S. 93 (Lincoln Co., 37°36'N, 114°14' W)	Same as Sample #6 except less hard (more typical)	Eastside of Dry Lake Valley	2.57	I
8	6	7.3 miles N of Hiway 93 on easternmost road (N-S) in Dry Lake Valley (Lincoln Co., 37°43'N, 114°44' W)	Highland Peak formation limestone	SW side of Dry Lake Valley	2.69	A
9	7	(Lincoln Co., 37°49'N, 114°42' W) westside of Dry Lake Valley	Eureka Quartzite	E side of Dry Lake Valley, S side of Railroad and Coal Valley. Probably hardest metasediment in these valleys	2.62	C,G
No sample	8	Hiway #93 W side of Dry Lake Valley (Lincoln Co., 37°37'N, 114°,56' W)	Similar to Sample #5	W side of Dry Lake Valley and S, SE and SW side of Coal Valley		
10	9	Hiway #93 W side of Dry Lake Valley (Lincoln Co., 37°37'N, 114°57' W)	Welded Tuff	W side of Dry Lake Valley and S, SE and SW side of Coal Valley	1.32	I
11	9	Hiway #93 W side of Dry Lake Valley (Lincoln Co., 37°37'N, 114°57' W)	Glassey Rhyolite	W side of Dry Lake Valley and S, SE and SW side of Coal Valley	1.85	I
12	10	(Northern Nye County, 38°03'N, 116°06' W) U.S. Rt. 25, 30 miles SE of Warm Springs, W side of Railroad Valley	Highly vesicular rhyolite	W and E sides of Railroad Valley; pieces of this rock cover portions of the valley floor, the finer size fractions of the soil have been blown away	1.74	I
13	11	U.S. Rt. 25, 25 miles SE of W side of Railroad Valley (N Nye Co., 38°09'N, 116°07' W)	Indurated basalt		2.35	H
14	12	U.S. Rt. 6, 26 km E of Tonopah on East slope of Ralston Valley (N Nye Co., 38°06'N; 116°57' W)	Dacite or Quartz rhyolite	NW side of Ralston Valley, N end Big Smokey Valley (sampling locality less certain)	2.43	I
15	13	15 km NNE Mud Lake (S Nye Co., 37°59'N; 117°09' W)	Quartz Lalite Flow	SE side of Ralston Valley (rock unit appears to be one of the hardest volcanic in Ralston Valley)	2.32	E
16	14	SE Big Smoky Valley, NW slope of "Lone Mountain" (Esmeralda Co., 38°04'N, 117°33' W)	Coarse granodiorite	Hardest rock in Big Smoky Valley. Associated with massive quartz veins and amphibolite dikes. Clasts of both dominate the valley fill in this area.	2.67	E

*See Figure 3.4.

In order to obtain realistic in-situ debris, once the percentage of geology represented by each rock unit was determined, representative rock samples were gathered from the rock units that cover the largest areas of the CDP. For example, rock unit I represented anywhere from 40 to 90% of the geology within the valleys considered; therefore, samples of siliceous tuff, rhyolite, and andesite rocks (samples #10, 11, 12 and 14 identified in Table 3.5) were obtained for additional characterization and mechanical testing. In rock units where a considerable amount of rock types was represented, only the rock units that were considered to contain hard rocks were sampled.

Figures 3.7 through 3.11 are photographs of the terrain within the valleys in the CSR. Figure 3.7a shows a panoramic view of Dry Lake Valley looking northeast. Vegetation is scarce with a predominant playa deposit occupying roughly sixteen square miles of the valley floor. Several river beds cut through the valley and provide natural exposures of the alluvium. These exposures indicate the character of the sedimentary layering of the alluvium (Figure 3.7b) and particle size distribution found in the valleys. Figure 3.7b shows the sedimentary layering at a creek bed in Dry Lake Valley. Figure 3.8 shows the same layering but to a depth of about ten feet*.

One of the valleys sampled, Railroad Valley, contained considerable indurated basalt. Figure 3.9a shows exposed basalt flows protruding from hills near the edge of the valley. The floor of this valley was covered with basalt and scoria as shown in Figure 3.9b. The basalt is represented by material #13 as listed in Table 3.5 and the scoria is material #12.

*In both figures a geological hammer (approximately 1 foot long) is shown to indicate size.

a) View of Dry Lake Valley Looking Northeast.

b) Example of sedimentary layering of the alluvium.

Figure 3.7. Dry Lake Valley, Nevada.

Figure 3.8 . Sedimentary Layering in Alluvium, Dry Lake Valley.

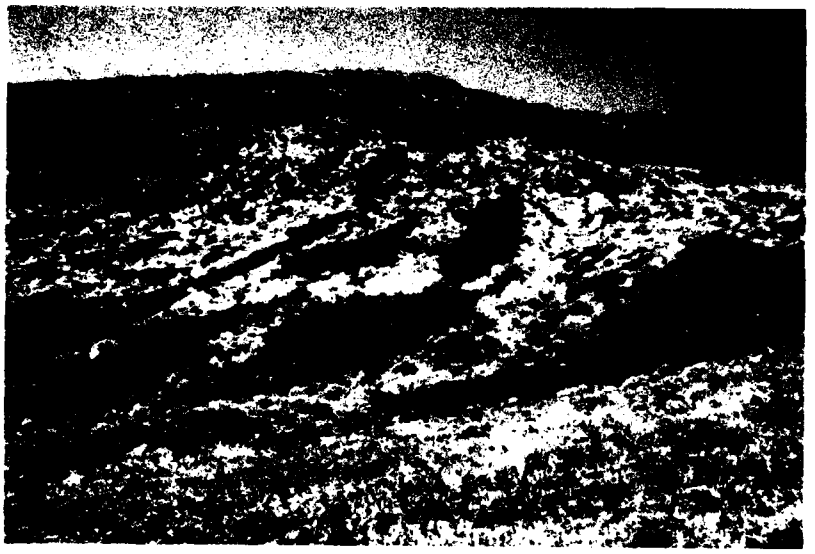

a) Indurated Basalt Flows.

b) Wind-stripped alluvium.

Figure 3.9. Railroad Valley, Nevada.

a) Granitic Rock Unit.

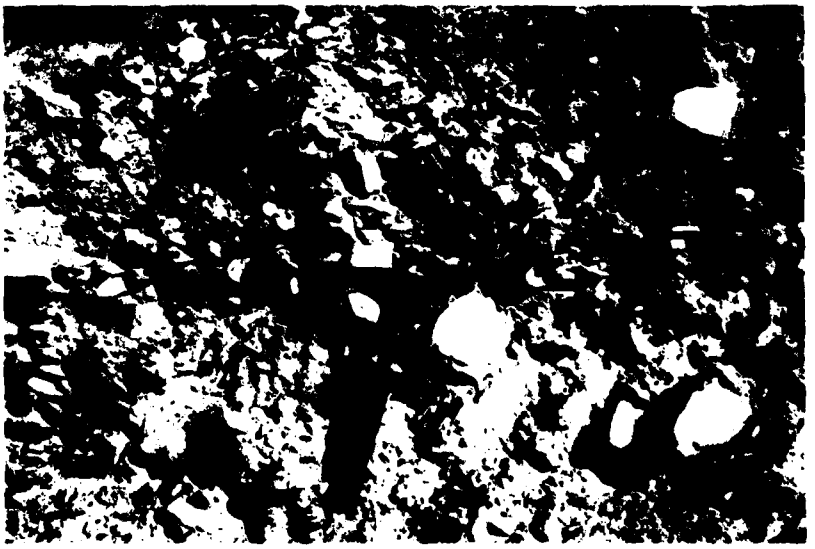

b) Crude cobble layering at base of Rock Unit.

Figure 3.10. Big Smoky Valley, Nevada.

Figure 3.11. Wind-stripped Alluvium Exposing Cobbles on Valley Floor, Big Smoky Valley.

The last valley visited, Big Smoky Valley, contained a large rock unit of granitic material (material #16 in Table 3.5) located near the southern edge of the valley. Figure 3.10a shows the rock unit as seen looking east across the valley. Near the base of the mountain there was considerable granite detritus present (Figure 3.10b) due to weathering. Figure 3.11 shows wind exposed cobbles on the valley floor that is also typical of the near surface geology for most of the valleys visited.

All samples acquired at the valleys were taken from fresh outcrop so that the specimens would be unweathered. Figure 3.12 shows examples of the typical sample sizes.

3.3 PETROGRAPHIC ANALYSIS

There are many factors associated with the formation of the major groups or rock types which influence their properties, including the following: mineral constituents, which in turn possess their own characteristic strength, hardness and durability; cementation, as it affects the bonding of the aggregate structure; texture, the term commonly used to describe the apparent grain size, for example, coarse or fine grain; fractures, joints, bedding planes, and weathering; chemical or physical weathering may serve to change the in-depth characteristics of the rock from a few inches to many feet. The sum total of events in the geologic history at a given site leads to a particular lithology. The lithology of a rock refers to its mineral composition, texture and fabric (the appearance or pattern produced by the shapes and arrangement of the crystal grains, including orientation features not evident from grain shape alone) (Hall, 1974).

In order to verify and further refine the field identification of the rocks collected in the field sampling, a petrographic analysis was undertaken. This analysis consists of grinding a thin slice of the rock material to a thickness approximately 0.001" thick and then examining the thin section with a petrographic microscope.

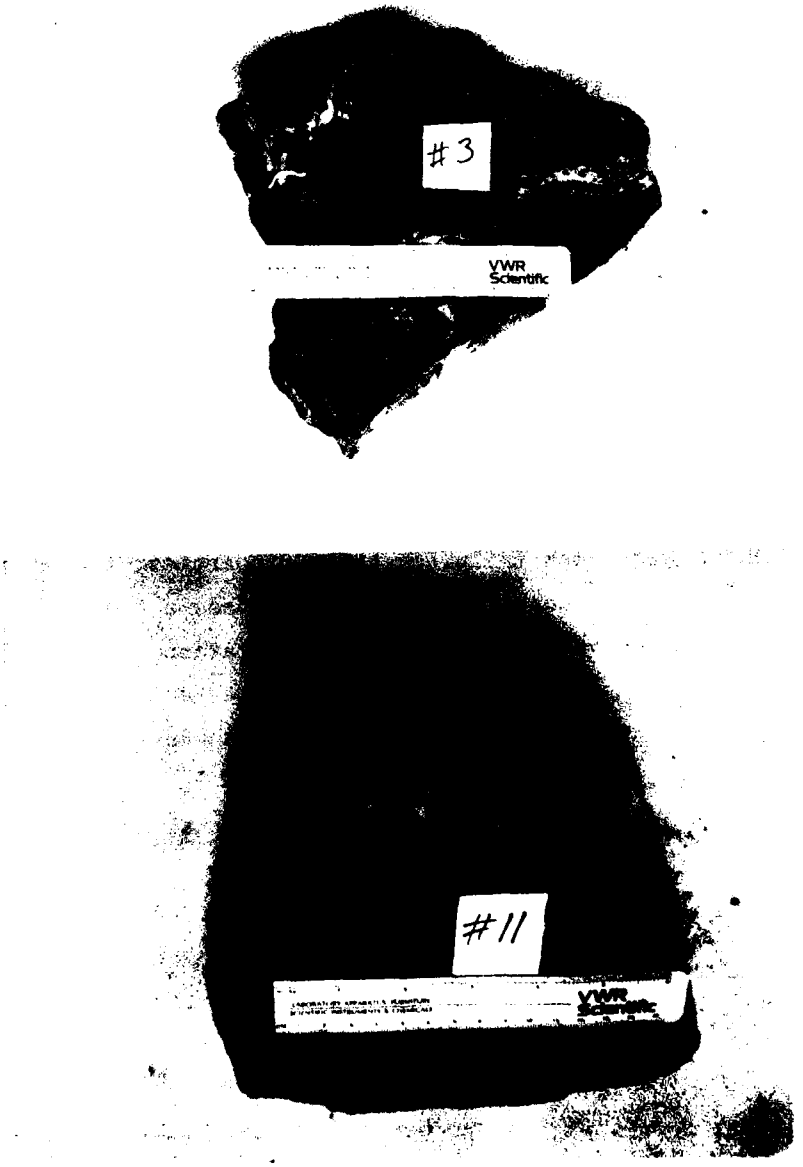

Figure 3.12. Examples of Rock Samples Obtained from Valleys.

Results of the analyses are given in Tables 3.6 and 3.7 with materials grouped into limestone, orthoquartzite, and volcanic classes. All the limestones are strongly cemented with calcite and have little or no porosity. The orthoquartzite is 100% quartz with zero porosity. In the volcanics, except for material #15, the higher the percentage of quartz and fledspar the stronger the material is expected to be. Material #15 is 80-85% microlite.*

Detailed analyses of all sixteen rock samples, including transmitted light micrographs, are provided in Appendix A.

*Lava has cooled slowly above ground resulting in the formation of very small crystals in the volcanic glass referred to as microlites.

Table 3.6. Thin Section Results for Limestones and Orthoquartzite.

	LIMESTONES
SAMPLE 1	Shell hash - ostracod shells dominant: 1.2 mm max., .6 mm average, porosity ∿1%. Other forms: foraminifera, fecal pellets (to .5 mm) sparry calcite grains (.5 mm average). Micrite (lime mud) fills in spaces between angular shell frags. 40% shell hash, 60% micrite.
SAMPLE 2	Micritized fossil forms in micrite mud. Observed: crinoid stem, echinoderm spine, foraminifera (10% of fossils), fecal pellets: 25-33% fossils, 70-80% micrite, 1-2% porosity. No strong bedding. Quartz grams being dissolved, replaced by calcite: extensive. Remnant grains now <0.5mm ∿1 mm calcite veins cut across slide - calcite filled. .1 - .3 mm average fossil size, angular fragments.
SAMPLE 3	Recrystallized limestone. Micritized pellets ∿50% .2-.4 mm = average micrite pellets. 5-10% = sparry calcite pellets, to 2 mm, .7 mm average. Relict quartz grains, all being dissolved replaced by calcite; .5 mm maximum size. Locally, micrite pellets recrystallizing to sparry calcite. All pellets sub-round to round.
SAMPLE 8	Micrite limestone. 95-98% lime mud. 2-5% quartz crystals, "resorbed" by calcite. Quartz grains now <.05 mm. Fractures in slide (.1-.5 mm) filled with sparry calcite. Indistinct banding, sub-parallel but highly distorted. No porosity.
	ORTHOQUARTZITE - METAMORPHOSED
SAMPLE 9	Metamorphic rock - 100% quartz. No porosity. Well-sorted grain size .15-.4 mm, .25 mm average. Numerous triple-point grain contacts. All quartz grains overgrown. No apparent bedding planes.

Table 3.7. Thin Section Results for the Volcanics.

SAMPLE NO.		% GLASS	% QUARTZ + FELDSPAR	% MAFICS	% PORE SPACE
RHYOLITES (EXTRUSIVE IGNEOUS)	4	70-75	20-25	Hematite present	5
	5	40-50	40-50	5-10	1-3
	6	40-50	50-60	5-7	-
	7	60-70	30-40	3-5	-
	10	90-95	5-10	(present)	1-3
	11	90-95	5-10	trace	1-5(?)
	12	30-40	20-30	1-2	40-50
	13	plagioclase	60-70	20-30 calcite	7-10
	14	60-70	30-40	1-2	-
	15	80-85 (Microlites)	10-20	2-3	1-2(?)
	16	Granodiorite	See Table A.16.		

% - Percent by volume.
(?) - Possible increased porosity due to chemical reaction during polishing process.

4.0 PENETRABILITY OF IN-SITU ROCK TYPES

In a hostile environment a missile payload shroud may encounter essentially two type of particle effects. The first is large pebble penetration and the second small particle erosion. Since the mass lofted and particle size distribution in the cloud does have temporal and altitude restrictions, the two effects can be evaluated separately. Large pebble penetration can be a problem during the initial phases of launch and small particle erosion effects may be more relevant at later stages of ascent. Large pebble penetration is the primary consideration in this report. However, site lithology is important to both effects since the constituents of the environment are determined by the in-situ geology.

This section discusses the site debris characterization phase of the program as illustrated in Figure 1.2. Specimen preparation and both uniaxial compression and ballistic impact testing of in-situ samples will be described. The uniaxial compression test is a relatively inexpensive test for screening and for ranking the various types of in-situ debris material in terms of average peak load to failure. A comparison of the results with ballistic impact response ranking is used to develop a material screening methodology as described in Section 4.4. The ballistic impact tests are used to compare the relative penetration capability of the in-situ debris, resulting in a comparison between sites and rock materials, to determine whether tonalite granite provides a conservative or nonconservative baseline projectile material for shroud material/concept testing. From these results a methodology is recommended for evaluation of shroud materials/concepts.

4.1 RELATED BALLISTIC IMPACT DATA

Hastings, et al. (1977), provide a compilation of impact pebble data covering various types of projectile and target materials. Data taken from this report shows an interesting effect of projectile type on ballistic limit.

Figure 4.1a and b are plots of impact angle versus impact velocity for several rock types. In both figures the rock materials are tonalite granite, Indiana limestone*, and an unspecified sandstone all in SAFR geometry. The test specimens were all titanium (6Aℓ-4V) 0.063" thick. Figure 4.1a is data for 0.625" diameter projectiles and Figure 4.1b is data for 1.0" diameter projectiles. In all cases the mass of the projectiles were essentially equivalent for the same diameter, except the 1.0" diameter granite SAFR's were approximately 10% heavier than either the limestone or sandstone SAFR's.

The lines drawn through the data are visual fits to the data indicating the approximate threshold conditions for penetration at the test conditions. For test conditions above the line penetration is expected for that particular rock type. Thus, the rock type considered most detrimental would be the lowest on the graphs. Figure 4.1a indicates that the granite is about 25% worse in terms of the ballistic response of the specimen than either the limestone or sandstone. Interestingly the limestone and sandstone response is apparently equivalent, but grain size and other physical properties for these particular projectiles are not available and could influence the response of the materials. Figure 4.1b is a plot of the 1.0" diameter data. Data at an impact velocity of 4000 feet per second is limited and thus the upper curves are extrapolated to the higher impact velocity test conditions. As opposed to the data in Figure 4.1a, the sandstone response is worse than the limestone response. In any event the ballistic response using granite is more than twice as severe as the ballistic response using limestone and sandstone, thus a definite particle type effect is noted.

Earlier tests using a SAFR projectile shape were conducted to investigage particle type effects but did not address any shape effects. This geometry was selected because spherical geological shapes could not be easily manufactured. The cone/cylinder/cone geometry made it possible

*Indiana limestone typically has the same density as tonalite granite but is more porous. It is not at all similar to limestone found at the CSR.

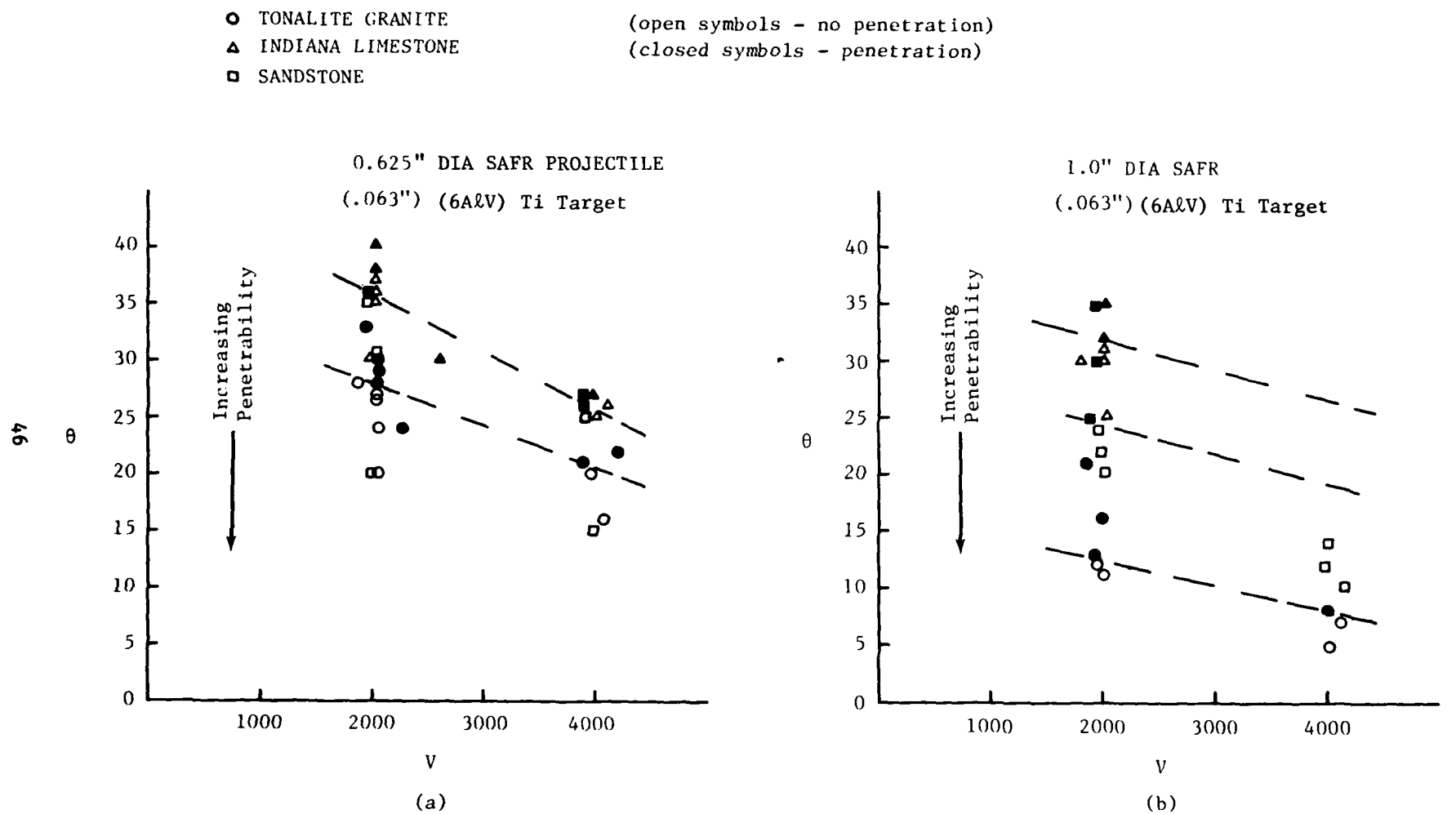

Figure 4.1. SAFR Particle Type Effect Data.

to obtain a nearly spherical geometry (volume essentially equivalent to a sphere of the same diameter) which could be launched successfully. Comparing data for the two geometries indicates a definite shape effect on penetrability. Figure 4.2 shows a plot of impact angle versus impact velocity of projectiles from three different materials and for spherical and SAFR shapes. The curves are reproductions of data fits for the ballistic limit of a titanium .063" thick target using .625" projectiles (Kong, 1978 and Hastings, 1977). The lower the curve in Figure 4.2, the more penetrating the projectiles for the particular impact conditions. For the SAFR geometry, the tonalite granite is more penetrating than either the sandstone or the Indiana limestone (a porous rock similar to sandstone). A definite increase in penetrability with velocity is noted for the spherical geometry compared with the SAFR data

Thus, it seems apparent that the shape of the projectiles may have a significant effect on their penetrability: in particular the harder materials. Since the harder rock masses will produce highly angulated pieces upon fragmentation (either as a result of weathering and/or nuclear explosion), the orientation of the sharp edges relative to the surface of the shroud will influence the degree of interaction with the impacted surface. Since the data shown in Figure 4.2 indicates a definite decrease in penetrability for nonspherical projectiles, this shape effect may significantly reduce the penetration threat from a cloud of highly angulated particulates.

Even though the data does indicate a particle shape effect, the spherical geometry was used for this effort since the primary objective was to evaluate particle type effects and most of the recent data base is for spherical tonalite granite projectiles. Also, the spherical geometry will minimize data scatter due to shape effects.

Due to the large amount of rock types and limited amount of testing available, a specific approach to material ranking and screening tests was employed as follows:

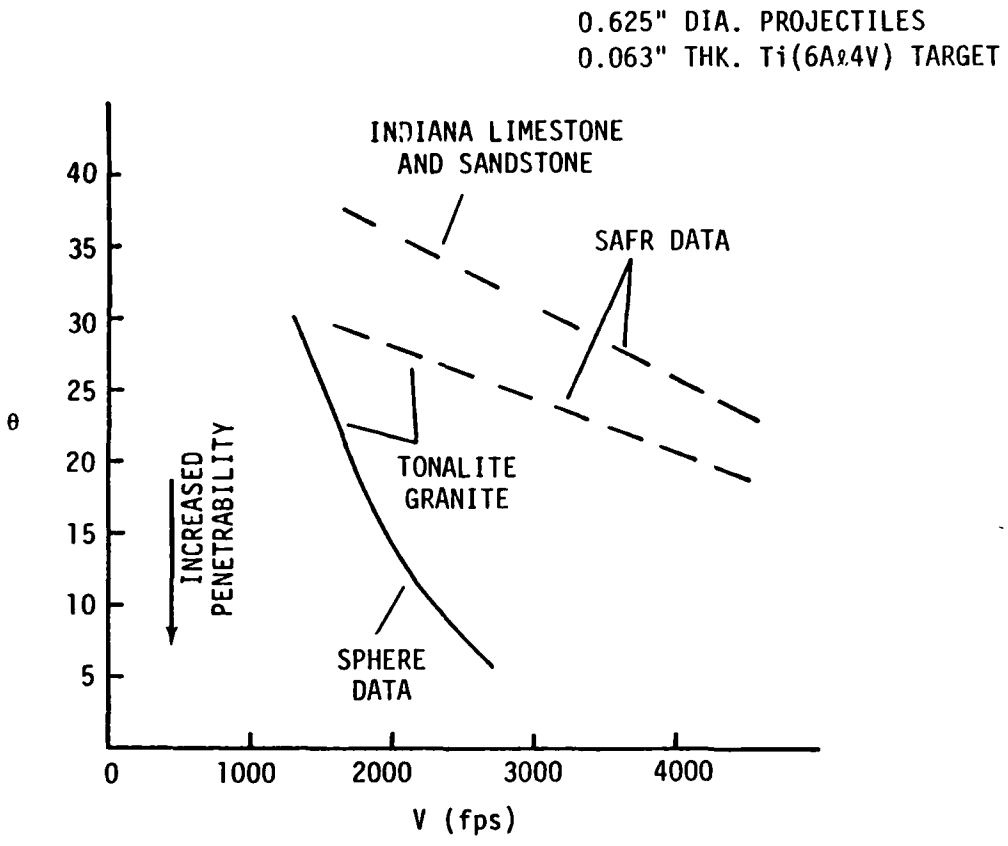

Figure 4.2. Effect of Particle Type and Shape on Penetrability.

1. Conduct uniaxial compression tests on in-situ debris samples and obtain a ranking of relative hardness. In this manner, rock types with similar compressive strengths and densities can be screened and grouped for ballistic testing.

2. Spherical projectiles are made from representative materials of each group and then ranked in terms of their ballistic response. Ballistic response is determined as a function of impact velocity and angle of impact for various types of rock materials to obtain curves similar to Figure 4.1.

This approach resulted in ballistic penetration curves of impact angle versus impact velocity which are compared with previous data. These curves represent the approximate ballistic limit with penetration occurring for conditions above the curve and no penetration below the curve.

4.2 TESTING PROCEDURES

With the test logic delineated, test specimens were manufactured for both the uniaxial compression test series and the ballistic impact test series. Each of these series of tests required unique specimen geometries as discussed in the following sections along with facility description and test techniques.

4.2.1 Specimen Preparation

As discussed by Vutukuri (1974), most mechanical property test specimens have a cylindrical geometry. Depending on the type of test, the length-to-diameter ratio of the cylinders should be between 0.2 and 3.0. However, the ratio is commonly fixed for each type of test.

For the uniaxial compression tests cylinders with a L/D = 2.5 were made by using a core drill. The ends of the cores were cut flat and parallel using a disc saw and then polished to minimize friction and to eliminate stress concentrations. All the samples from each rock type were cored in the same direction to attempt to minimize material anisotropy.

It was the purpose of these tests to establish a ranking relative to tonalite granite and not to determine a compressive strength value for the rock specimens. In order to determine a compressive strength value, large numbers of tests per rock material would be necessary along with an evaluation of anisotropic effects. For this effort three test points per material were obtained.

To obtain baseline material for the tests, tonalite granite cores were obtained from Cedar City, Utah, from which specimens were made. Soda lime glass cylinders (L/D = 2.5) were obtained commercially for comparison with the rock materials.

Dry bulk density measurements were made after the cylindrical specimens were machined. Figure 4.3 shows a plot of bulk density versus material in decreasing density. It was expected that a comparable ranking would be obtained from the uniaxial compression test series to be discussed in Section 4.2.2.

Material ranking by bulk density, as seen in Figure 4.3, was not definitive except for materials #10, #11, and #12. This type of ranking was used strictly for guidance during the uniaxial compression tests.

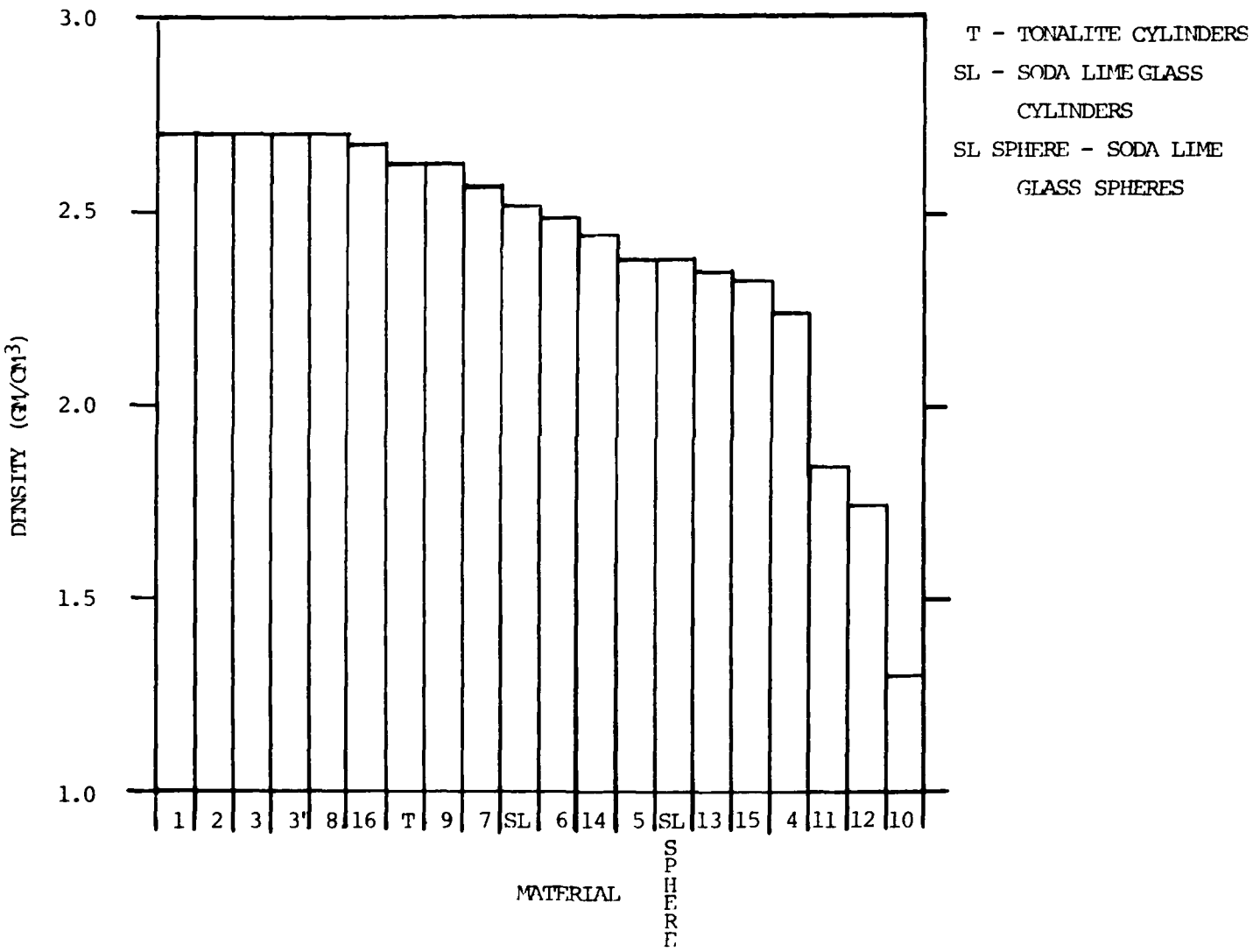

Figure 4.3. Bulk Density Ranking of In-Situ Samples.

The ballistic test series consists of testing titanium (6Aℓ4V) targets for ballistic limit response using 0.625" diameter spheres made from eight of the rock materials. The eight materials, for a wide range of hardness, were chosen based upon results from the uniaxial compression tests.

All of the spherical ballistic test specimens were manufactured by ETI in a two-step grinding process. The first step was a rough machining into a quasi-spherical shape and then a fine grinding in a sphere-making machine. The resulting spheres are 0.615" $\pm$ 0.010" in diameter.

4.2.2 Dynamic Compression Tests

The degree of damage (penetration) sustained by a missile during the initial ascent portion of the flight will depend upon a number of parameters. One such parameter will probably be the compressive strengths of the dust and debris (i.e., rocks). The magnitude of the stress generated by the rock impacts is dependent on the equation of state and Hugoniot of the target and rock materials. However, the degree of penetration is dependent on both the compressive strength of the rocks and the material response to absorbed energy which is manifested as material damage.

Dynamic* compression is a test technique used to rank in-situ materials in terms of their average peak load to failure and is a screening technique to minimize the number of ballistic impact tests required. The objective was to compare the material ranking from this test series with the relative ballistic penetrability for use in developing a test methodology.

When a cylindrical specimen is loaded in axial compression in a testing machine, the compressive strength is given by the relation

$$\sigma_p = \frac{F}{A} \tag{4.1}$$

*Dynamic refers to loading rates of 48 in/second as compared to static of 0.008 in/second.

where σ_p = compressive strength of the material

F = applied force at failure

A = initial cross-sectional area normal to the direction of the force.

Of importance to the determination of σ_p are material properties (e.g., mineralogy, grain size, and porosity), friction between platens and end surfaces, specimen geometry (shape, height to diameter ratio L/D, size), rate of loading, and environment (moisture content, temperature, etc.).

Vutukuri (1974) made the following conclusions concerning compressive strength testing:

a) Cylindrical specimens with a L/D ratio of 2.5 - 3.0 should be used.

b) Specimen ends should be flat and parallel with ends polished to minimize frictional effects.

c) Steel platens of the same diameter as the specimens should be used.

d) Specimens should be tested in an environment comparable to in-situ conditions.

e) Rate of loading will have a variable effect on the compressive strength of rocks.

Following the procedures outlined above, test specimens with L/D = 2.5 were tested using a drop tower to achieve loading rates approximately 48 in/sec (static loading rates are typically 0.008 in/sec). The test fixture employed is illustrated in Figure 4.4. The striker (tup) attached to the falling weight is strain gaged and calibrated to measure the compressive loading of the specimen. The instrumented tup is interfaced to an ETI Model 300 data automated acquisition and analysis system. The basic components of this system consist of a velocity measuring/triggering unit, microprocessor unit, a printer/plotter unit, and a floppy disk drive unit. A schematic of the system is shown in the block diagram in Figure 4.5.

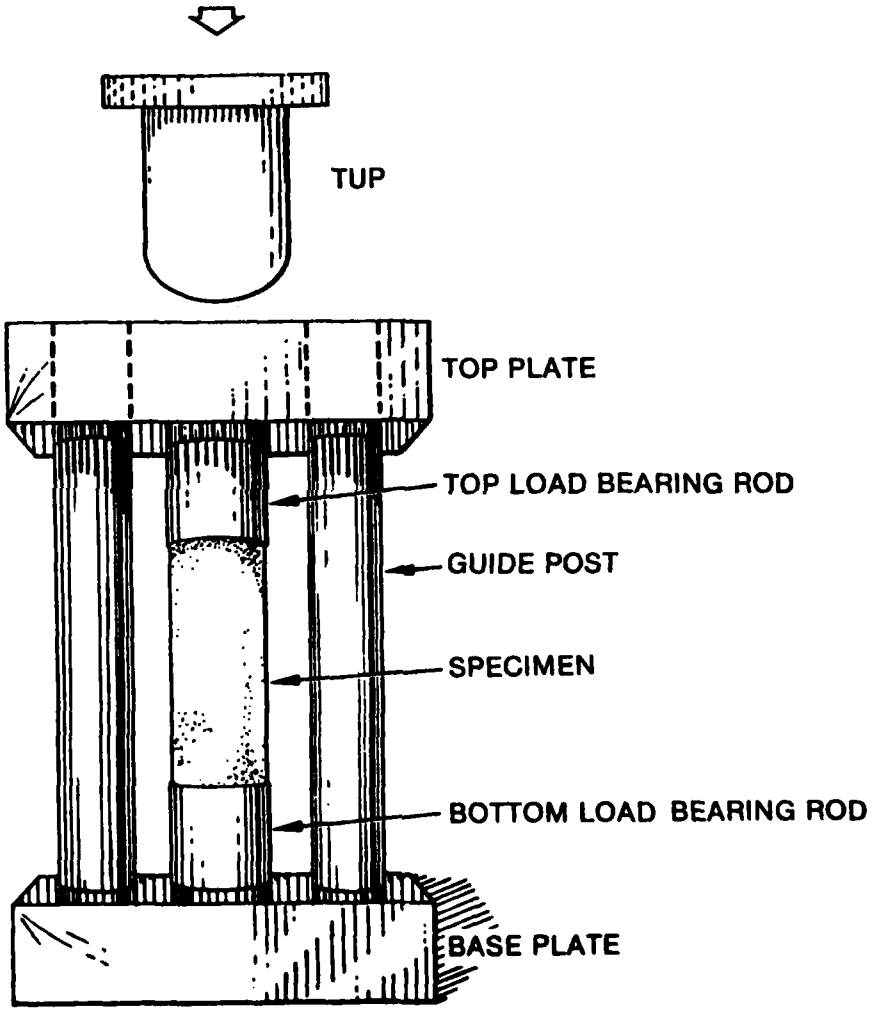

Figure 4.4. Dynamic Compression Test Fixture.

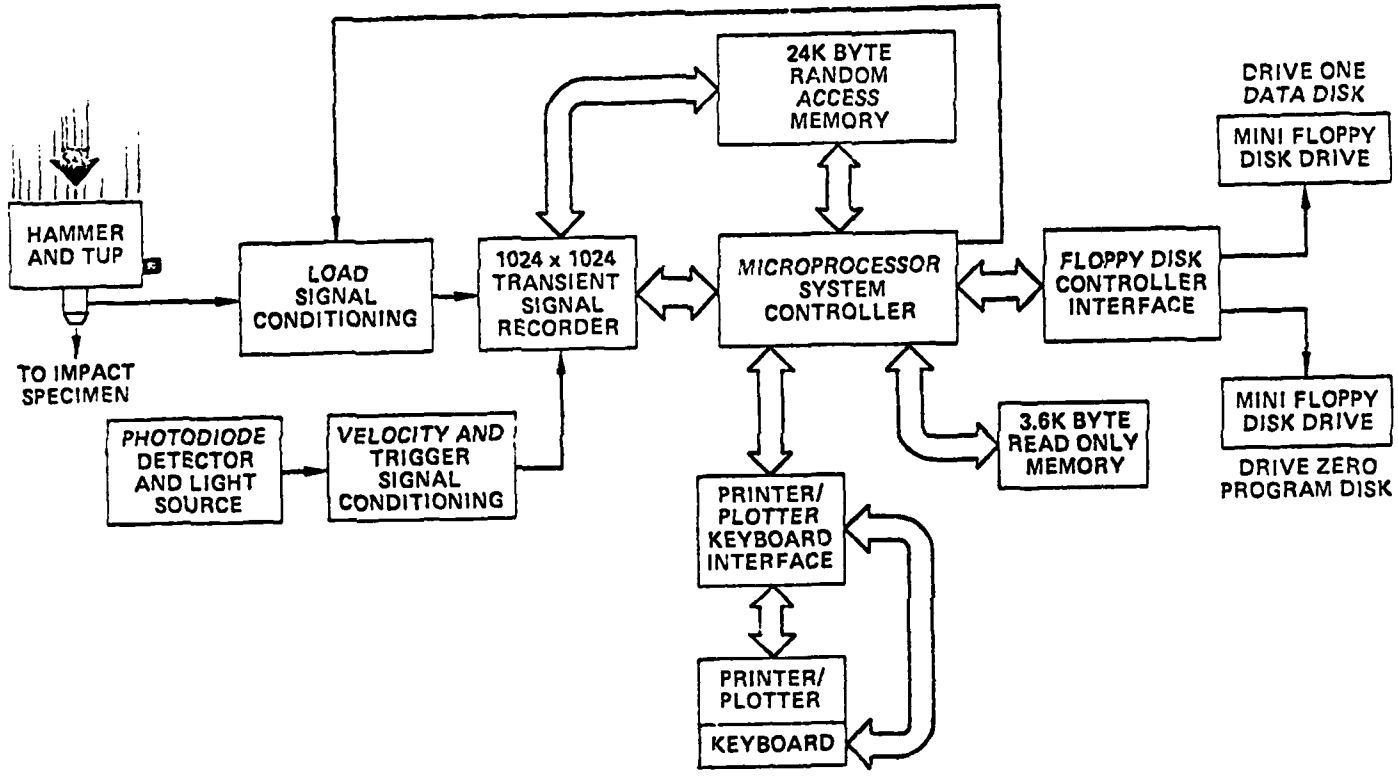

Figure 4.5. Block Diagram for Automated Instrumented Impact System.

The velocity/trigger unit measures initial impact velocity for use in computer analyses of the instrumented tup signal. It also supplies the trigger for the data acquisition system. The microprocessor unit consists of the computer hardware and software as well as a transient signal recorder. Utilization of the microprocessor assures the data capture and analysis is performed using consistent procedures and permits the use of in-depth data analysis on a routine basis. The printer/plotter unit permits operator communication with the equipment and provides automatic printing of test data and plotting of the computer analyzed curves on a graph. Figure 4.6 shows a representative load-energy trace for an instrumented impact test on material #9 (pure quartzite). The upper curve is load versus deflection and the lower curve is energy versus deflection. The energy curve is just the integral of the area under the load curve.

Dynamic compression tests were conducted on all sixteen in-situ materials plus baseline tonalite granite and soda lime glass cylinders with a maximum of three data points per material. A Model 8100 Drop Tower was used with a crosshead weight of 490 lbs. for the first six tests and 1000 lbs. for the remaining tests. The initial tests resulted in noisy traces due to inertial effects associated with specimen loading. To get a load trace that would minimize these effects, the drop height was reduced from 6 to 3 inches and crosshead weight increased from 490 to 1000 lbs. Tape was used on the test fixture to damp out extraneous noise to the strain gages in the tup. These test parameters were used for the remaining tests. The two test parameters described above did not appear to influence the peak load measured, only the trace noise.

The results of the dynamic compressive strength tests on the various types of rock are summarized in Table 4.1. In addition to average maximum load (P_{max}), the table also includes the energy corresponding to the total energy (E_T) to failure for each specimen. Although the initiation energy has arbitrarily been defined as the energy required to reach maximum load,

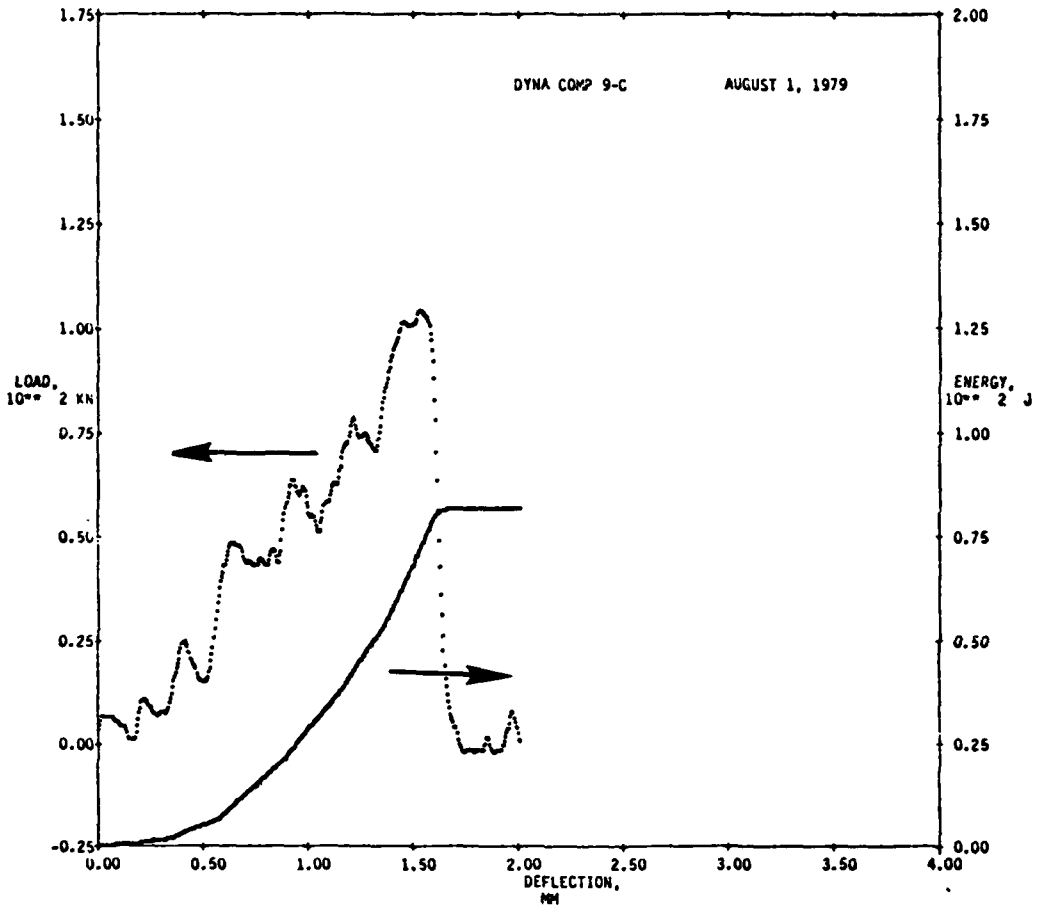

TEST	TEMP C	IMPACT VELOCITY M/S	ENERGY J	TIME,10** 0 MSEC INIA	TOTAL	LOAD,10**-1KN MAX	ENERGY,10** 0 J INIA	PROP	TOTAL
9-C	23.0	1.23	342.5	1.31	1.73	1044	72.1	10.0	82.2

Figure 4.6. Representative Load-Energy Trace.

Table 4.1. Summary of Dynamic Compression Test Results of In-situ Samples.

MATERIAL NUMBER	$\bar{P}_{MAX}$ (KN)	$\bar{E}_T$ (J)
1	152	116
2	163	129
3	133	99
3'	73	50
4	59	37
5	49	29
6	50	24
7	60	44
8	89	65
9	110	84
10	7	4
11	51	34
12	26	10
13	62	44
14	53	27
15	88	66
16	76	64
Soda Lime	205	190
Tonalite	67	43

the extent of microcracking prior to maximum load was not investigated. However, in all the tests, catastrophic failure was found to initiate at the maximum load.

Material ranking in terms of decreasing density, decreasing average peak load and decreasing average peak energy are summarized in Table 4.2. A plot of average peak load with decreasing density is given in Figure 4.7 to compare with Figure 4.3. Figure 4.7 indicates a trend of decreasing load with decreasing density for all materials except the soda lime glass, and materials #9 and #15. Replotting the results of the figure gives a slightly different material ranking with average peak load (Figure 4.8). As discussed in Section 4.1, materials #2, 8, 9, 13, and 16 were originally considered to be strong materials as is indicated by these tests. Materials #8, 9, 10, 11, 12 and 13 were considered to be the most predominant ($\sim$90% geology) in the valleys sampled. As can clearly be seen from Figure 4.8, the materials identified above represent a good cross section of relative hardness and density. Thus these eight materials were manufactured into spheres for ballistic testing and penetrability ranking.

Also shown in Figure 4.8 is the scatter band for the three tests conducted on each sample (except materials #3 and #3')*. After each test, sample pieces were recovered and examined. The lowest data points for a given material correspond to those specimens which fractured into the fewest pieces (i.e., they had the largest fragments). This fracture behavior probably resulted from the formation of a few large cracks in the material and propagating along planes of weakness, such as joints.

The highest load and energy absorbing specimens fractured into many small pieces as a result of the formation of a large number of small, individual cracks.

*Due to limited material, only two tests were conducted on these materials.

Table 4.2. Ranking of Materials by Average Peak Load, Average Peak Energy and Bulk Density.

)ECREASING LOAD	DECREASING ENERGY	DECREASING DENSITY
Soda Lime	Soda Lime	1
2	2	2
1	1	3
3	3	3'
9	9	8
8	15	16
15	8	Tonalite
16	16	9
3'	3'	7
Tonalite	13	Soda Lime
13	7	6
7	Tonalite	14
4	4	5
14	11	13
11	5	15
6	14	4
5	6	11
12	12	12
10	10	10

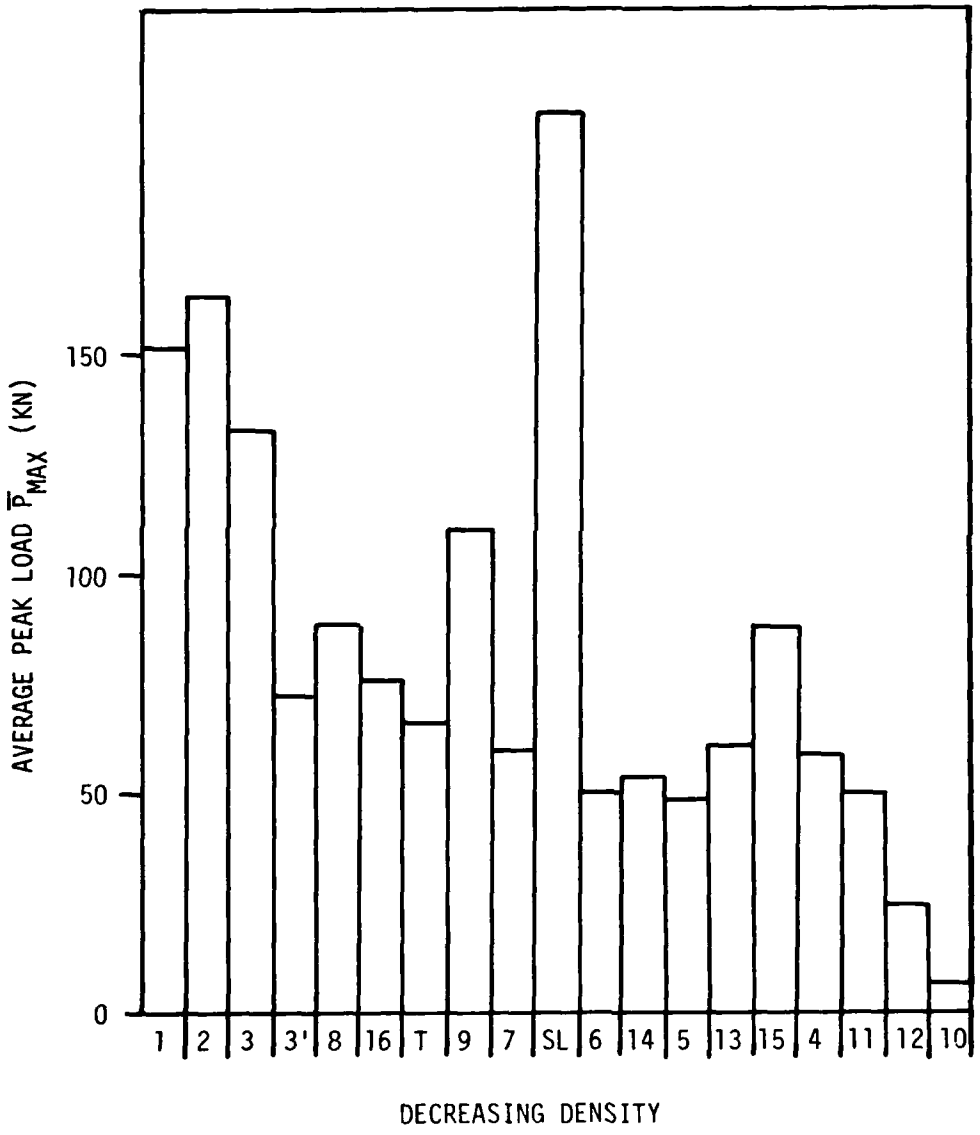

Figure 4.7. Comparison of Average Peak Load with Ranking of Materials by Density.

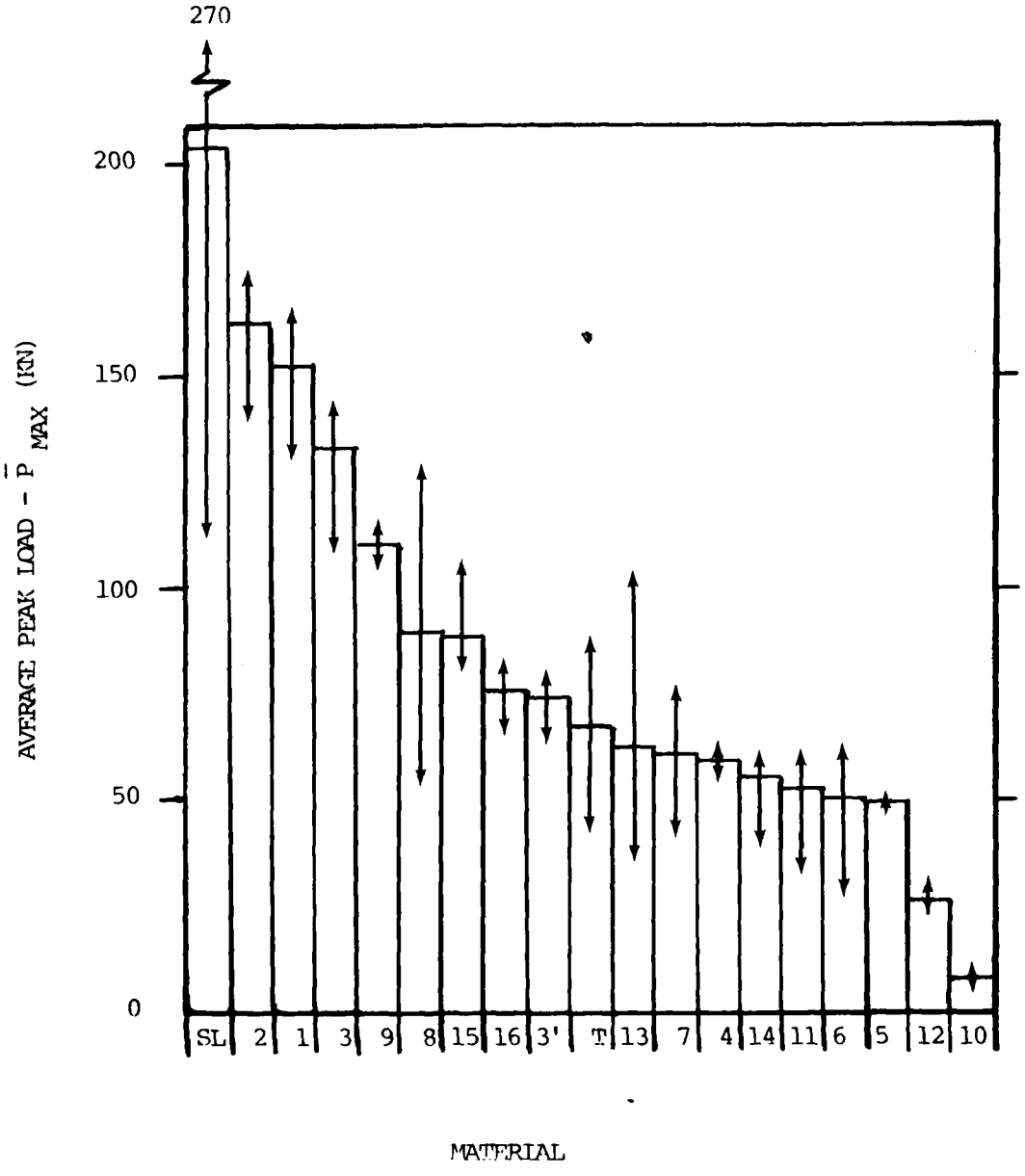

Figure 4.8. Material Ranking by Average Peak Load.

The petrographic analysis in Section 3.3 resulted in grouping the materials as limestones, orthoquartzites, or volcanics. Comparing the petrographic analysis results with Figure 4.8, one quickly sees that the limestones and orthoquartzites are the harder materials and the volcanics the weaker. All the limestones are cemented with calcites, have small grain size, and have little or no porosity. The orthoquartzite is 100% quartz, small grains with zero porosity. In the volcanics, the higher the percentage of quartz and feldspar the higher ranking achieved in Figure 4.8. On the other hand, the higher the percentage of volcanic glass the weaker the material. The only exception is material #15 which contains 80 to 85% microlite glass which is different from volcanic glass because during the much slower cooling process a very fine crystal structure is formed.

Thin section analysis substantiated the dynamic compression ranking and indicated that the strongly cemented, nonporous limestones can sustain the higher load before fracturing. Vutukuri (1974) found that mineralogy, grain size, and porosity are the intrinsic properties controlling rock strength. The compressive strength of rocks is found to decrease as the binding material varied from quartz to calcite to ferrous minerals with the weakest being clay-like binding materials. The strength of rocks increases with decreasing grain size and with decreasing porosity.

The ability of a rock material to sustain high loads prior to failure accounts for the small pieces recovered after testing. Vutukuri (1974) observed three modes of failure in materials tested.

1) The first consists of a general crumbling by development of multiple cracks parallel to the direction of applied force at mid-height of the specimen near the surface and its extension to the ends and into the center of the specimen. This results upon failure in conical end segments and long slivers of rock around the periphery.

2) The second type of failure occurs with development of one or more major cracks (called slabbing or vertical splintering) parallel to the direction of the applied force resulting in a series of columns.

3) The third type of failure is the shearing of the test specimen along a single oblique plane.

All three modes or combination thereof were observed as a result of the dynamic compression test series. The mode of failure appears to be a function of material type and/or material flaws. The higher ranked materials (soda lime glass, #1, 2, 3, and 9) literally exploded into small pieces after failure. Interestingly, material #9 had closed cracks running the length of the cylindrical specimens, yet they did not fail by shear along these flaws. All these materials, except the soda lime glass, had minimal data scatter in the test results. It is not clear why the apparently homogeneous soda lime glass cylinders had considerable data scatter.

Material #8, a limestone, had fractures filled with sparry calcite (see Figure A.8) that extended throughout the cylinders. Recovered specimens indicated that failure was not along these fractures.

Material #8 through #5 in Figure 4.8, inclusive, all appeared to fail as a result of the first two modes discussed above. Any low data point indicated in Figure 4.8 was a result of failure by shear. Materials #10 and 12 both appeared to fail by shear. This difference in failure mode would appear to be a combined material and geometry* effect which did not have an influence on the ballistic test results.

*The first mode of failure described by Vutukuri (1974) is usually attributed to the end constraints by the loading platens.

4.2.3 Ballistic Impact Tests

Figure 4.9 illustrates the gun facility which can be operated either as a powder gun (velocity range 800 to 5000 ft/sec), or as a gas gun (velocity range 200 to 800 ft/sec). For both operating modes the sabot is identical. Serrated sabots made of polyethylene are machined to accommodate the projectile. The sabots are machined so that upon exit from the launch tube the aerodynamic forces separate the sabot from the projectile. After separation occurs, the projectile passes through a sabot stripper which prevents sabot fragments from impacting the target. The distance from the sabot stripper to the target is about 1.5 feet. It is over this distance that the impact velocity is measured (see Figure 4.10).

A DYNATUP Model 502 Velocometer is used for the impact velocity measurements. The major components of this system are two velocometer main frames and two laser heads. Figure 4.10 shows a schematic of the velocity detector system currently employed at the facility. The orientation of the laser beams and photodiodes in the velocometer units is such that the projectile will traverse and interrupt the laser beams. The photodiodes are adjusted for a ten volt offset when completely saturated by the laser beam. Upon interruption of the beams by the projectile the output reverts to its baseline voltage. Thus a signal similar to the one shown in Figure 4.10 is obtained on an oscilloscope. The output of the first velocometer triggers the scope so that a complete velocity trace is obtained. This output was also used for triggering flash units for shadowgrams and frontlit photographs.

Test specimens are mounted in a test stand as shown in Figure 4.11a and clamped down along all four edges. The test stand is adjusted to orient the specimen at any incident angle desired (0° to 90°) using a Mitutoyo universal bevel protractor and vernier height gage. Due to the high aiming accuracy ($\leq$1/8") impacts at very low glancing angles on 6"x6" specimens are possible.

POWDER/AIR G
FOR PARTICLE IMP

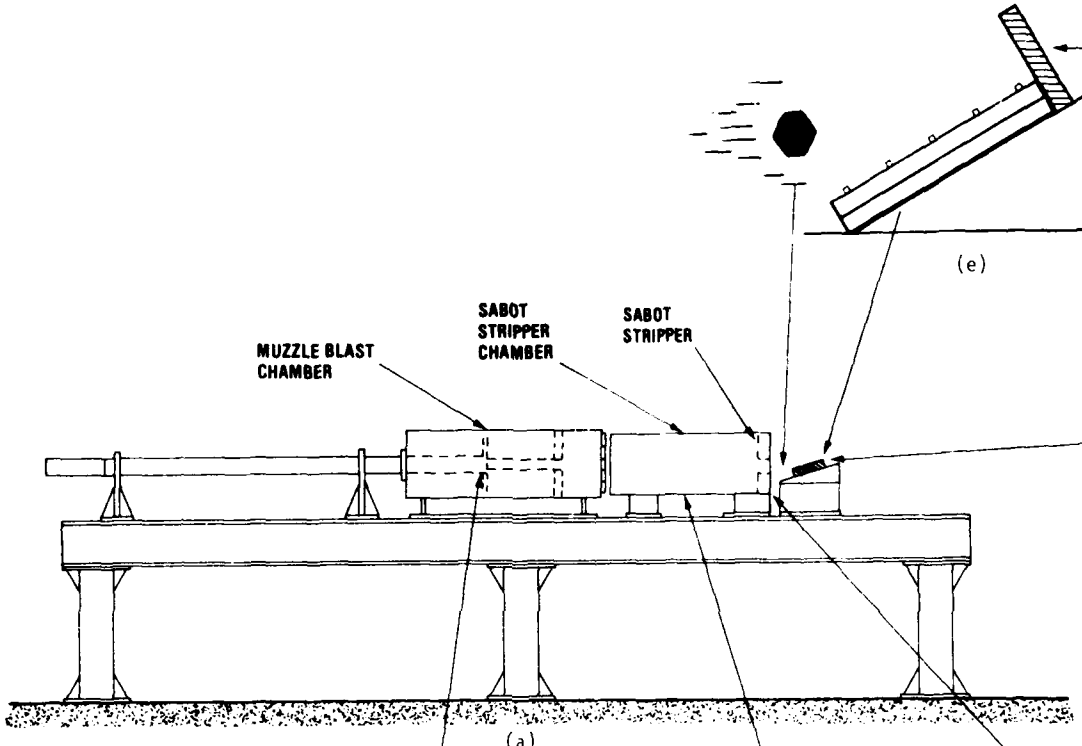

(a)

(e)

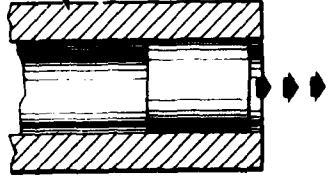

SABOT SERVES TWO MAIN FUNCTIONS

(1) ACTS AS OBTURATOR WHILE CARRYING THE PROJECTILE DOWN THE LAUNCH TUBE

(2) PROTECTS THE PROJECTILE FROM EROSIVE GUN GASES

(b)

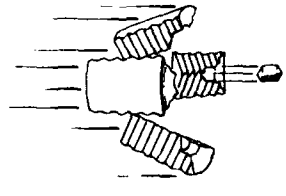

AERODYNAMIC FORCES SEPARATE SABOT FROM PROJECTILE

(c)

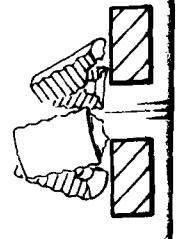

SABOT FRA
ON SABOT S
PROJECTILE
TARGET

ETI EFFECTS TECHNOLOGY, INC.
A SUBSIDIARY OF FLOW GENERAL, INC.
5383 HOLLISTER AVENUE
SANTA BARBARA, CA. 93111

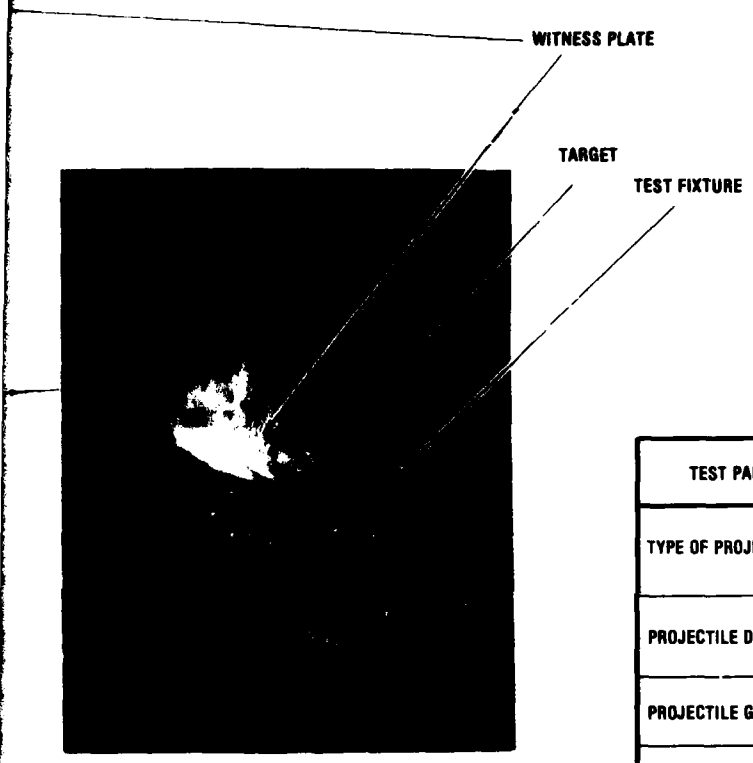

(f)

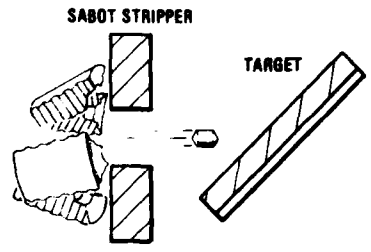

SABOT FRAGMENTS IMPACT ON SABOT STRIPPER, ALLOWING PROJECTILE TO IMPACT TARGET

(d)

CAPABILITIES

TEST PARAMETERS	RANGE	DIAGNOSTICS
TYPE OF PROJECTILE	GLASS, STEEL, GRANITE, ICE, ETC.	
PROJECTILE DIAMETER [cm]	0.2 — 2.2	
PROJECTILE GEOMETRY	SPHERE, CYLINDER, CYLINDER CONE, ETC.	
PROJECTILE CONDITION IN-FLIGHT	INTEGRITY, ORIENTATION	HI-SPEED PHOTOGRAPHY
IMPACT VELOCITY Vp [m/s]	17 — 2000	HI-SPEED FRAMING CAMERA LASER BEAM/PHOTO DIODES FOIL GAGES
TARGET ORIENTATION θ [°]	0 — 90	ADJUSTABLE SPECIMEN MOUNT
TARGET GEOMETRY	AS REQUIRED	
TARGET/PROJECTILE INTERACTION		WITNESS PLATE HI-SPEED FRAMING CAMERA
TARGET RESPONSE	PRESSURE-TIME DAMAGE	CARBON GAGE QUARTZ GAGE STRAIN GAGE PHOTOMICROGRAPHS

Figure 4.9.

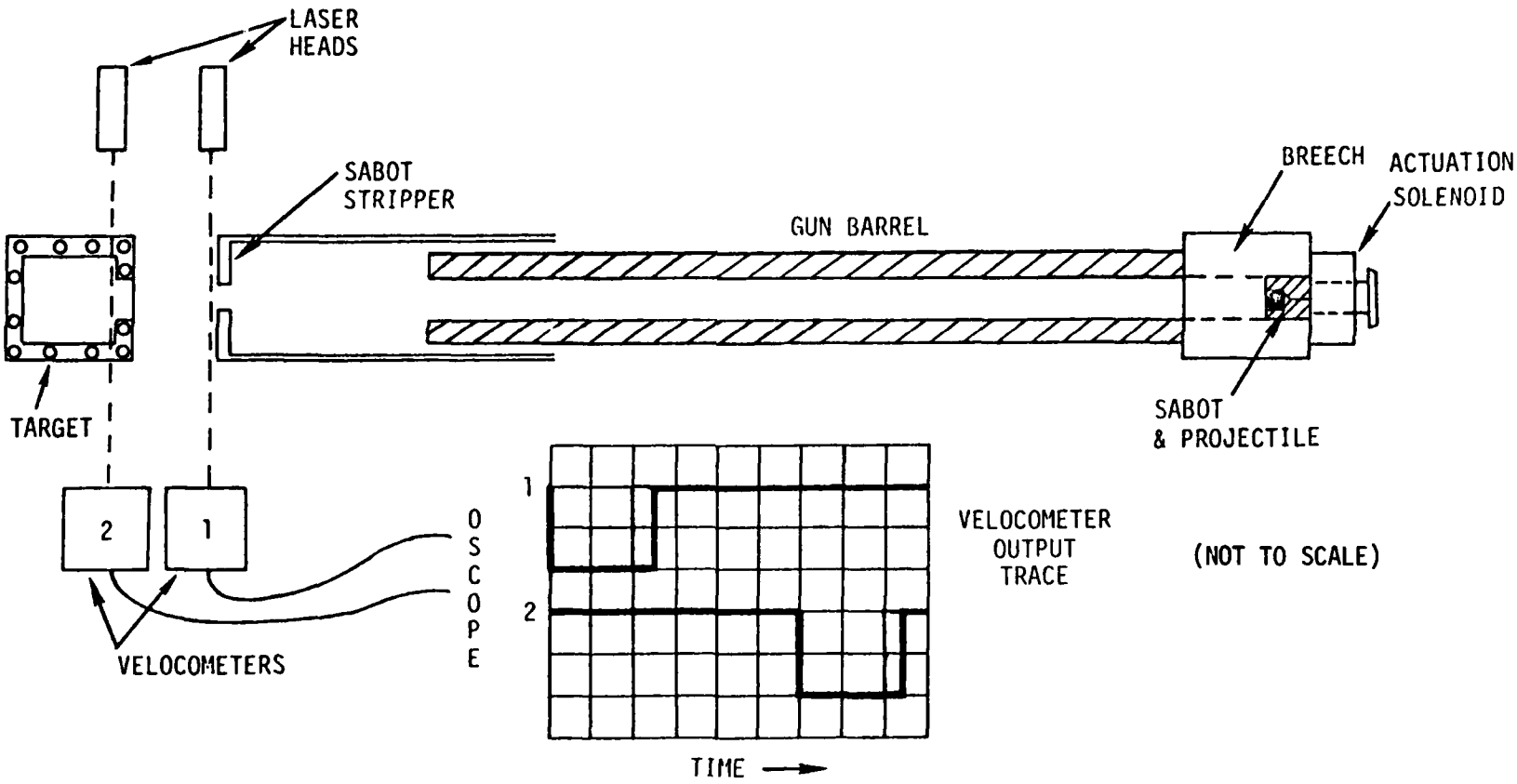

Figure 4.10. Impact Velocity Diagnostics.

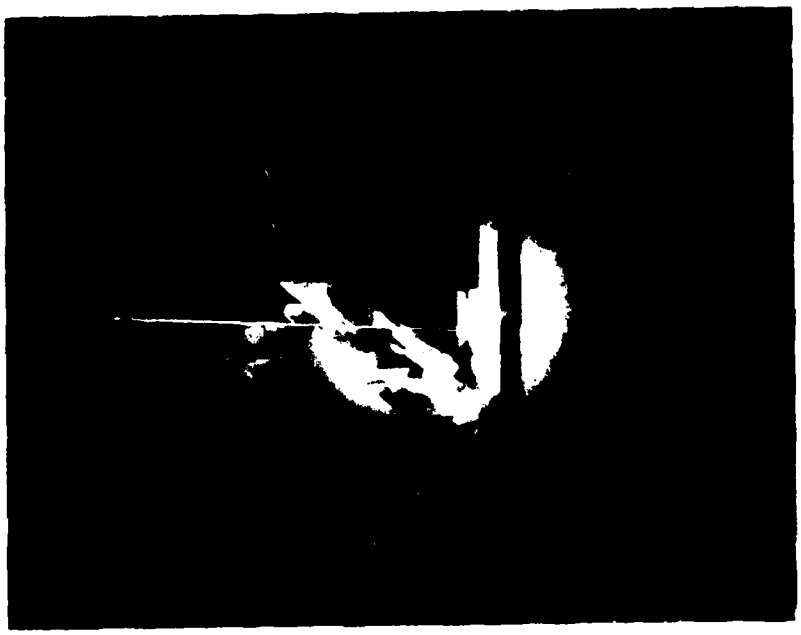

a) Time exposure of impact (note impact flash).

b) *Time exposure of projectile just before impact.*

Figure 4.11. Test Fixture and Diagnostics.

A total of eighty-three (83) tests were conducted using spherical projectiles manufactured from materials #2, 8, 9, 10, 11, 12, 13, 16, tonalite granite (both spheres and SAFRs) and soda lime glass. The projectiles were all nominally 0.625" diameter. Titanium (6Aℓ4V)* 0.019" thick and 6" square was used as test targets.

The objective of the tests was to determine the ballistic limit of the titanium panels for various impact conditions. The ballistic limit is defined as the conditions at which the specimen just tears. At times this had to be a judgment since a slight variation of velocity would cause no penetration or vice-versa. Tests were conducted with parameters varied until tearing of the specimen just occurred. The mode of failure of the titanium was distinctive enough (large dent to tear to complete punch out) that an estimate of ballistic limit is possible.

In most cases, except for the soda lime spheres, the projectiles broke up or were pulverized by the impact. At very shallow angles, most of the spheres ricocheted off the specimen intact (with the exception of materials #10 and 12).

Photographs of the projectiles prior to impact indicate that all of the materials are capable of being launched and impact the target intact as shown in Figures 4.11a and b. Figure 4.11a is a photograph that depicts the test fixture, laser beams, sphere prior to impact, and material response to impact. The timed flash illuminated the sphere just prior to impact and since the shutter was still open, the impact flash was also recorded. Figure 4.11b is a higher magnification photograph that shows the projectile just prior to impact.

*MIL SPEC 9046 Type 3 Composition C.

Using the procedure and diagnostics discussed above, spherical projectiles made from volcanic tuff (density of 1.3) were successfully launched without breakup prior to impact. Very porous materials (for example, scoria) were also successfully launched using this same technique. It is apparent from these results that any of the rock materials representative of the in-situ debris can be successfully launched to velocities of interest.

Ballistic impact tests were conducted for increasing impact angles at constant impact velocity until titanium penetration (or tearing) occurred. The test results are summarized in Table 4.3 and shown graphically in Figure 4.12*. A considerable spread of penetrability of rock types at the lower velocities is evident, while the penetration capability of many of the rock types converges at higher velocities. The penetrability of the baseline tonalite granite is comparable to several of these rock types at the higher velocities and of the CDP's evaluated represent (in rock units) approximately 30 to 60% of the geology. Clearly materials #10 and 12, volcanic tuff and scoria, respectively, do not fall in this grouping, however they represent rock units that constitute from 40 to 90% of the geology surveyed.

4.3 DISCUSSION AND RESULTS

The objective of the uniaxial compression test series was to provide a material ranking for the various geological materials thereby providing a possible screening test for the ballistic impact test series. By normalizing the average peak load to the baseline tonalite granite response a qualitative ranking is obtained (Figure 4.13) that is a definitive, more distinctive, and somewhat different ranking than by material density (Figure 4.3).

*Penetration for a particular rock type would occur at conditions above the ballistic limit curve for that rock type.

Table 4.3. Summary of Ballistic Impact Data.

PROJECTILE MATERIAL	BALLISTIC LIMIT CONDITIONS	
	IMPACT VELOCITY (ft/sec)	IMPACT ANGLE (°)
T-SAFR*	580	20
T-SAFR*	1100	12
2	550	33
2	1150	12
2	1380	8
T	550	42
T	1150	12
T	1480	6
SL	550	42
SL	1150	12
9	550	44
9	1280	12
16	550	44
8	550	45
8	1460	6
13	550	52.5
13	1400	8
13	1590	6
11	550	55
11	1370	12
11	1540	8
12	550	80
12	1230	30
12	1800	6
10	1300	60
10	1660	30

*SAFR - Cylinder cone shape of Standard Air Force Rock.

†See Tables 3.6 and 3.7 for material type.

SL = Soda Lime Glass

T = Tonalite Granite

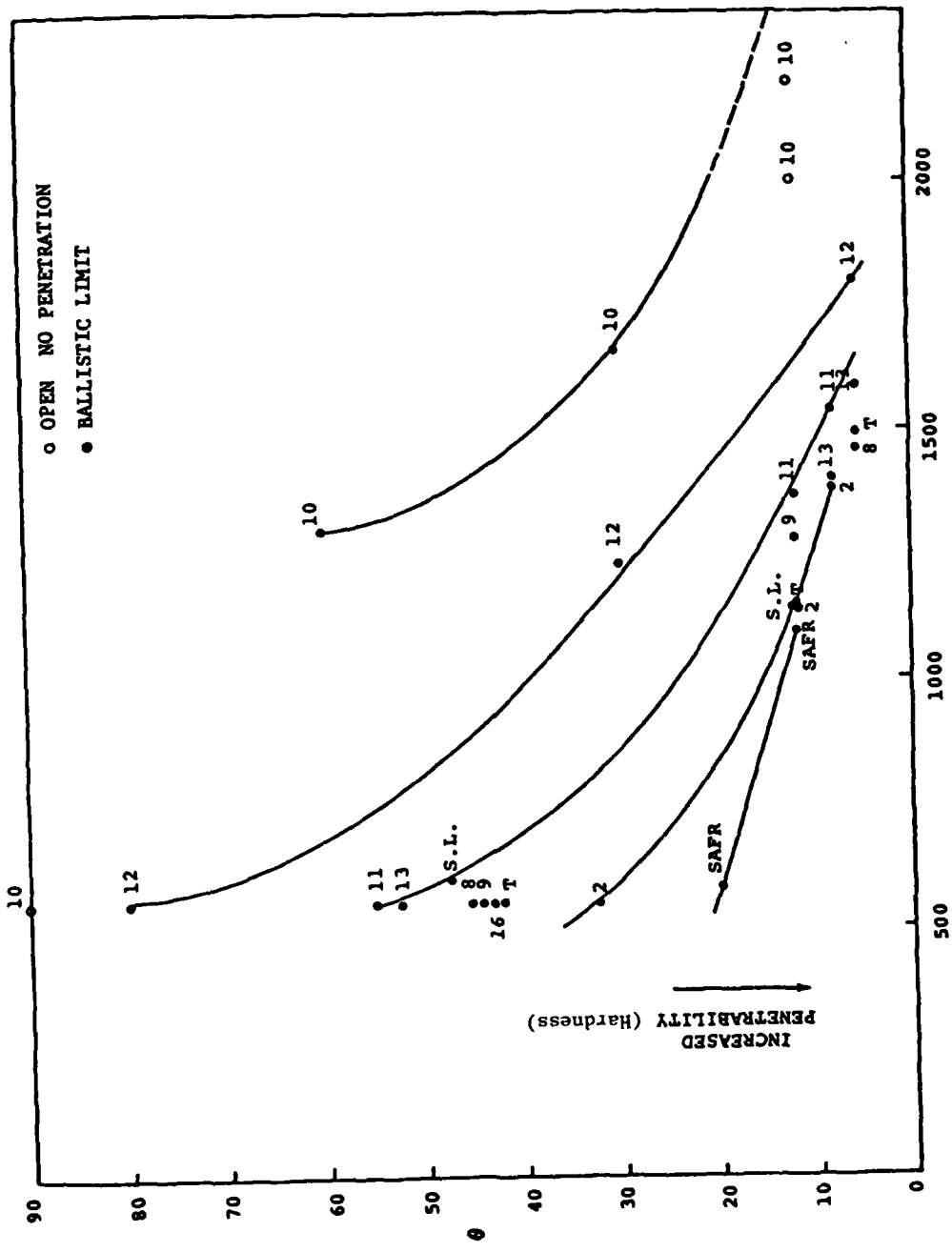

Figure 4.12. Results of Particle Type Ballistic Impact Tests.

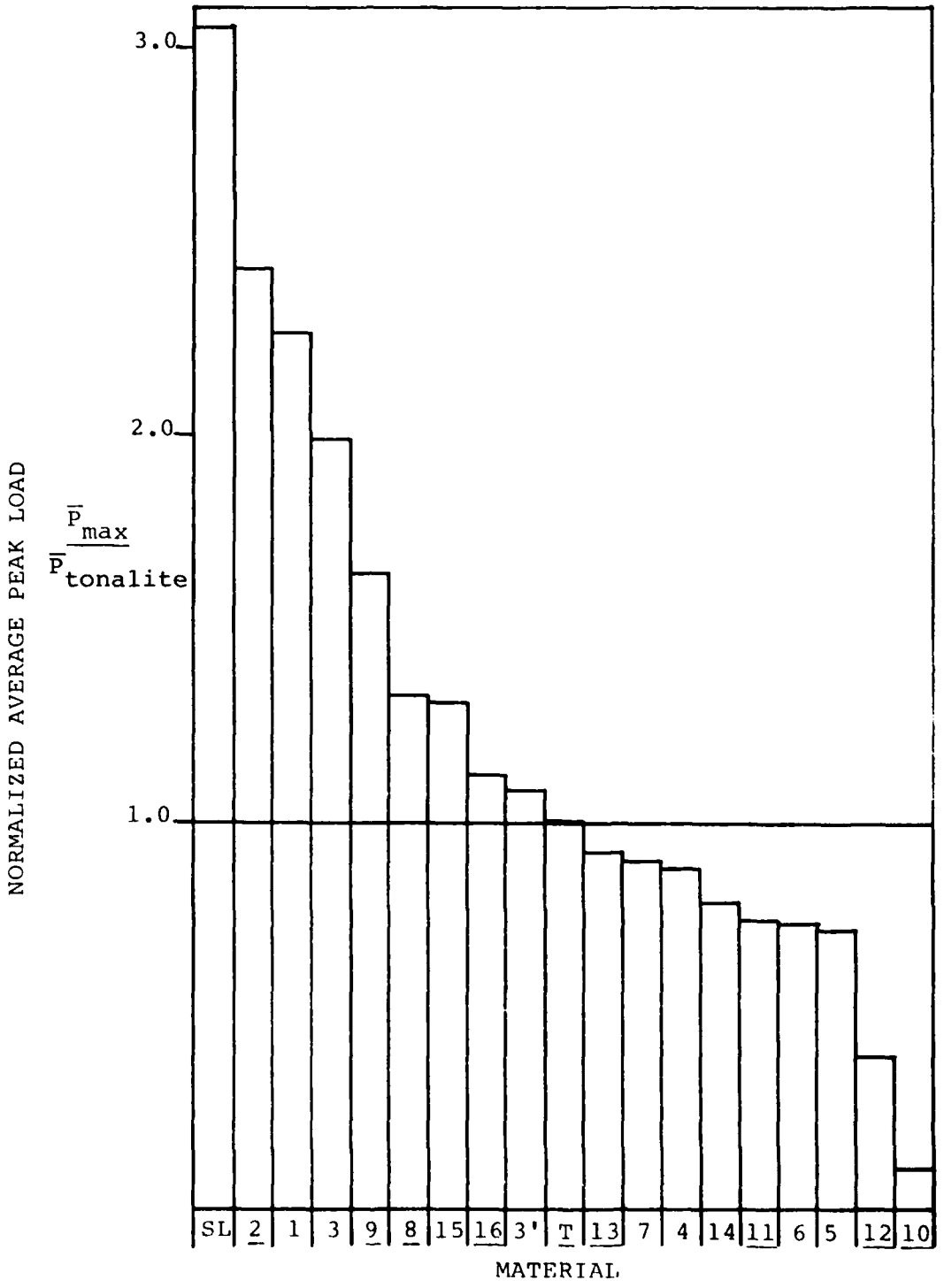

Figure 4.13. Material Ranking from Dynamic Compression Tests.

Comparing Figures 4.12 and 4.13 for spherical projectiles at impact velocities of 550 feet per second the relative penetrability response ranks in the same order as shown by the dynamic compression test results. The soda lime sphere data is comparable to the tonalite data, but was on the average able to sustain over three times the load for tonalite granite prior to failure. As stated before this may be a geometry and material effect. As the impact velocity is increased the response of the materials tend to group due to the thin target material.

It would appear that the use of dynamic compression testing as a screening test for many geological materials prior to ballistic testing would be of value. This will need to be clarified for increased target thicknesses as discussed below.

In order to apply the particle type data shown in Figure 4.12 to the penetration resistance of a titanium shroud, a representative shroud design was selected. Shroud geometries (forward, mid, and aft) at various angles of attack are considered.* A plot of angle versus velocity for the various sections of the shroud in different D&D environments is constructed (Figure 4.14a). The aft section of the shroud poses no survivability concern.† However, the fore and mid sections suggest that rock unit materials, which tonalite represents, would penetrate but materials #12 and #10 would not.

Using t/d (thickness/particle diameter) data and extrapolating for impact velocities $\leq$ 1000 fps indicates, as shown in Figure 4.14b, that 40 mils of titanium on the fore and mid sections would insure survivability. This varied thickness data shows the expected trend of the ballistic limit curve shifting up and to the right with increased titanium thickness. It is also reasonable to expect the ballistic limit

*Angle of attack taken from Reference Trajectory (Polich, 1979) was added to the shroud angle to give a maximum incident angle with time (i.e., velocity).

†Penetration will not occur for test conditions below the curves of the various rock types.

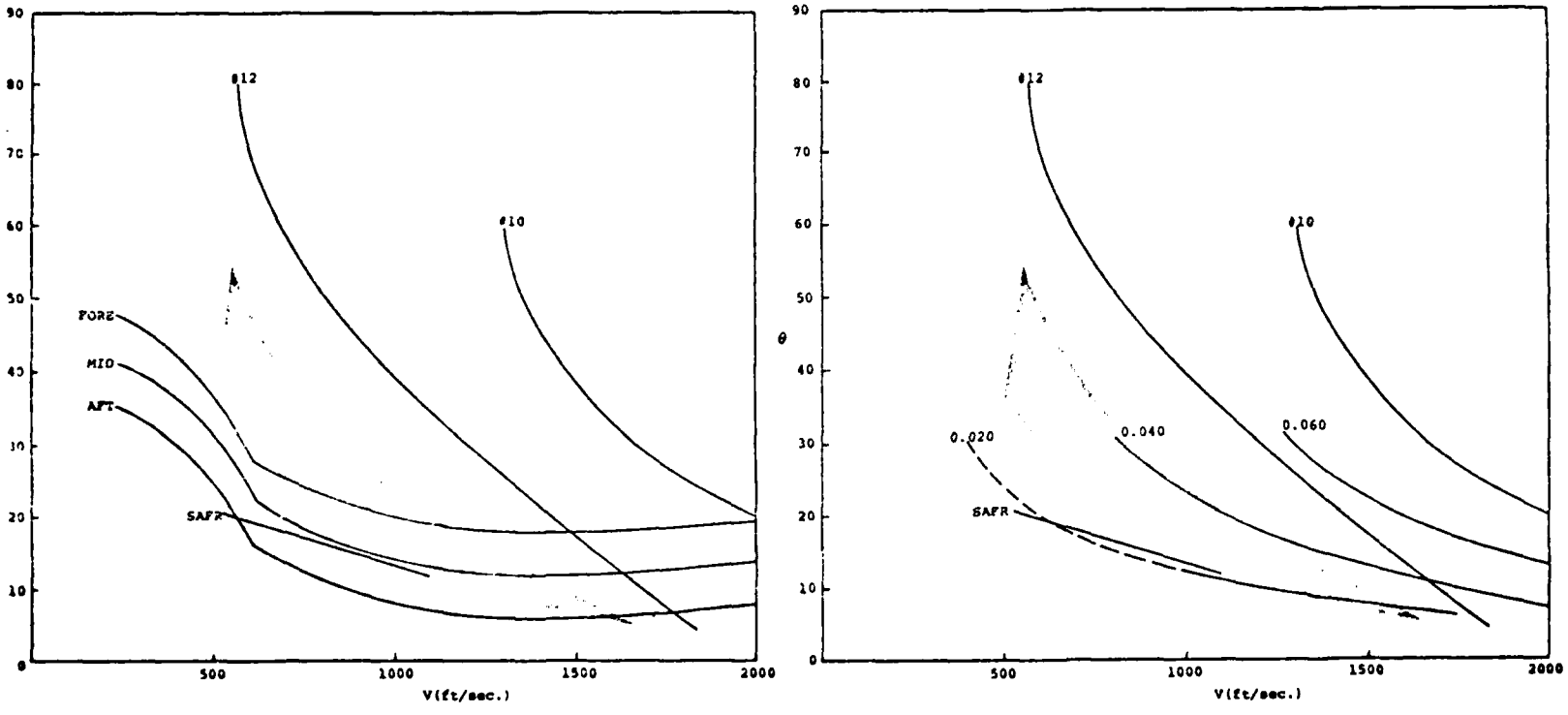

(a) (b)

Figure 4.14. Summary of Particle Type Ballistic Impact Tests. (Shaded area: grouping of materials comparable to tonalite response.)

curves for the various material types to shift in the same manner as target thickness is varied. Comparing Figures 4.14a and b suggests that 40 mils of titanium would be required for at least the mid and aft sections and possibly the fore section of the shroud to insure cloud survivability to materials represented by tonalite (30 to 60% of geology). It is also obvious that rock types similar to materials #10 and #12 (representing 40 to 90% of the rock units in the geology) pose no concern for the postulated titanium shroud.

4.4 CONCEPT/MATERIALS EVALUATION METHODOLOGY

From the approach used for the geological survey discussed in Section 3 and the ballistic impact test results, a methodology was established as depicted in the flow chart in Figure 4.15. This methodology is recommended to survey proposed basing areas and to evaluate advanced ICBM concepts and materials relative to the in-situ debris.

The first step in this evaluation is a determination of flyout environment conditions from system requirements. If the type of environment and source (natural and nuclear augmented) are well known, then material/concept evaluations can be conducted in terms of design and system issues. If the environmental concerns are not well known, for example in an augmented particle environment, the approach is to determine the locality (basing areas) of the proposed systems and then conduct a geological survey of the areas. From the survey it will be apparent if sampling is required. If the survey indicates a geology represented by tonalite granite, no sampling is required and test projectiles can be manufactured from tonalite for missile material/concept evaluation. If sampling is required, an effort is necessary for in-situ sample acquisition, petrographic sample analysis, and test projectile fabrication. Uniaxial compression tests can be used as a screening test to determine the relative performance and impact ranking of the rock types compared with

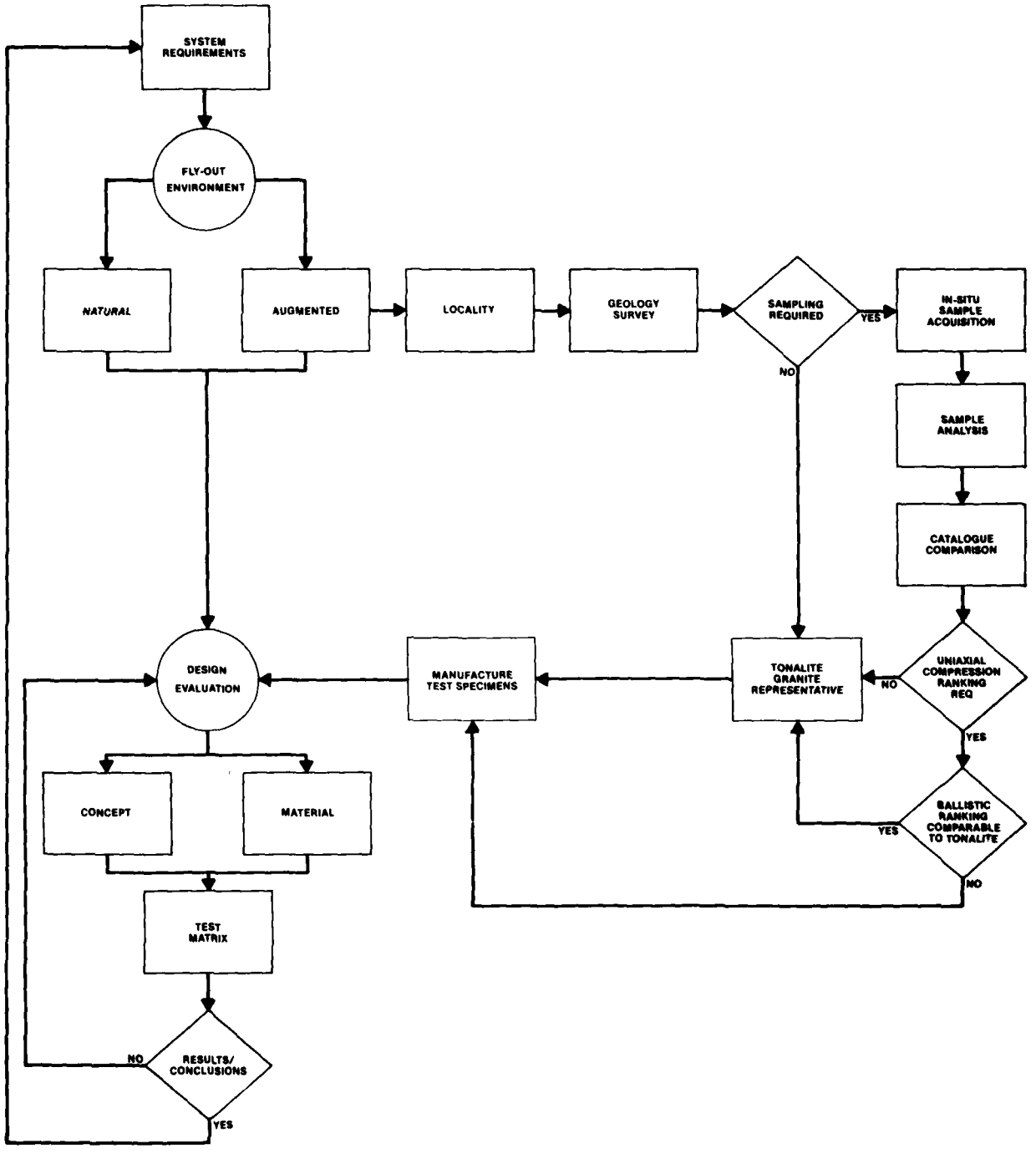

Figure 4.15. Concept/Materials D&D Evaluation Methodology.

tonalite. If the results indicate performance comparable to tonalite, testing proceeds the same as if sampling was unnecessary. If results indicate the need for further evaluation, then ballistic impact tests are conducted for further comparison with tonalite granite. Based upon these results, a selection is made regarding the use of tonalite as a representative material or the use of actual in-situ materials for advanced ICBM external material/concept D&D evaluations.

5.0 CONCLUSIONS AND RECOMMENDATIONS

The objective of the program was to evaluate the use of in-situ materials for penetration testing and to establish the difference in penetrability that would result using these materials versus the current baseline tonalite granite. To accomplish this a test methodology was developed to rank in-situ debris materials against the baseline tonalite granite. This methodology included uniaxial compression tests on rocks and ballistic impact tests on monolithic titanium.

5.1 CONCLUSIONS

As a result of this effort, tonalite granite appears to be a somewhat conservative material for use as a test projectile for advanced missile material evaluations. Tonalite granite is representative of rock units that make up 10 to 30% of the geology at the CDPs evaluated in this program. Rock types that are representative of rock units that make up 40 to 90% of the geology are about two to three times less penetrating than equivalent tonalite granite projectiles. These results indicate a definite rock type effect with the more widely disseminated geology being less penetrating than the tonalite granite material. Applying the current data to a representative shroud design suggests that materials representative of from 40 to 90% of the geology in any one CDP would probably pose no single particle penetration threat.

From this effort a methodology has been developed for ranking in-situ debris materials that are representative of proposed basing sites. This methodology is applicable to any geology considered as a possible cloud particulate source.

A compilation of in-situ particle size distribution obtained from recent geotechnical efforts is summarized in this report. Analysis indicates that particle size distribution for either the competent rock or the previously considered missile site representative geologies are orders of magnitude larger than for the in-situ geology.

Historically, spherical projectiles are used for particle impact simulation to minimize data scatter due to particle shape effects and to provide conservatism. However this spherical geometry is more representative of the softer, more easily fragmented, in-situ materials. Thus, the spherical projectile is more representative of the less detrimental materials (e.g., volcanic tuff) and it is not apparent at this time what affect this geometry restriction has on the degree of penetrability for the harder rock types.

It seems apparent from previous data as well as from data generated during this program that the shape of the projectiles may have a significant effect on their penetrability: in particular the harder materials. Since the harder rock masses will produce highly angulated pieces upon fragmentation (either as a result of weathering and/or nuclear explosion), the orientation of the sharp edges relative to the surface of the shroud will influence the degree of interaction with the impact surface.

The important aspects of particle coupling effects (multiple impacts, erosion, etc.) were not addressed due to limited scope of this effort. The program objective was evaluation of particle type effects on penetration thresholds of advanced missile materials; therefore, only large particle impacts were considered.

As a result of this effort several important issues and recommendations warrant consideration and evaluation:

- All of the proposed and/or selected CDPs were not geologically investigated within this effort (Figure 5.1), and it is not apparent at this time whether the extended areas are geologically similar to the valleys discussed here.

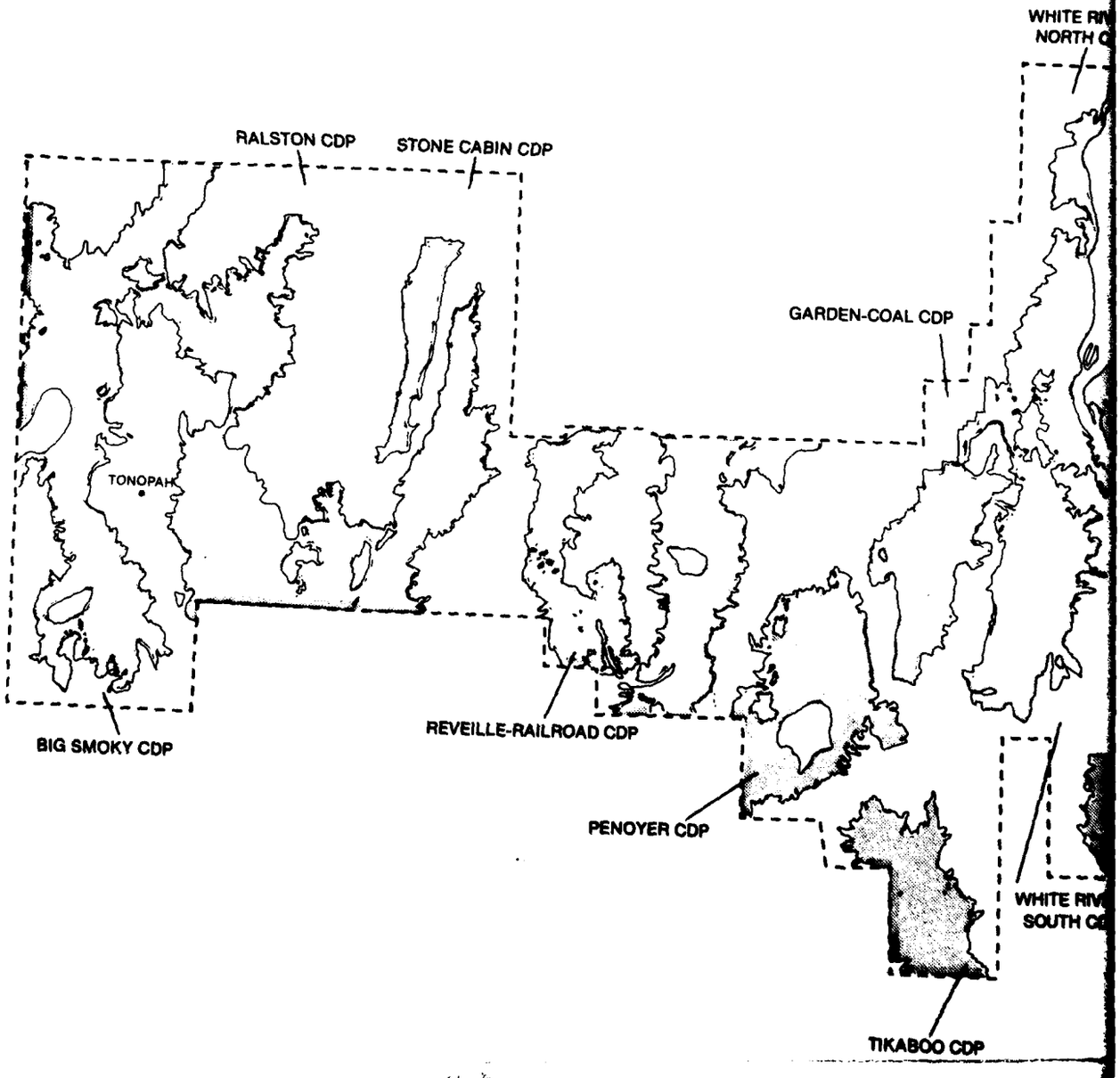
WHITE RIV
NORTH C
RALSTON CDP
STONE CABIN CDP
GARDEN-COAL CDP
TONOPAH
BIG SMOKY CDP
REVEILLE-RAILROAD CDP
PENOYER CDP
WHITE RIV
SOUTH C
TIKABOO CDP

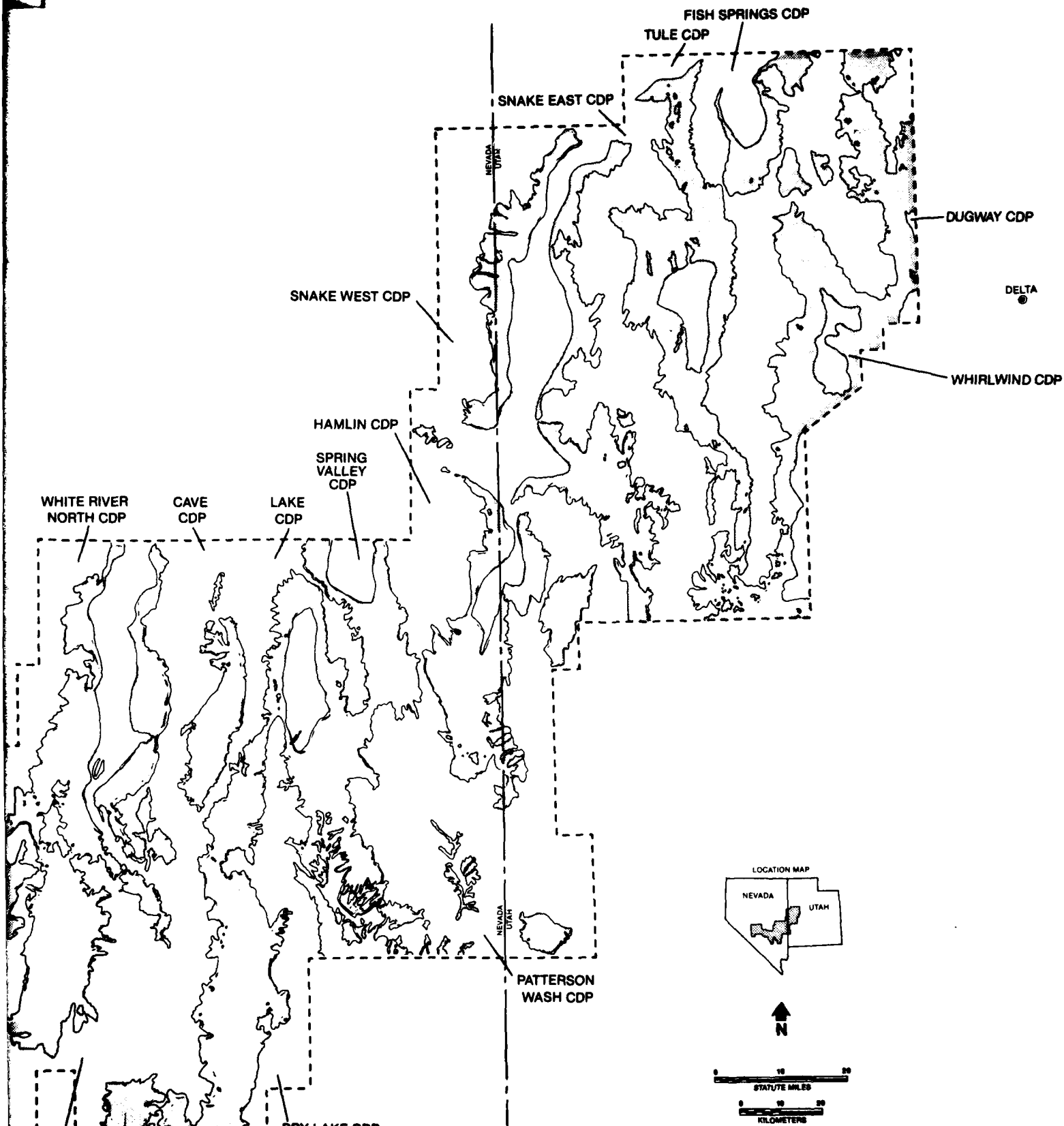

Figure 5.1. CDPs Currently Being Considered for Evaluatio

- The influence of increased titanium thicknesses on the t/d data trend shown in Figure 4.14b (especially for velocities less than 1000 feet per second) is not apparent from the results of the current effort.
- An increased thickness of titanium may both increase the spread between the ballistic limit curves and shift the curves of the various materials (i.e., materials #2, 16, 8, 9, 11, and 13) compared to tonalite granite.
- A spread in penetrability response may affect the penetrability ranking of the various rock types.
- The reasonableness of using a competent rock (i.e., tonalite granite) or a soft rock (i.e., tuff) geology or some combination of the two for cloud modeling and particle size distribution is not apparent.
- The limited data accumulated during this program does not address the effect of particle shape on material/concept response to an augmented D&D environment.
- Of primary importance is the influence of the above issues in the generation of realistic specifications of the advanced missile ascent environment.

REFERENCES

MX Siting Investigation Geotechnical Summary Prime Characterization Sites Great Basin Candidate Siting Province, Fugro National, Inc., for SAMSO, Norton AFB, California, 15 February 1979.

R.S. Bertke and D.D. Preonas, "Response of Materials to Pebble Impacts," University of Dayton Research Institute, UDRI-TM-PC-75-1, November 5, 1975.

W.J. Hall, N.M. Newmark and A.J. Hendron, Jr., (1974), "Classification, Engineering Properties and Field Exploration of Soils, Intact Rock and In-Situ Rock Masses," Directorate of Regulatory Standard, U.S. Atomic Energy Commission, Washington, D.C., May 1974, WASH-1301.

C.J. Hastings, J.H. Alexander, P.L. Anderson and E.W. Sims, "Pebble Impact Data, A Compilation," Systems, Science and Software, SSS-R-77-3173, April 1977.

W.F. Polich, Personal Communication TRW, El Segundo, California, MX Reference Trajectory, January 19, 1979.

G. Ramanjaneya, Project Manager/Engineering, Fugro National, Inc., Long Beach, California, Personal Communication, 1979.

M. Rosenblatt, "Dice Calculations," California Research and Technology, Inc., Woodland Hills, California. Viewgraph presentation for Advanced Missile F'vout Survivability Programs Review held at SAMSO/NAFB, California, 13-14 June 1979.

V.S. Vutukuri, R.D. Lama, and S.S. Saluja, Handbook on Mechanical Properties of Rocks, Volume I, Trans Tech Publications, Ohio, 1974.

APPENDIX A

RESULTS OF PETROGRAPHIC ANALYSIS

As discussed in Section 3.3 a necessary requirement in identifying rock samples as well as in determining the lithology of the in-situ debris is a petrographic analysis. Results of the thin section analysis is given in Section 3.3 with photomicrographs, using transmitted light, of the thin sections shown in Figure A.1 through A.16. Tables A.1 through A.16 give detailed results of the analysis.

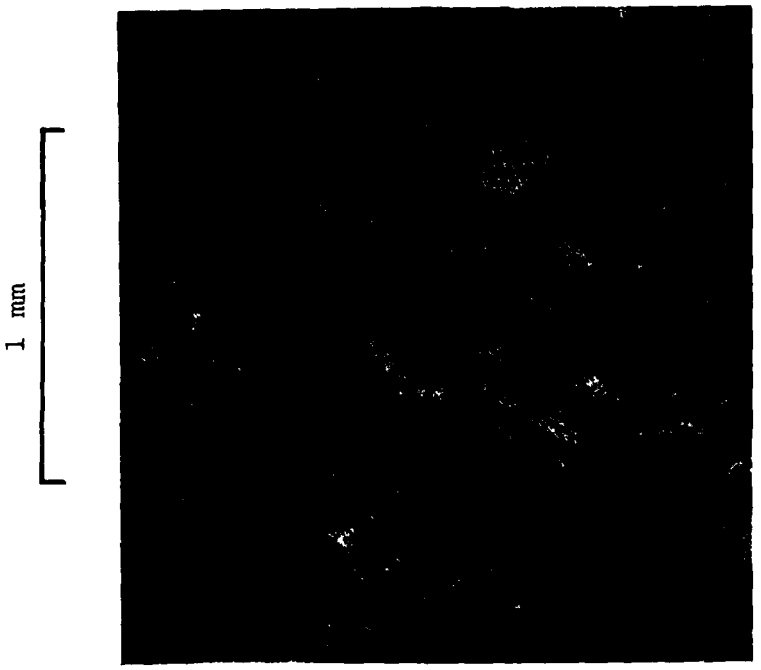

Figure A.1. Photomicrograph of Thin Section from Material #1.

Table A.1. Slide 1 Limestone - 100% Calcite (Angular Fragments).

SHELL HASH—OSTRACODS—DOMINANT—TO 1.2 MM MAX., .6 AVERAGE

FORAMS

BEDDED

SPARRY CALCITE GRAINS—.5 MM AVERAGE

MICRITE LOCALLY ABUNDANT—INFILLS ALL SPACES BETWEEN SHELL HASH

POROSITY ~1%

FECAL PELLETS TO .5 MM

40% SHELL HASH

60% MICRITE

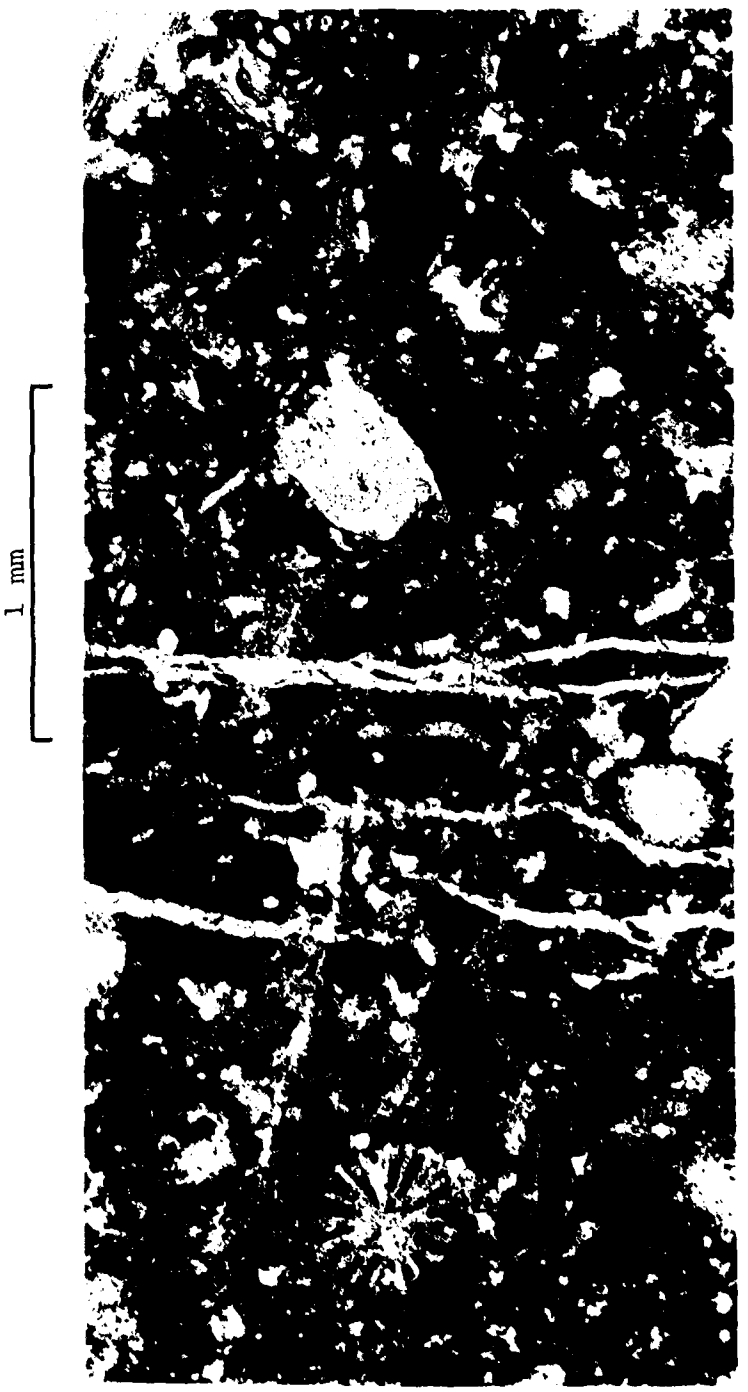

Figure A.2. Photomicrograph of Thin Section from Material #2.

Table A.2. Slide 2 Limestone (Angular Fragments)

CRINOID STEM

FORAMINIFERA - 10% OF FOSSILS (SPARRY MOTTLED FOSSILS)

FECAL PELLETS

FRACTURES .1 MM CUT ACROSS SLIDE, CALCITE FILLED,
BEDDING

QUARTZ GRAINS - DISSOLVED, REPLACED BY CALCITE <.05 MM
REMNANTS

AD-A089 186 EFFECTS TECHNOLOGY INC SANTA BARBARA CA F/G 8/7
MISSILE SITE ROCK CHARACTERIZATION AND PENETRATION TEST RESULTS--ETC(U)
DEC 79 J D CARLYLE DNA001-79-C-0115
UNCLASSIFIED DNA-5144F NL

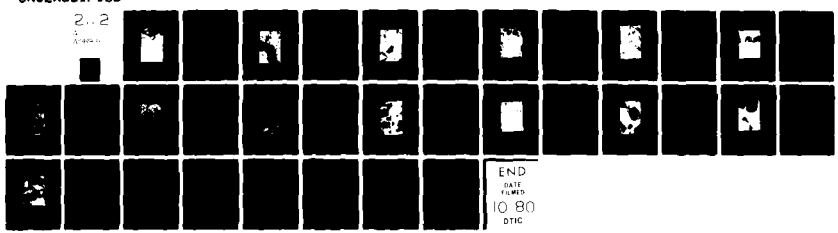

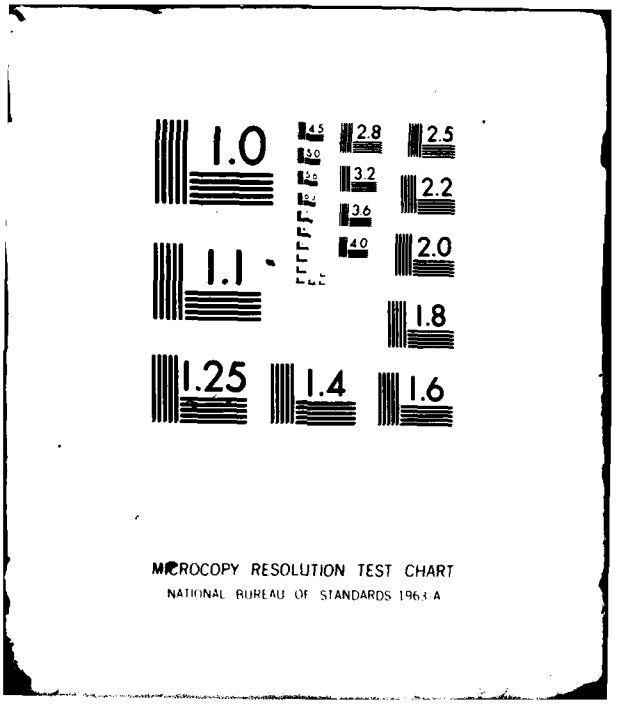
1.0
1.1
1.25
1.4
1.6
1.8
2.0
2.2
2.5
2.8
3.2
3.6
4.0
4.5
5.0
MICROCOPY RESOLUTION TEST CHART
NATIONAL BUREAU OF STANDARDS 1963 A

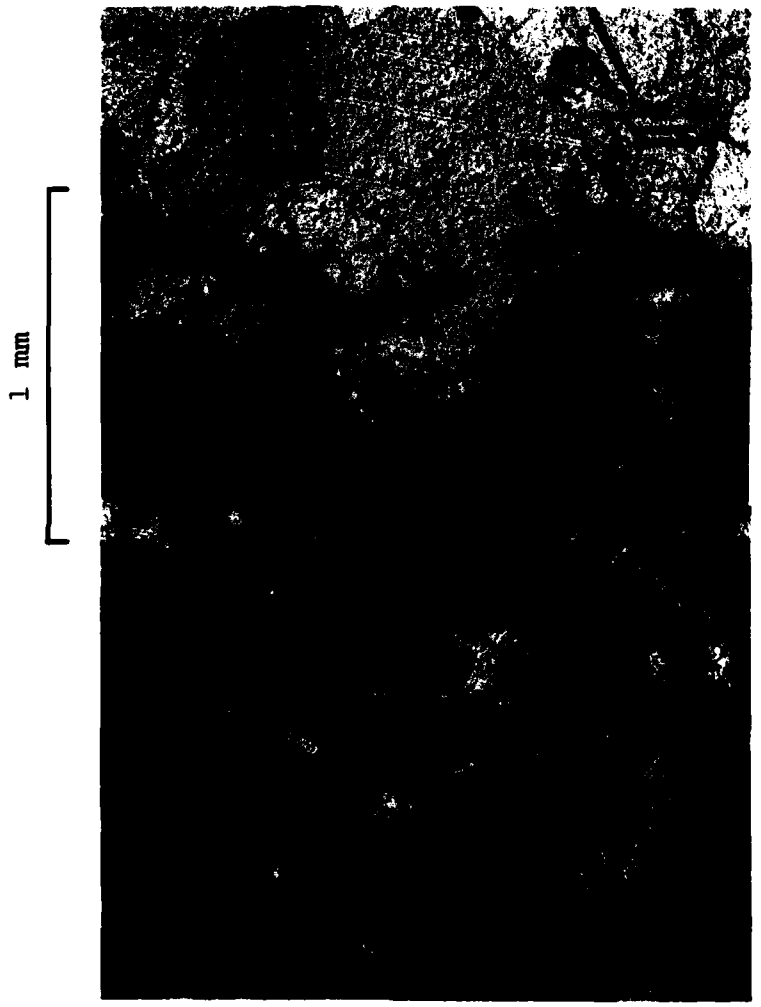

Figure A.3. Photomicrograph of Thin Section from Material #3.

Table A.3. Slide 3 Recrystalized Limestone.

MICRITE PELLETS ∿50%

SPARRY PELLETS - VOID FILLINGS OR RECRYSTALIZATION TO 2 MM

AVERAGE = 5 - 10%, .7 MM PELLETS ROUNDED

SPARRY CALCITE CEMENT

QUARTZ GRAINS - RECRYSTAL - MOST ALL HAVE BEEN DISSOLVED
BY CALCITE ∿.5MM MAX ∿1%

Figure A.4. Photomicrograph of Thin Section from Material #4.

Table A.4. Slide 4 Rhyolite.

70—75% DEVITRIFIED GLASS

20—30% QUARTZ SANDSTONE

PORE 5% SPACES FILLED WITH SMALL QUARTZ-CRYSTALS (VESICLES)

RELICT SHARDS PRESENT

SANIDINE .5—1 MM AVERAGE

Figure A.5. Photomicrograph from Thin Section from Material #5.

Table A.5. Slide 5.

40—50% GLASS—BROWN, DEVITRIFIED TO CHLORITE

PORE SPACE 1—3%

OPAQUES - BIOTITE HORNBLENDE IN PERCENTAGE

BIOTITE—LATHS—UNSTRAINED—UP TO 1 MM
(GREEN, BROWN) HORNBLENDE .3—.5 MM
} 5—10%

QUARTZ + FELDSPAR
40—50%
} TO 4 MM
4 MM AVERAGE

SUBHEDRAL TO EUHEDRAL WEAKLY DEFINED FLOW BANDING

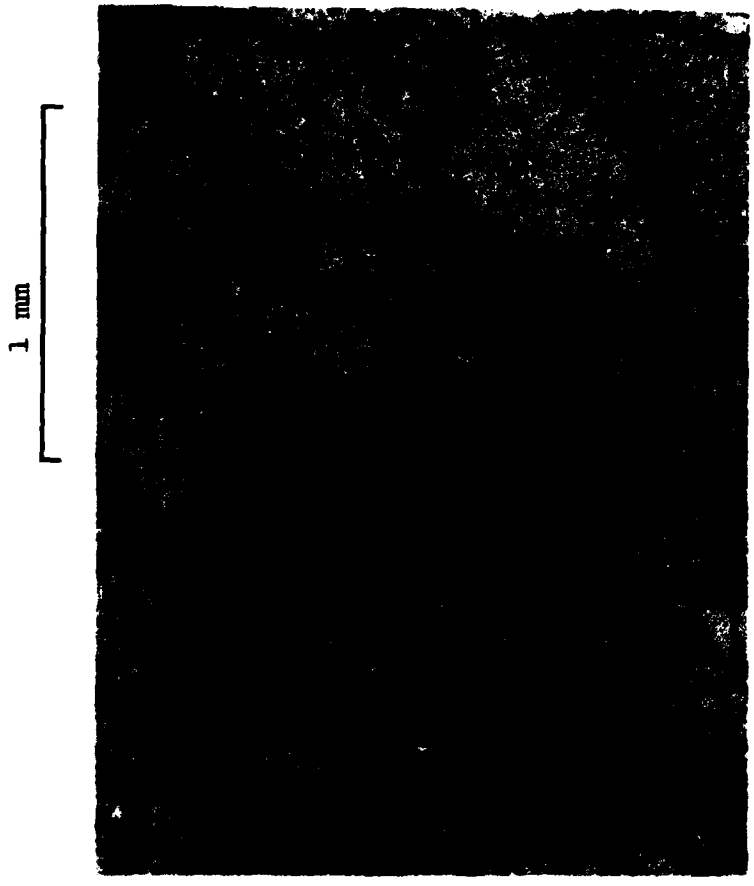

Figure A.6. Photomicrograph of Thin Section from Material #6.

Table A.6. Slide 6.

ABUNDANT PHENOCRYSTS IN CLEAR UNALTERED GLASS

5—7% BIOTITE, SLIGHTLY BENT, BROWN, GENERALLY TABULAR
TO .5 MM LONG

50—60% PLAGIOCLASE + SANDINE TO 2 MM .5—.7 MM AVERAGE
HORNBLENDE TO 2 MM

ROCK FRAGMENTS WITH SMALL PLAGIOCLASE LATHS + OPAQUES NO PORE
SPACES (VESICLES)

NO FLOW BANDING, NO VESICLE WALLS

CRYSTALS ALL ANGULAR

2 MM = MAX PHENOCRYST SIZE

GLASS: 40—50%

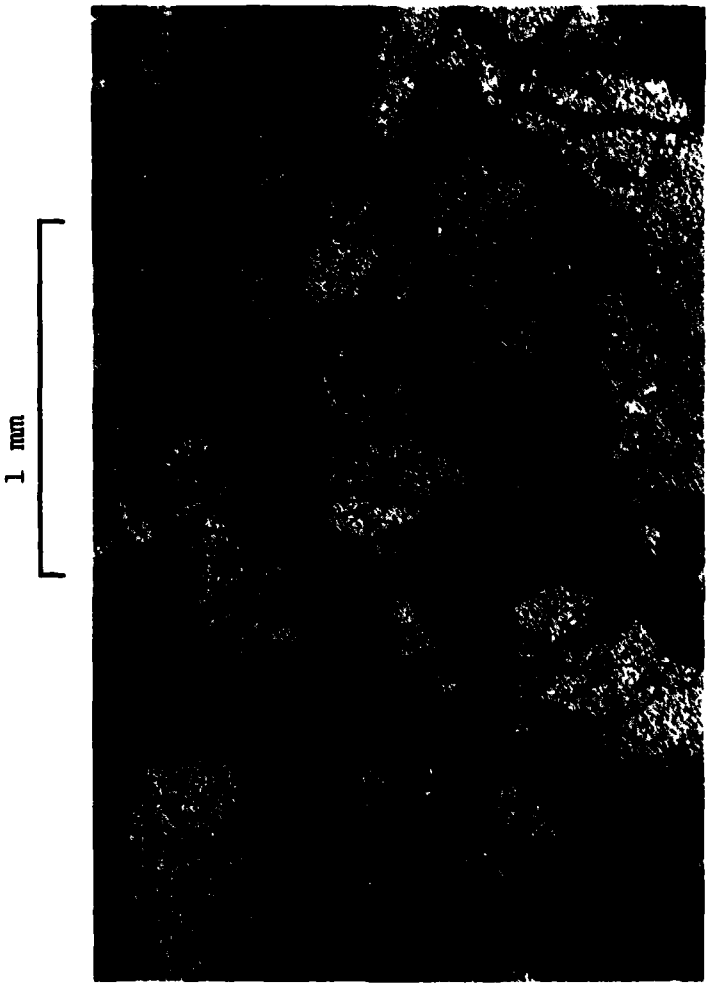

Figure A.7. Photomicrograph of Thin Section from Material #7.

Table A.7. Slide 7 Rhyolite.

BIOTITES—BROWN—SLIGHTLY BEND .5—.7 MM

GLASS—BROWNISH—DEVITRIFIED

HORNBLENDE

1 MM AVERAGE 30—40%

PLAGIOCLASE—MODERATELY ZONED—TWINNED (CARLSBAD)

QUARTZ —TO 3 MM

HEMATITE

MAGNETITE

POOR SORTING OF CRYSTAL SIZE

PHENOCRYSTS ARE ANGULAR (SUBHEDRAL TO EUHEDRAL)

NO PORE SPACES

GLASS BANDED AROUND CRYSTALS—COLLAPSED SHARDS

PHENOCRYST TO PHENOCRYST CONTACTS NOT COMMON

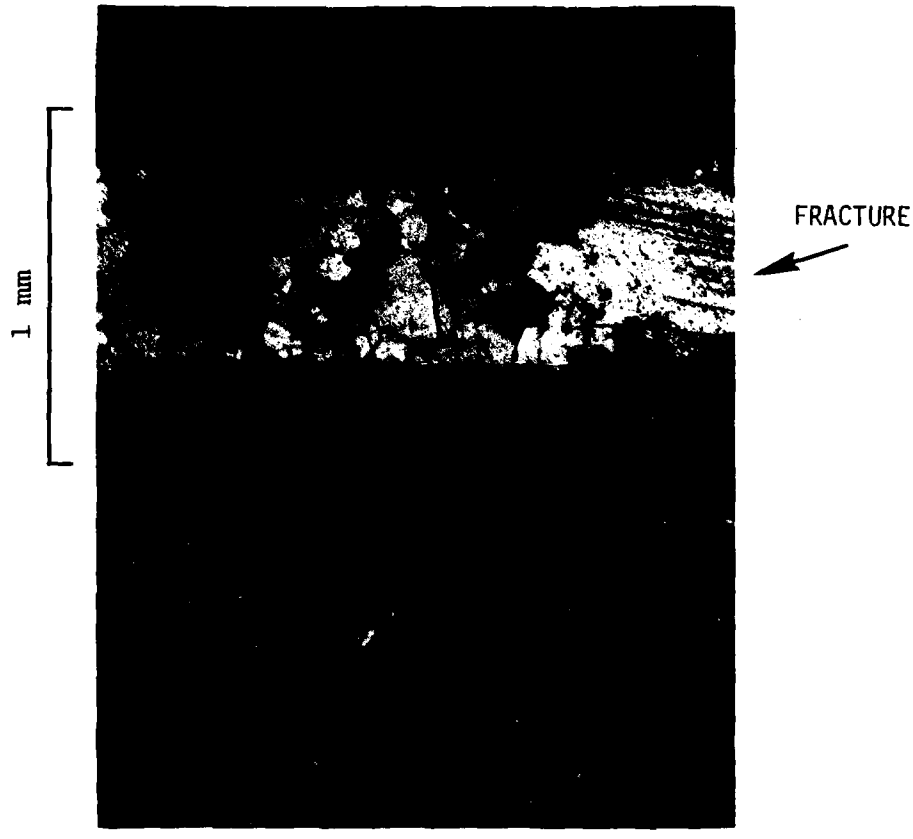

Figure A.8. Photomicrograph of Thin Section from Material #8.

Table A.8. Slide 8 Micrite Limestone.

90—95% LIME MUD

QUARTZ GRAINS—ATTACKED BY CALCITE—SMALLER THAN SILT (<0.5 MM)

FRACTURES IN SLIDE (.1 MM—.5 MM) FILLED WITH SPARRY CALCITE

INDISTINCT BANDARY—SUB-PARALLEL BUT HIGHLY DISTORTED,
LIKE ALGAL MATTES

THESE BANDS MARKED BY SLIGHT INCREASE IN CALCITE CRYSTAL SIZE

NO PORE SPACES

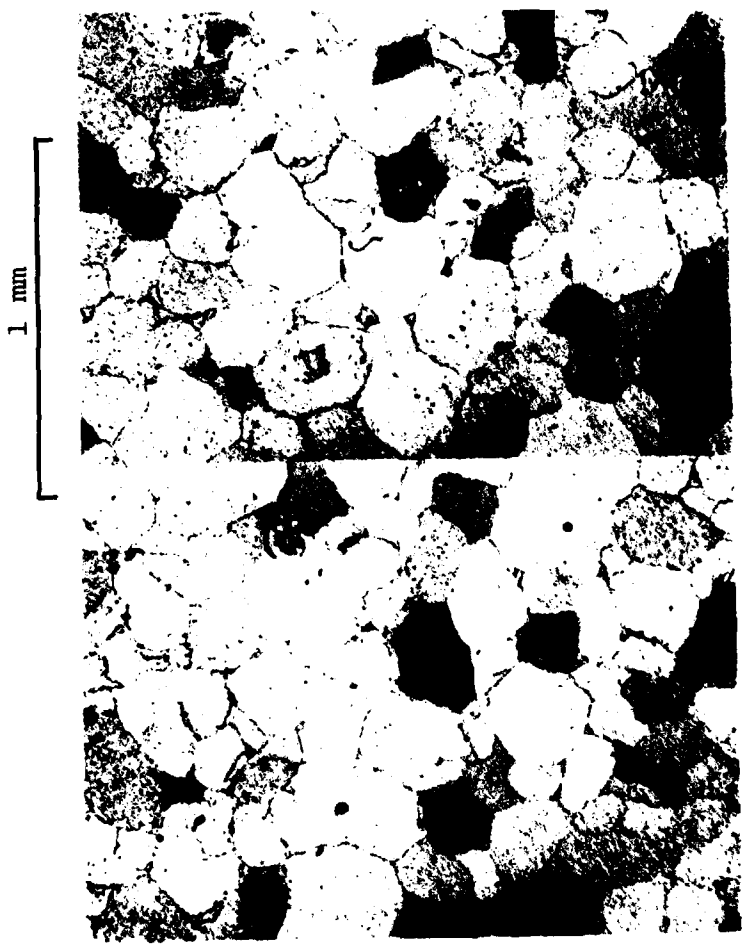

Figure A.9. Photomicrograph of Thin Section from Material #9.

Table A.9. Slide 9 - Orthoquartzite.

METAMORPHIC—100% QUARTZ

NO PORE SPACES

WELL-SORTED

.15—.4 MM, MOST AROUND .25 MM

NUMEROUS TRIPLE-POINT GRAIN CONTACTS

ALL QUARTZ GRAINS OVERGROWN

VERY CLEAN ROCK

WHITE IN HAND

SPECIMEN COLOR

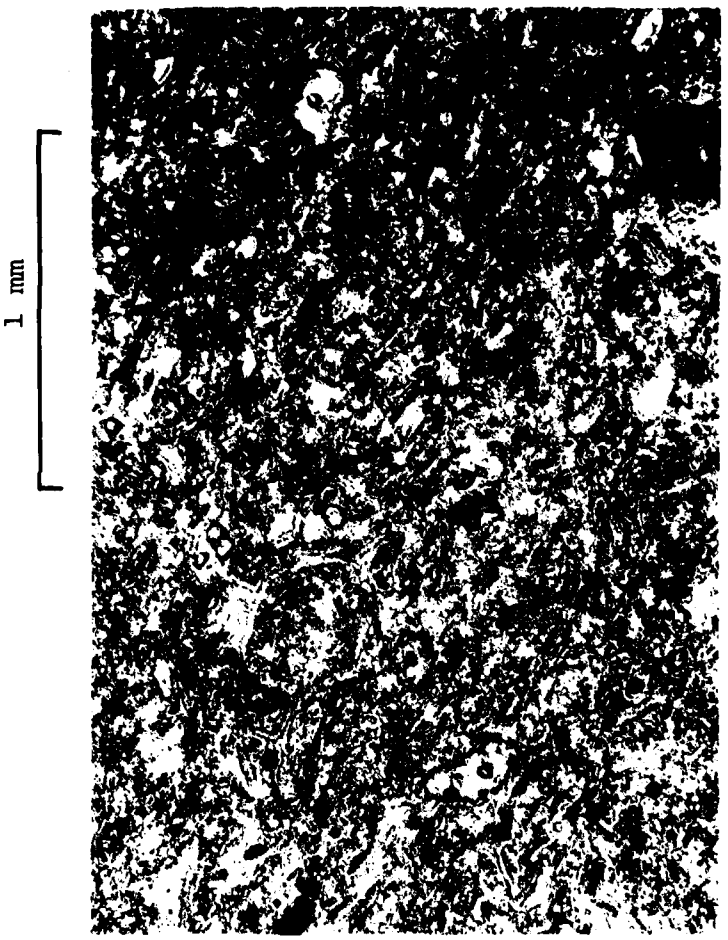

Figure A.10. Photomicrograph of Thin Section from Material #10.

Table A.10. Slide 10.

90-95% DEVITRIFIED GLASS WITH CLEAR RELICT SHARD STRUCTURE

MODERATE RELICT FLOW BANDING

SANIDINE + QUARTZ TO 1.7 MM, MOST SMALLER (∿.1—.5 MM)

SOME LINED VESICLES—BOLATED, 1—3% .3 MM AVERAGE SIZE

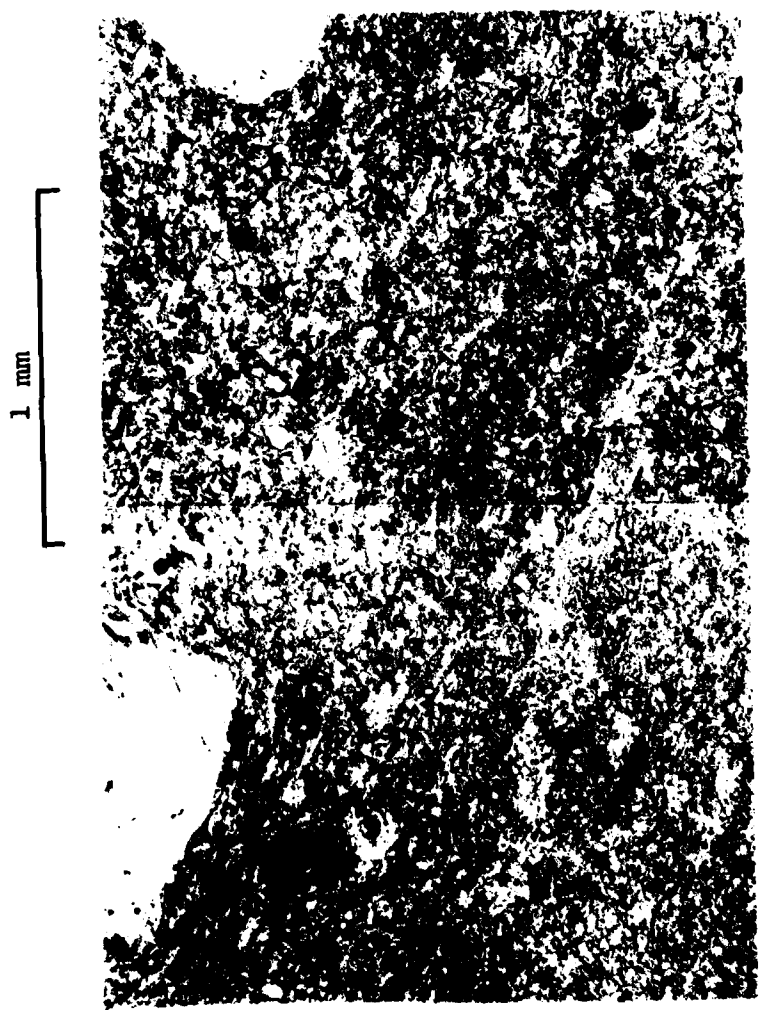

Figure A.11. Photomicrograph of Thin Section from Material #11.

Table A.11. Slide 11 Devitrified Glass.

90—95% DEVITRIFIED GLASS

MODERATE FLOW BANDING EXHIBITED BY COLLAPSED RELICT SHARD STRUCTURES

HORNBLENDE

5—10% SANIDINE + QUARTZ CRYSTALS TO 2 MM, .15—2 MM COMPLETE SIZE SPECTRUM

BIOTITE—TRACE

COLLAPSED VESICLES HAVE BEEN FILLED, REPLACED BY QUARTZ/CHALCEDONY (?)

MAY BE SOME POROSITY—HARD TO DETERMINE

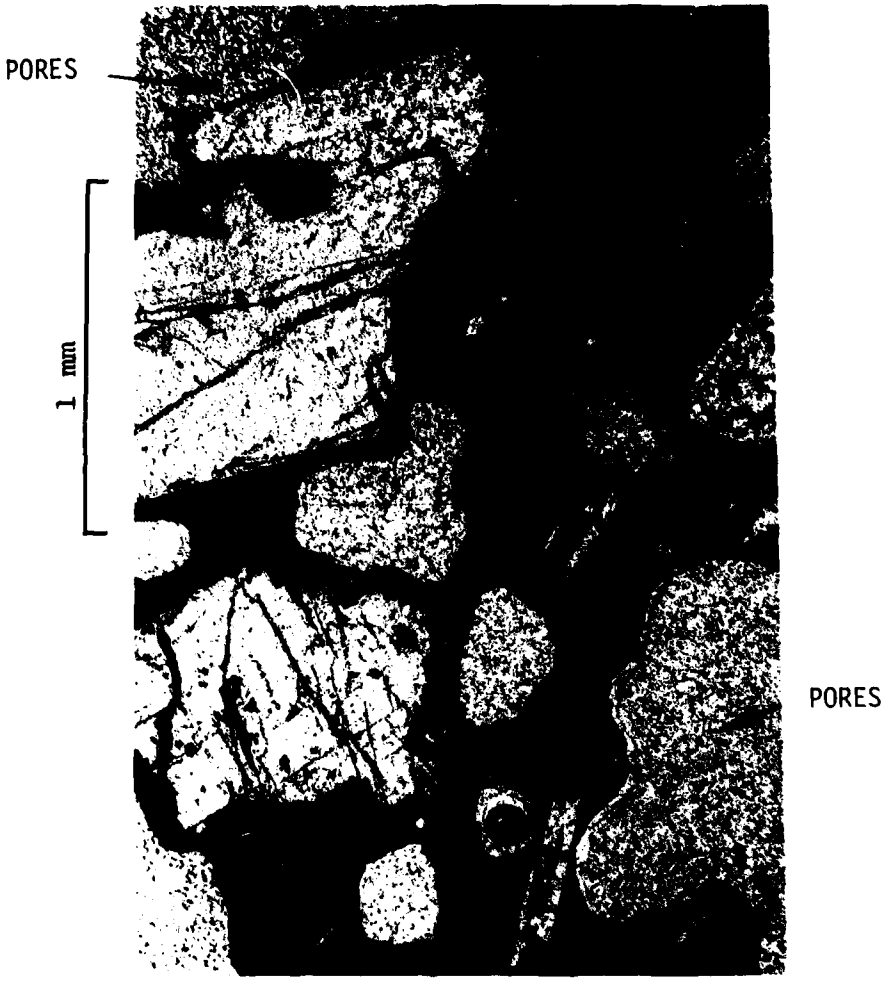

Figure A.12. Photomicrograph of Thin Section from Material #12.

Table A.12. Slide 12.

50—60% GLASS (PLAGIOCLASE MICROTITES + DEVITRIFIED GLASS)

VESICULAR 40—50% POROUS

EUHEDRAL PLAGIOCLASE PHENOCRYSTALS—TO 1.5 MM TWINNED

PYROTENE—AUGITE—TO .3 MM, 1—2%

MOST VESICLES HAVE THIN ALTERATION (CLAYS) LINING VESICLE WALLS

PLAGIOCLASE LATHS ALIGNED, MOST MICROTITES, .1—.3 MM

PLAGIOCLASE = 97—99% OF PHENOCRYSTLS (30—40% TOTAL ROCK)

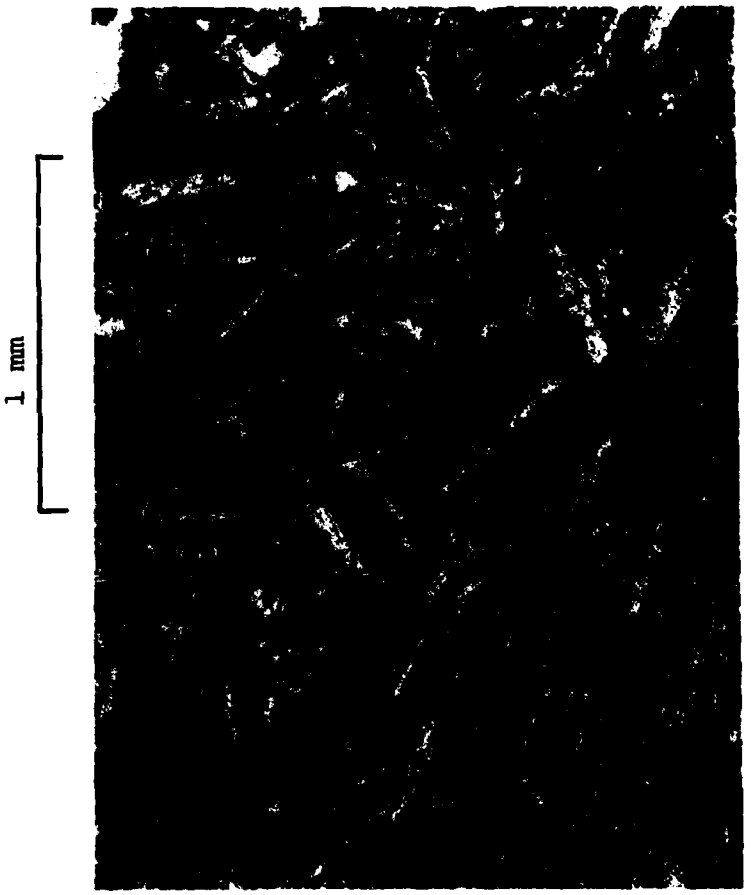

Figure A.13. Photomicrograph of Thin Section from Material #13.

Table A.13. Slide 13.

PLAGIOCLASE LATHS, CALCITE MAKE UP BULK OF ROCK

1 RESORBING PLAGIOCLASE PHENOCRYST ∿3.5 MM LONG

PLAGIOCLASE 60—70% = .1—.2 MM AVERAGE

CALCITE 20—30% <.05 MM—ALTERATION PRODUCT

OPAQUES 7—10%

PORE SPACE 7—10%

ILL-DEFINED THROUGH-GOING CRYSTAL ALIGNMENT—LOCALLY STRONG CRYSTAL ALIGNMENT; ZONES ADJACENT TO ONE ANOTHER CAN BE AT RIGHT ANGLES

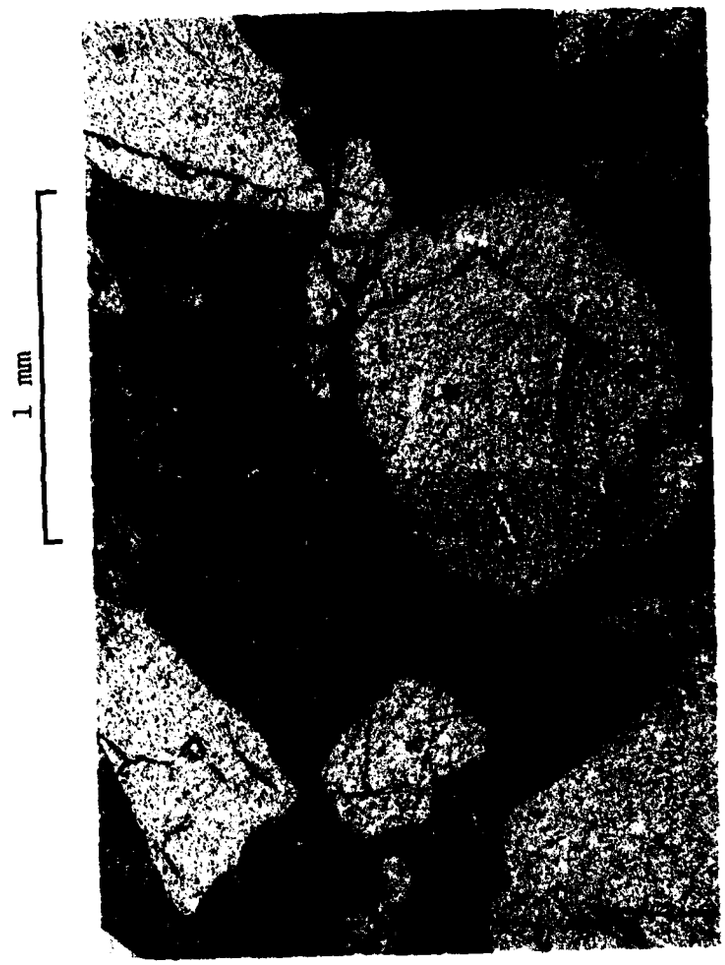

Figure A.14. Photomicrograph of Thin Section from Material #14.

Table A.14. Slide 14.

PLAGIOCLASE—LOCALLY EMBARGED AVERAGE = .6 MM FOR LARGER SIZE SET
.5 FOR SMALLER SIZE SET

BIOTITE TO .3 MM

QUARTZ

LIGHT BROWN GLASS—DEVITRIFIED TO PLAGIOCLASE + CHLORITE (?)

RELICT SHARDS PSEUDOMORPHS PRESENT

NO STRONG FLOW BANDING OBSERVED

SANIDINE

2.5 MM SANIDINE

BIMODAL PHENOCRYST SIZE DISTRIBUTION LARGER CRYSTALS SUBSEQUENT, SUBHEDRAL

60—70% DEVITRIFIED GLASS

30—40% QUARTZ + FELDSPAR

1—2% BIOTITE

Figure A.15. Photomicrograph of Thin Section from Material #15.

Table A.15. Slide 15.

80—85% GLASS

MICROLITE LATHS IN GLASSY GROUND MASS CREATE FLOW BANDING

LATHS VERY SMALL .05 MM LONG DIMENSION

BIOTITE 2—3% .5 MM LONG

PLAGIOCLASE BEING RESORBED—TO 2.5 MM AVERAGE .8—1.2 MM

PORE SPACES (VESICLES)—PSEUDOMORPH

RELICT PLAGIOCLASE PHENOCRYSTLS—PLUCKED

GRAINS?—1—2%

Figure A.16. Photomicrograph of Thin Section from Material #16.

Table A.16. Slide 16.

QUARTZ GRAINS STRAINED—POLYGONALIZATION IS ATTEMPT TO REXTALIZE, RELIEVE STRAIN

GRANODORITE

50—60% PLAGIOCLASE—ALBITE TWINNED 1—2.5 MM

2—5% EPIDOTE—CLINOZOBITE .4—.8 MM

15—20% QUARTZ—SOME POLYGOND GRAINS 2 MM POLY CLOTS

TRACE HEMATITE .2 MM

5—10 CHLORITE—NOT BENT

GREEN BIOTITE 1—5 MM

2 MM = AVERAGE CRYSTAL SIZE RANDOM CRYSTAL ORIENTATION—"ISOTROPIC"

5—10% KSPAR—ORTHOCLASE—GRAMOPHYRES LOCALLY TO 6 MM

CRYSTAL BOUNDARIES NOT SHARP—AS IF ITS SLIGHTLY REXTALIZED, BUT NOT EXTENSIVELY. CLOTS OF QUARTZ HIGHLY POLYGONALIZED.

APPENDIX B

AUTHOR'S RESPONSE TO QUESTIONS

During the initial technical review, several questions were raised by the Contracting Officers Representative. The body of the letter in response to these questions is presented here to clarify several points raised in the report.

Body of letter to Capt. A. T. Hopkins DNA/SPAS dated 22 January 1980.

"Most of the questions raised during the report review were addressed in the report, but I think it is appropriate that others be discussed further in terms of the program objective and approach. I have responded to the questions as encountered in the report.

On page 15 and elsewhere in the report, there is the continuing question for doing the petrographic analysis. In order to determine the lithology (numerical composition, texture and fabric) of the rocks that were sampled, petrographic analysis is the primary technique available. It is an inexpensive process that provides positive identification of the type of rock and therefore the rock unit sampled. As discussed in Tables 3.6 and 3.7 and in Section 3.0, the petrographic analyses were used to substantiate the uniaxial compression tests ranking by indicating that the limestones were able to sustain a higher load to fracture than the volcanics, due to their low porosity. Also, the percent pore space determined by the analysis was found to be an important factor in the penetration response of the rock materials. Results of the analysis are also important in determining a representative material for erosion effects studies since particle type is an important consideration with respect to erosion. Chemical constituent of the in-situ material can be used to determine their hardness relative to MgO for erosive effects evaluations.

Once the type of geology present was determined, the next step was to determine the extent of the geology (percentage). This was accomplished by a geological survey using available maps as discussed in Section 3.1. The results are shown graphically in Figures 3.4 and 2.1(a). From Figure 3.4 one can see that rock unit I is representative of anywhere from 40 to 90 percent of the geology in any one of the CDPs investigated. Figure 2.1(a) shows the percentage of total geology represented by the rock units for all five CDPs combined. This figure

shows that rock unit I represents upwards of 60 percent of the total geology. Obviously rock unit I is representative of the most prevalent geology at the CDPs investigated.

This brings us to the reason for sampling. As discussed on page 23, the valleys are located between linearly extending mountains which are the source of the geological material that fills the valleys. The source of the nuclear cloud particulates is the alluvial fill, thus the need to evaluate the in-situ samples in terms of their penetrability. An understanding of the relative penetrability of the in-situ debris and tonalite granite will help determine the response of an ascent shroud to a nuclear generated debris cloud.

Obviously, the survey and sampling conducted under this effort had to be limited due to the enormous land area involved. However, a logical approach was used to delineate what were considered to be the more detrimental rock units for evaluation. The extent and relative hardness of the rock unit samples were of primary importance in sample selection. Identification of the individual rock units had to be based upon the available geological map data since an extensive and individual field survey would be extremely expensive. Unfortunately, most of the available data are aerial surveys. To conduct an accounting of the subsurface geology is well beyond the scope of the program, but representative valley profiles (e.g., Figure 3.6) are available from other sources and have been referred to in the report.

The objective of this program was to evaluate the relative penetrability of in-situ debris and tonalite granite and to develop a methodology for evaluation of shroud and motorcase materials/concepts. As a part of the methodology, an inexpensive uniaxial compression test is suggested for debris material screening prior to any relatively expensive ballistic impact test. This screening would be invaluable if the geological source for an augmented environment is different from the one evaluated under this program, as pointed out in Section 4.4. At the present, there does not appear to be a direct correlation between the compression test results and the ballistic impact test results except for relative ranking of the response for the various geological materials."

DISTRIBUTION LIST

DEPARTMENT OF DEFENSE

Assistant to the Secretary of Defense
Atomic Energy
ATTN: Executive Assistant

Defense Advanced Rsch. Proj. Agency
ATTN: TIO

Defense Communications Agency
ATTN: CCTC

Defense Intelligence Agency
ATTN: DT-2
ATTN: DT-1C
ATTN: DB-4D
ATTN: DT-2, T. Dorr

Defense Nuclear Agency
ATTN: RATN
ATTN: SPSS
ATTN: SPTD
ATTN: STSP
ATTN: STVL
3 cy ATTN: SPAS
4 cy ATTN: TITL

Defense Technical Information Center
12 cy ATTN: DD

Field Command
Defense Nuclear Agency
ATTN: FCTMOT
ATTN: FCPR
ATTN: FCTMOF
ATTN: FCTMD

Field Command
Defense Nuclear Agency
Livermore Division
ATTN: FCPRL

Joint Chiefs of Staff
ATTN: SAGA/SFD
ATTN: SAGA/SSD
ATTN: J-5, Nuclear Division
ATTN: J-5, Force Planning & Program Division

Joint Strat. Tgt. Planning Staff
ATTN: JPTM
ATTN: JLTW-2
ATTN: JPST
ATTN: JLA, R. Haag
ATTN: JPST, G. Burton

NATO School (SHAPE)
ATTN: U.S. Documents Officer

Undersecretary of Defense for Rsch. & Engrg.
ATTN: Engineering Technology, J. Persh
ATTN: Strategic & Space Systems (OS)

DEPARTMENT OF THE ARMY

BMD Advanced Technology Center
Department of the Army
ATTN: ATC-T, M. Capps

DEPARTMENT OF THE ARMY (Continued)

BMD Systems Command
Department of the Army
ATTN: BMDSC-H, N. Hurst

Deputy Chief of Staff for Ops. & Plans
Department of the Army
ATTN: DAMO-NCZ

Deputy Chief of Staff for Rsch., Dev., & Acq.
Department of the Army
ATTN: DAMA-CSS-N

Harry Diamond Laboratories
Department of the Army
ATTN: DELHD-N-TF
ATTN: DELHD-N-P, J. Gwaltney
ATTN: DELHD-N-P

U.S. Army Ballistic Research Labs.
ATTN: DRDAR-BLV
ATTN: DRDAR-BLT, J. Frasier
ATTN: DRDAR-BL, R. Eichelberger
ATTN: DRDAR-BLT, R. Vitali
ATTN: DRDAR-BLV, W. Schuman, Jr.
ATTN: DRDAR-BLE, J. Keefer

U.S. Army Material & Mechanics Rsch. Ctr.
ATTN: DRXMR-HH, J. Dignam

U.S. Army Materiel Dev. & Readiness Command
ATTN: DRCDE-D, L. Flynn

U.S. Army Missile Command
ATTN: DRDMI-TRR, B. Gibson
ATTN: DRSMI-RKP, W. Thomas
ATTN: DRDMI-XS

U.S. Army Nuclear & Chemical Agency
ATTN: Library

U.S. Army Research Office
ATTN: P. Radowski, Consultant

U.S. Army TRADOC Systems Analysis Activity
ATTN: ATAA-TDC, R. Benson

DEPARTMENT OF THE NAVY

Naval Research Laboratory
ATTN: Code 2627
ATTN: Code 6770, G. Cooperstein
ATTN: Code 7908, A. Williams

Naval Sea Systems Command
ATTN: SEA-0352, M. Kinna

Naval Surface Weapons Center
ATTN: Code R15, J. Petes
ATTN: Code K06, C. Lyons
ATTN: Code F31

Naval Weapons Evaluation Facility
ATTN: P. Hughes
ATTN: L. Oliver

DEPARTMENT OF THE NAVY (Continued)

Office of Naval Research
ATTN: Code 465

Office of the Chief of Naval Operations
ATTN: OP 604-E14, R. Blaise
ATTN: OP 65
ATTN: OP 604C3, R. Piacesi

Strategic Systems Project Office
Department of the Navy
ATTN: NSP-272
ATTN: NSP-273
ATTN: NSP-2722, F. Wimberly

DEPARTMENT OF THE AIR FORCE

Aeronautical Systems Division
Air Force Systems Command
2 cy ATTN: ASD/ENFTV, D. Ward

Air Force Flight Dynamics Laboratory
ATTN: FXG
ATTN: FBAC, D. Roselius

Air Force Geophysics Laboratory
ATTN: LY, C. Touart

Air Force Materials Laboratory
ATTN: MBE, G. Schmitt
ATTN: MBC, D. Schmidt
ATTN: LLM, T. Nicholas

Air Force Rocket Propulsion Laboratory
ATTN: LKCP, G. Beale

Air Force Systems Command
ATTN: SOSS
ATTN: XRTO

Air Force Technical Applications Center
ATTN: TF

Air Force Weapons Laboratory
Air Force Systems Command
ATTN: DYV, A. Sharp
ATTN: DYS
ATTN: DYT
ATTN: DYV
ATTN: NTES, K. Filippelli
ATTN: SUL
ATTN: HO, W. Minge
ATTN: DYV, E. Copus
ATTN: DYV, D. Newlander
2 cy ATTN: NTO

Arnold Engineering Development Center
Air Force Systems Command
ATTN: Library Documents
ATTN: DOOP, G. Cowley

Ballistic Missile Office
Air Force Systems Command
ATTN: MNNXH, Capt Blankenship
ATTN: MNNP
ATTN: MNNX
3 cy ATTN: MNN, M. Baran

DEPARTMENT OF THE AIR FORCE (Continued)

Deputy Chief of Staff
Operations, Plans and Readiness
Department of the Air Force
ATTN: AFXOOSS

Deputy Chief of Staff
Research, Development & Acq.
Department of the Air Force
ATTN: AFRD
ATTN: AFRDQSM

Foreign Technology Division
Air Force Systems Command
ATTN: SDBG
ATTN: TQTD
ATTN: SDBS, J. Pumphrey

Headquarters Space Division
Air Force Systems Command
ATTN: DYS

Headquarters Space Division
Air Force Systems Command
ATTN: RST
ATTN: RSS
ATTN: RSSE

Strategic Air Command
Department of the Air Force
ATTN: DOXT
ATTN: JSTPS/JLA, R. Haag
ATTN: XOBM
ATTN: XPQM
ATTN: XPFS

DEPARTMENT OF ENERGY

Department of Energy
ATTN: OMA/RD&T

DEPARTMENT OF ENERGY CONTRACTORS

Lawrence Livermore National Laboratory
ATTN: L-262, J. Knox
ATTN: L-125, J. Keller
ATTN: L-92, C. Taylor
ATTN: L-24, G. Staihle

Los Alamos National Scientific Laboratory
ATTN: R. Dingus
ATTN: J. Taylor
ATTN: R. Thurston
ATTN: D. Kerr
ATTN: J. McQueen
ATTN: R. Skaggs

Sandia National Laboratories
Livermore Laboratory
ATTN: H. Norris, Jr.
ATTN: T. Cook
ATTN: Library & Security Class. Div.

Sandia National Laboratories
ATTN: M. Cowan
ATTN: A. Chabai
ATTN: T. Cook

DEPARTMENT OF DEFENSE CONTRACTORS

Acurex Corp.
ATTN: R. Rindal
ATTN: C. Powars
ATTN: C. Nardo

Aerojet Solid Propulsion Co.
ATTN: R. Steele

Aeronautical Rsch. Assoc. of Princeton, Inc.
ATTN: C. Donaldson

Aerospace Corp.
ATTN: H. Blaes
ATTN: J. McClelland
ATTN: W. Barry
ATTN: R. Crolius

AVCO Research & Systems Group
ATTN: J. Gilmore
ATTN: Document Control
ATTN: A. Pallone
ATTN: W. Broding
ATTN: J. Stevens
ATTN: W. Reinecke
ATTN: P. Grady

Battelle Memorial Institute
ATTN: E. Unger
ATTN: M. Vanderlind
ATTN: R. Castle

Boeing Co.
ATTN: B. Lempriere

California Research & Technology, Inc.
ATTN: K. Kreyenhagen
ATTN: M. Rosenblatt

Effects Technology, Inc.
ATTN: R. Parisse
ATTN: R. Wengler
ATTN: J. Green
5 cy ATTN: J. Carlyle

General Electric Co.
ATTN: D. Edelman
ATTN: C. Anderson
ATTN: G. Harrison

General Electric Co.
ATTN: P. Cline
ATTN: B. MaGuire

General Electric Company—TEMPO
ATTN: DASIAC
ATTN: B. Gambill

Harold Rosenbaum Associates, Inc.
ATTN: G. Weber

Hercules, Inc.
ATTN: P. McAllister

Institute for Defense Analyses
ATTN: J. Bengston
ATTN: Classified Library

Lockheed Missiles & Space Co., Inc.
ATTN: F. Borgardt

DEPARTMENT OF DEFENSE CONTRACTORS (Continued)

Kaman Sciences Corp.
ATTN: J. Hoffman
ATTN: J. Harper
ATTN: D. Sachs
ATTN: F. Shelton
ATTN: J. Keith

Lockheed Missiles & Space Co., Inc.
ATTN: R. Walz
ATTN: A. Collins

Martin Marietta Corp.
ATTN: J. Potts
ATTN: L. Kinnaird
ATTN: G. Aiello

Martin Marietta Corp.
ATTN: E. Strauss

McDonnell Douglas Corp.
ATTN: E. Fitzgerald
ATTN: J. Garibotti
ATTN: H. Berkowitz
ATTN: L. Cohen
ATTN: H. Hurwicz
ATTN: D. Dean
ATTN: P. Lewis, Jr.
ATTN: G. Johnson
ATTN: R. Reck
ATTN: J. Kirby

National Academy of Sciences
ATTN: D. Groves

Pacific-Sierra Research Corp.
ATTN: H. Brode
ATTN: G. Lang

Physics International Co.
ATTN: J. Shea
ATTN: D. Guthrie

Prototype Development Associates, Inc.
ATTN: J. Dunn
ATTN: M. Sherman
ATTN: J. McDonald

R & D Associates
ATTN: P. Rausch
ATTN: C. MacDonald
ATTN: W. Graham, Jr.
ATTN: F. Field
ATTN: J. Carpenter

Rand Corp.
ATTN: J. Mate
ATTN: R. Rapp

Rockwell International Corp.
ATTN: B. Schulkin

Science Applications, Inc.
ATTN: O. Nance
ATTN: D. Hove
ATTN: J. Stoddard
ATTN: W. Yengst
ATTN: G. Ray
ATTN: J. Warner

DEPARTMENT OF DEFENSE CONTRACTORS (Continued)

Science Applications, Inc.
ATTN: G. Burghart

Science Applications, Inc.
ATTN: J. Cockayne
ATTN: W. Layson

Science Applications, Inc.
ATTN: A. Martellucci

Southern Research Institute
ATTN: C. Pears

SRI International
ATTN: P. Dolan
ATTN: H. Lindberg
ATTN: D. Curran
ATTN: G. Abrahamson

System Planning Corp.
ATTN: F. Adelman

DEPARTMENT OF DEFENSE CONTRACTORS (Continued)

Systems, Science & Software, Inc.
ATTN: R. Duff
ATTN: G. Gurtman

Thiokol Corp.
ATTN: J. Hinchman

TRW Defense & Space Systems Group
ATTN: T. Mazzola
ATTN: M. King
ATTN: A. Ambrosio
ATTN: D. Baer
ATTN: P. Brandt
ATTN: G. Arenguren
2 cy ATTN: A. Zimmerman
2 cy ATTN: I. Alber

Terra Tek, Inc.
ATTN: S. Green

TRW Defense
ATTN: W. Polich
ATTN: E. Wong
2 cy ATTN: V. Blankenship